Materials Science Corporation

NASA CONTRACT REPORT 165778

DEVELOPMENT OF AN ENGINEERING ANALYSIS OF PROGRESSIVE DAMAGE IN COMPOSITES DURING LOW VELOCITY IMPACT

E. A. HUMPHREYS

National Aeronautics and Space Administration
Langley Research Center
Hampton, Virginia 23665

MSC TFR 1205/0208.
JULY, 1981

Materials Sciences Corporation

DEVELOPMENT OF AN ENGINEERING ANALYSIS OF PROGRESSIVE DAMAGE IN COMPOSITES DURING LOW VELOCITY IMPACT

Technical Final Report
MSC TFR 1205/0208
July, 1981

Prepared by:
E. A. Humphreys

Prepared for:
National Aeronautics and Space Administration
Langley Research Center
Hampton, Virginia

Gwynedd Plaza II, Bethlehem Pike, Spring House, PA • 215-542-8400

DEVELOPMENT OF AN ENGINEERING ANALYSIS OF PROGRESSIVE DAMAGE IN COMPOSITES DURING LOW VELOCITY IMPACT

E. A. HUMPHREYS

Materials Sciences Corporation

SUMMARY

This report describes the development and implementation of a methodology to predict damage initiation and growth in composite laminates when subjected to low velocity, low mass, lateral impact. The methodology incorporates a transient dynamic finite element analysis with composite stress and failure analyses. The procedure incorporates damage, as it is predicted, into the displacement solution. Thus, the damage predicted during any time step is incorporated into the dynamic solution at future time steps. This coupling of damage and dynamic response is the heart of the computerized procedure.

Utilizing a perfectly plastic impact assumption, the impact phenomenon is reduced to an initial velocity dynamics problem with the impacting mass lumped at appropriate locations. The displacement time response of the laminated plate is predicted using the transient analysis. Composite ply stresses and interlaminar shear stresses are computed based on nodal moments and forces and laminate models. Failure analyses are performed and appropriate elemental properties degraded within the displacement solution matrices.

The analysis procedure has been utilized to simulate the impact of a 1.59 cm. steel sphere on an eight ply, $[45/0/-45/90]_s$ Gr/Ep laminate. The damage predicted included interlaminar shear failures, laminate back face splitting and the progression of damage within the plane of the plate and through the thickness of the plate.

FOREWORD

This report summarizes the work done for the NASA Langley Research Center under Contract NAS1-15888 during the period August 3, 1979 through July 1, 1981. Mr. Walter Illg was the NASA Technical Representative and the author wishes to express appreciation for the many technical discussions held with him.

The Principal Investigator for MSC was Mr. E. A. Humphreys. The Program Manager for MSC was Dr. B. Walter Rosen and the author wishes to express sincere appreciation for the many technical inputs and discussions provided by him.

TABLE OF CONTENTS

I. INTRODUCTION

With the ever increasing use of laminated composites in structural applications, an interesting phenomenon has become apparent. This phenomenon concerns the real possibility of invisible damage within a composite structure caused by low velocity, low mass impacts. This type of loading environment is most easily envisioned as the impact of a dropped workman's tool on a structure or, perhaps, runway debris ejected onto a structure.

The primary concern related to this type of loading environment is the introduction of performance degrading damage within the composite structure. This damage may not be visually apparent during subsequent inspections of the structure and, hence, the performance degradation will also not be immediately apparent.

The subject of impact related phenomena has been studied by many investigators utilizing many different approaches. Much of this work has been related to ballistic type impact and, hence, is not applicable here. In ballistic impact, the velocities involved are high enough to promote large stress wave propagation effects.

Prior work in the analysis of the low speed impact problem has established that it is reasonable to neglect the stress wave propagation problem and to focus on the transient structural dynamic approach. Different approaches have appeared in the literature to combine contact effects with dynamic effects. The Hertz contact problem has been extended to the problem of dynamic contact and also to the problem of contact of anisotropic bodies (see ref. 1). These approaches treat impact with a semi-infinite target. In the present case, one is concerned with a target in which the dynamic response of the target is important in the sense of transient structural motion rather than material displacement. This problem appears to have been addressed first by Timoshenko (ref. 2), as described by Goldsmith (ref. 3). Timoshenko studied the problem of the impact of a beam where the contact between the bodies was governed by Hertz's law for contact deformations. Karas (ref. 4) extended the Timoshenko

approach to the study of plate impact (see ref. 5). Moon (refs. 6, 7) has utilized the Hertz impact theory in combination with a Mindlin plate theory (ref. 8) to model a similar approach for impact of plate structures. This particular approach yields a nonlinear mathematical problem and extended numerical analysis is required to obtain solutions. The procedure is sufficiently complex to motivate consideration of alternate approaches.

Two such approaches are based on simplifications of the contact force analysis. In one case, it is considered that the impact takes place during a time period which is very short compared to the period of the first natural frequency. In this case, it appears reasonable to regard the impact as having imparted an impulse locally to the plate and to then study the dynamic response of the composite plate target to that impulsive loading. This approach (see ref. 9) is appropriate as the structural stiffness increases and the impacting mass decreases.

Another line of approach initiated by Clebsch (ref. 10) as described by Goldsmith (ref. 3) assumes that upon impact, the projectile moves with the plate and that the velocity of the projectile becomes an initial velocity condition. Thus, the analysis is the structural dynamic response of the plate with the attached mass. McQuillen et al. (ref. 11) applied this approach to a beam. They minimized some of the numerical problems by considering the contact zone between projectile and target to have finite width. This approach tended to minimize the contribution of the higher frequency modes and, thus, numerical procedures were more successful. However, even with these assumptions, the work of reference 11 shows that modes of vibration other than the fundamental mode can be excited by impact, particularly if the striker mass is small. This approach, which is expanded somewhat in references 12 and 13, is being utilized in the current effort.

In the present study, the primary emphasis has focused on the prediction of damage initiation and propagation during the impact event and subsequent dynamic plate response. The difficulty posed

here is that any induced damage will alter the plate stiffness locally and, hence, affect the subsequent dynamic response. Thus, the closed form analytical approach taken in references 11-13 is not applicable.

The approach taken has included the use of a transient dynamic finite element code, modified for composites analysis. The code selected for this purpose was SAP IV (ref. 14). The modifications made within the finite element code have allowed for the computation of composite laminate properties, prediction of layer and interlaminar stresses, failure analysis and incorporation of predicted damage into the subsequent dynamic response.

The finite element method is well suited for this type of analysis since spacial variations in material properties are easily incorporated. Thus, local damage can be included without affecting the stiffness of adjacent material.

The computerized analysis procedure, CLIP (Composite Laminate Impact Program), has been utilized to predict the dynamic response of a laminated plate subjected to low velocity impact. The predictions included damage initiation and growth during time of the dynamic response. A description of the code and users guide are included as an appendix to this report.

II. ANALYTICAL METHODOLOGY

The analysis of laminated composites subjected to impact loadings consists of several distinct procedures. The dynamic response of the system is required. Coupled with this are laminate stress and failure analyses. Additionally, predicted damage must be incorporated back into the dynamic response predictions. The analysis operates in a fashion where each procedure is dependent on the others. The dynamic response affects the stresses. The stresses affect the failure modes and locations. The failure modes and locations in turn affect the dynamic response.

Each of these areas and their effects upon the other procedures are discussed here.

DYNAMIC ANALYSIS

The dynamic analysis routines used in developing the CLIP code were taken from SAP IV. The routines which were utilized include an anisotropic thin shell finite element, capable of bending and membrane loading, and a time integration scheme which integrates the equations of motion to predict the time dependent structural response.

Thin Shell Finite Element

The finite element used in the analysis combines a bending element with a linear curvature field and a membrane element with a constant strain field. The two elements are combined in such a fashion that bending-extensional coupling cannot be modeled. Thus, it is required that laminates modeled be mid-plane symmetric.

The element as formulated in SAP IV used the same material properties for bending and extension. This has been modified such that nonhomogeneous materials can be properly modeled with different properties in extension and bending. The shell element does have the capability to model both extensional-shear coupling and bending-

twisting coupling as it utilizes a full plane stress stiffness matrix in its formulation and, as such, is well suited for composites analysis.

For dynamic analysis, it is required that a mass matrix also be formulated. The method used in formulating the thin shell element consists of generating a lumped mass vector. Hence, only diagonal mass terms are formed. Additionally, no rotary inertial terms are included. Thus, the mass is distributed at translationary degrees of freedom only.

Since dynamic responses typically may include the effects of material damping, some provision must be made for these effects in an analysis. The method used in SAP IV consists of Raleigh damping. This is a convenient formulation as it does not require the formulation of elemental damping matrices. The effects of damping are included at the global mass and stiffness level and, hence, will be discussed in the next section.

Time Integration Routines

The transient time analysis is performed using the Wilson-Θ method (refs. 14, 15). This procedure is a modification of the linear acceleration scheme. The method is unconditionally numerically stable for any choice of time step. The results of the analysis are dependent on the time step, however, due to numerical damping.

The effects of numerical damping can be overcome by judicious time step selection. The approach involves determining the highest structural frequency of interest and then selecting a time step which is a small fraction of the period of this frequency. In reference 15, it is shown that for the Wilson-Θ method an amplitude decay of one percent per cycle can be expected for a time step to bending mode period ratio of approximately 0.045.

The scheme used for material damping in the analysis consists of Raleigh damping. In this method, the damping is assumed to be proportional to both the stiffness and mass matrices. This is convenient since no elemental damping matrices are required. Also,

since typically the structure to be analyzed with CLIP will be of one material, this type of damping is most suitable.

Initial Conditions

The impact analysis performed by CLIP assumes a perfectly plastic impact. This implies that the impacting mass attaches to the plate and remains in contact. This type of impact also implies a conservation of momentum within the system.

These effects are incorporated by lumping the impact mass at specified nodes on the plate structure. An initial velocity is then applied at these nodes. The velocity used is scaled such that the product of impact mass and impactor velocity is equal to the product of impact mass plus nodal masses and the applied initial velocity, thereby conserving the impact momentum.

There are provisions which have been added to allow for the impacting mass to rebound from the plate structure. The contact force between the impactor and plate is computed based on the product of the accelerations of the impacted nodes and the impactor mass. When this force becomes tensile, the mass detaches and the analysis becomes a free vibration problem.

COMPOSITE AND STRESS ANALYSIS

The purpose of the composites analysis is two-fold. First, laminate properties must be generated for input to the thin shell finite element and second, composite inter- and intralaminar stresses must be predicted for use with a failure analysis. The generation of properties and in-plane stress analysis of undamaged finite elements directly follows classical lamination theory and as such will not be detailed here. The areas which need explanation include the generation of stress, moment, and transverse shear resultants from the nodal forces and moments, and the prediction of transverse (interlaminar) shear stresses from the shear resultants.

The stress recovery portions of the thin shell finite element in SAP IV are designed to generate both stresses and moment resultants within a triangular or arbitrary quadrilateral element. The capability for predicting transverse shear resultants did not exist, however. In order to include this capability and minimize redundancy within the CLIP code, the SAP IV stress recovery routines were removed. The shell element procedures were then modified to produce nodal forces and moments directly from the elemental stiffness matrices. By using equilibrium considerations, stress, moment and transverse shear resultants are generated directly from these nodal forces and moments. These considerations are detailed in Appendix A.

As a consequence of the required removal of the SAP IV stress recovery routines, and the inclusion of the alternate method used, all shell elements within the CLIP code are required to be rectangular. Additionally, all elements must be aligned with the global coordinate system.

It is still possible to use nonrectangular quadrilateral elements and obtain the correct displacement response but the subsequent stress analysis would be in error.

The prediction of transverse (interlaminar) shear stress follows closely the method used in classical strength of materials texts for beam bending shear stresses. The finite element models used do not include shear deformation and, therefore, the transverse shear resultants are determined through equilibrium. This method produces satisfactory results if the thickness of the plate is small and the bending response dominates the overall deflections.

The method used for interlaminar shear stress calculation in both intact and damaged elements is detailed in Appendix B. Predicting interlaminar shear stresses in damaged elements is considerably more difficult and will be discussed in a later section.

The calculation of interlaminar normal stresses within the laminated plate is possible through the use of stress equilibrium. However, these stresses should have significant magnitude only directly under the impacting mass. Thus, the effort required to do a rigorous

analysis was deemed too extreme. As a first approximation, interlaminar normal stresses are computed directly under the impact site as a linear function of the thickness. The contact force is distributed over the affected elements and scaled such that the stress on the back face is zero.

Failure Analysis

As the inter- and intralaminar composite stresses are computed, it is necessary to evaluate whether or not failure has occurred. This evaluation must predict both the presence of failure and the type or mode of failure. The mode of failure is required such that the specific elastic properties affected can be modified without affecting the other material parameters.

The failure criteria selected for use in the CLIP code are listed in table 1. These criteria are applied ply by ply for in-plane failure analysis, and interface by interface for interlaminar failure analysis. The components of stress used in the failure analysis are described in figure 1.

Incorporation of Predicted Damage

The primary goal of the current study is to track damage accumulation and growth throughout the impact event. This involves calculating damage at selected time steps and incorporating the effects of this damage back into the dynamic solution. The failure criteria described in the previous section are used to calculate the modes of failure within the shell finite elements. When the modes of damage are found in an element, its stiffness matrix is reformed and the new element is incorporated into the dynamic analysis. This procedure is accomplished by subtracting out the original element from the unfactored global stiffness matrix and adding the new, damaged element. This, of course, requires that the global stiffness matrix be decomposed again.

Ply Damage

When the damage mode predicted consists of ply damage, it is necessary to compute new laminate stiffnesses for bending, extension and bending-extensional coupling. The new bending and extensional properties are input back into the shell finite element routines for formulating the new elemental stiffness matrix. The bending-extensional coupling terms are used only in the stress recovery information since, as was mentioned before, this type of material behavior cannot be modeled in the displacement solution.

The way in which the laminate properties are changed depends upon the type of ply damage. If the ply damage includes fiber failure, then the entire ply is removed from the laminate model. If, however, matrix failure is the only failure mode, it is assumed that the fiber can still carry load. Thus, only the transverse properties of the ply are removed. These laminate modifications apply to the specific element under consideration. Thus, if only one element sustains damage, the other elements are not affected.

When an interior ply fails under the dynamic loading, it is assumed that the constraint of the adjacent material will cause the strain distribution to remain linear through the laminate thickness. Because of this, it is not necessary to compute properties for two or more separate laminates for the damaged shell elements. This type of damage does, however, pose some difficulties in finding the interlaminar stresses. The methodology used for predicting interlaminar shear stresses is described in Appendix B.

Within the CLIP code, the types and locations of damage are saved for each damaged element. This information is then used to evaluate subsequent damage modes. Under certain circumstances, it might be possible for the numerical procedure to predict the same damage mode and location more than once. This is physically unrealistic though, and if the CLIP code senses this, the analysis is stopped.

Interlaminar Damage

When interlaminar damage is predicted due to the dynamic loading, the procedure used is different from that for ply damage. Because of the assumption that adjacent material restrains the curvature and strain distribution when local damage is present, the only effect of a delamination is an adjustment to the transverse shear stress field. The shell finite element does not consider shear deformation and, therefore, the increased shear deformation associated with a crack tip singularity cannot be modeled. The introduction of interlaminar delaminations does not require a reformulation of the elemental or global stiffness matrices. A full description of the assumptions implicit in this method, the effects on the shear stress distribution, and the formulation of the shear stress calculations is contained in Appendix B.

SUMMARY OF ANALYSIS METHODOLOGY

The analysis methodology described previously including Appendices A and B detail the approach taken for analyzing low velocity impact of composite plates. The assumptions implicit in this methodology, as well as the capabilities and limitations of the analysis, are summarized here for clarity.

Analysis Assumptions

1. Small Deflection Analysis

   The displacements of the plate structure are sufficiently small such that the original geometry is applicable throughout the analysis.

2. Displacement Fields

Only bending and membrane displacements are modeled. The effects of shear deformation are insignificant with respect to bending deformations. Typically, this condition is satisfied if the plate thickness is small compared to the other plate dimensions.

3. Material Properties

Static material constants and strengths are used. The effects of time-dependent material properties are insignificant in a realistic structural laminate. This is primarily due to the presence of fibers in many directions.

4. Superposition of Static and Dynamic Displacements

Static pre-stress displacement fields are added directly to the dynamic displacements. No stability analysis is performed as a consequence of (1).

5. Laminate Modeling

Bending-extensional coupling is not included in the analysis. This effectively requires that all laminates modeled be mid-plane symmetric. The assumption is made that damage induced bending-extensional coupling will be highly localized and, therefore, negligible.

6. Perfectly Plastic Impact

The impact involves a complete momentum transfer from the impacting mass to the composite plate structure. This

also implies that contact effects (Hertzian Contact) and wave propagation effects are negligible. Additionally, since contact effects are not modeled, the impact mass can only rebound due to plate dynamics.

7. Interlaminar Normal Stresses

Interlaminar normal stresses are computed only directly under the impacting mass. A linear approximation is used through the thickness of the plate such that the back surface has zero stress and the impacted surface carries the contact force distributed over all affected elements.

Damage Modes

8. Matrix Ply Damage

Damage produced by combined σ_{22}, σ_{12} stress fields. Matrix dominated ply moduli E_2 and G_{12} are set to zero in the affected ply within the affected finite element.

9. Fiber Ply Damage

Damage produced by σ_{11} stresses. All lamina moduli are set to zero in the affected ply within the affected finite element.

10. Interlaminar Delamination

No stiffness effects as a direct consequence of (2). Increased shear deformations associated with a singular shear stress distribution at the crack tip are not modeled.

Damage Stress Effects

11. Matrix Ply Damage

Lamina stresses σ_{22} and σ_{12} are automatically set to zero as a consequence of (8). Additionally, interlaminar stresses σ_{xz} and σ_{yz} are set to zero within the damaged ply.

12. Fiber Ply Damage

Lamina stresses σ_{11}, σ_{22} and σ_{12} are automatically set to zero as a consequence of (9). Additionally, interlaminar stresses σ_{xz} and σ_{yz} are set to zero within the damaged ply.

13. Interlaminar Delamination

Interlaminar stress components σ_{xz} and σ_{yz} are set to zero at the affected ply interface within the affected finite element.

Damage Propagation

14. Ply Damage

Damage predicted in plies propagated due to load redistribution. The load distribution is changed because of local stiffness changes (8), (9).

15. Interlaminar Delamination

Delaminations do not propagate to adjacent elements. Delaminations may occur in adjacent elements due to shear force distributions but these distributions are not changed as a result of interlaminar damage (10).

III. LOW VELOCITY IMPACT ANALYSIS

The analysis methodology described in the previous sections has been utilized to predict the response of a clamped rectangular laminated composite plate subjected to a low velocity, low mass impact. The analyses performed have provided information relating to the modes and locations of impact induced damage, the displacement response of the composite plate and the contact force between the impacting mass and the plate structure. This information is generated at various times throughout the duration of the impact event.

In the course of predicting the response of the plate, it was required to make several computer analyses. These included solutions with the entire impact mass lumped at a single, central node and solutions with the impacting mass distributed over a group of centrally located nodes.

The laminate configuration, impact parameters, finite element models and the results of the various analyses are described and discussed here.

ANALYSIS PARAMETERS

Before discussing the various analyses performed, the various parameters relating to the materials, finite element models and impact conditions need to be described. The analyses performed were part of an effort to model one of many impact experiments which have been performed at NASA Langley. Hence, the materials and configurations correspond to this experiment.

Laminate Configuration

The laminate selected for the impact analysis was an eight ply, quasi-isotropic configuration. The stacking sequence analyzed was $[45/0/-45/90]_S$. The material properties used correspond to a T300/5208 Gr/Ep system and are listed in table 2. The unidirectional properties used are typical static data and were taken from refer-

ence 16. It should be noted that variation in these properties could greatly affect the solution. Therefore, a design application of the analysis would require the characterization of the material under consideration to avoid the wide variation in material data reported in the literature.

The ply thickness used was 0 01321 cm. yielding a total laminate thickness of 0.1056 cm. This laminate configuration exhibits bending-twisting coupling which must be taken into account in the finite element model.

Finite Element Models

The finite element model used for most of the analyses made is shown in figure 2. The model encompasses the entire plate structure as required by the bending-twisting coupling present in the laminate to be analyzed. The model dimensions are 10.16 cm. by 15.24 cm.

In figure 2, the shaded area represents the elements which were selected for stress analysis. The CLIP code has been developed such that only specified elements have stress calculations performed (see Appendix C). This was done in an effort to maximize computational economy.

The central section of the plate was chosen for stress calculations as this is the area where any impact induced damage should occur. More elements could have been selected for stress analysis but this was deemed unnecessary since the impact site was directly at the center of the plate.

The model was developed to represent a clamped plate and as such, the edge nodes are constrained against all rotations and displacements. The model contains 704 elements, 759 nodes and 1953 active degrees of freedom. The number of active degrees of freedom is minimized by constraining all in-plane displacements.

In the finite element model, the maximum element aspect ratio is eight. Within the area where stress calculations are performed, the maximum element aspect ratio is 4.

In order to verify the validity of this model, a static solution was run. The loading consisted of a uniform pressure distributed over the entire plate surface. The results of this solution were then compared with a one-term Ritz solution taken from reference 17. For this comparison, it was necessary to assume that the quasi-isotropic $[45/0/-45/90]_s$ laminate behaves as a specially orthotropic laminate. Hence, the bending-twisting coupling terms, D_{16}, D_{26} are ignored. Even with this approximation, the two solutions compare within 3.3%. Hence, the model has been shown to be valid.

During the course of performing the impact analyses, it was necessary to develop another finite element model. This model is shown in figure 3. The only difference between the two models is the removal of four elements and one node at the center of the plate in the second model. The rationale for developing this second model will be discussed later in this report.

Impact Parameters

The impact mass and velocity modeled in the analyses are listed in table 3. All of the analyses used these parameters. The various analyses did in some cases represent different distributions of the impact mass on the plate, however. The different distributions used are depicted in figure 4. Each of the sections shown are representative of the geometric center of the plate. Obviously, the third impact mass distribution shown in figure 4 was utilized with the second finite element mesh which had the four central elements removed.

Integration Time Step

The selection of the integration time step is one of the more critical steps in defining the impact model. The time step selected must be small enough to adequately determine the response of all critical bending modes while not requiring an excessive number of

time steps to investigate the impact event. The approach is to compute the periods of the plate natural frequencies and determine which are critical.

An analysis was made using a solution given in reference 17 to determine the natural frequencies for the clamped plate in question. As before, it was necessary to model the plate without the bending-twisting coupling terms. This implies that all frequencies calculated are higher than actual since neglecting the coupling terms effectively increases the plate bending stiffnesses. Additionally, the predictions were made without including the effects of impact induced damage. Thus, the stiffnesses were again higher in the predictions than can be expected in the impact analyses. Hence, the computed frequencies can be expected to be somewhat higher than the actual natural frequencies

Based on these calculations, a time step of 1 μsec was selected for the initial impact analysis. This corresponds to approximately 1/19 of the 10-10 bending mode period. The results of the initial impact analysis indicate that the 1 μsec time step was considerably smaller than required. The bending shapes of the plate did not involve frequencies this large and, hence, for the remaining analyses, a time step of 2.5 μsec was used with no apparent degradation of the results.

In conjunction with the time step selection, it must be determined how often to perform stress calculations. In each of the analyses made where stress calculations were included, the frequency of stress calculation was every five time steps. In terms of computing damage growth, the optimum frequency of stress calculation would be to compute them every time step. Considerations of the cost and time involved precluded this, however.

IMPACT ANALYSES

In order to predict the response of the laminated plate described when subjected to the impact conditions also described, it was necessary to perform four separate analyses. The first three analyses

were performed with the finite element model shown in figure 2. The last analysis was made using the model in figure 3.

The first analysis was made without the inclusion of stress calculations. This analysis was performed in order to verify the time step selection and determine the duration of the impact event. (See Appendix C.)

The second and third analyses were full analyses including stress analysis. In the second analysis, the impact mass was lumped at the center node of the finite element model. The results of this analysis prompted the distributed impact mass utilized in the third analysis. In both of these solutions, the damage computed was so extensive that computerized procedure terminated the solution.

The fourth solution was made in an attempt to model the damage growth beyond the point at which the computer program had terminated in the second and third solutions. Hence, the removal of the four central elements in figure 3.

Convenient groupings of the damage predictions of these analyses can be found in table 4. The information in table 4 will aid in comparisons of the growth of damage between solutions and in comparisons of the types of damage within each solution.

Displacement Solution

The first analysis performed was simply a dynamic displacement response solution. The impact mass was lumped at the center plate node. The integration time step was 1.0 μsec.

The displacement response of the laminated plate plotted through the center of the plate, along the axis corresponding to the smaller dimension of the plate, is shown in figures 5 and 6. The displacements in figure 5 represent the very short time response of the plate while figure 6 depicts the longer time response.

Comparing the two figures demonstrates a fundamental difference between the early displacement fields (fig. 5) and later displacement fields (fig. 6). At very early times in the impact event, the displacements can be characterized as a local phenomenon. At $T = 2.5 \times 10^{-5}$ seconds, the major displacement response can be seen to exist at the center of the plate, with the rest of the structure

remaining nearly motionless. As time progresses, the extent of the plate with significant displacements can be seen to be progressing outwards to the edges of the plate.

The progress of outward spreading of the major displacement response is complete at T = 2.0×10^{-4} seconds, as can be seen in figure 6. All of the displacement fields in figure 6 can be characterized as a predominance of the third bending mode shape. The third mode rather than the first mode is excited due to the clamped boundary conditions.

Another aspect of the mode shapes excited relates to the integration time step selected. Previously it was stated that the 1 μsec. time step was sufficient to characterize the 10-10 bending mode shape of the impacted plate. It is quite obvious from figure 5 that the mode shapes present do not approach the 10-10 mode. Hence, for all remaining analyses, the time step was increased to 2.5 μsec.

In setting up the analysis, two unfortunate situations were included. First, the printing of displacements was set up in such a fashion that it was not possible to observe the displacement fields along the longer dimension of the plate. This is apparently of little consequence since the displacements of figures 5 and 6 have provided sufficient information. The second problem involves the amount of time required for the duration of the impact event. The solution was set up with five hundred time steps. Hence, the total time allowed was 5×10^{-4} seconds. At the end of this time, and therefore the end of the solution, the impact mass had not rebounded and the maximum displacements had not yet been reached. This caused some difficulty since part of the rationale for performing this solution involved determining the time duration of the impact event.

In order to make an estimate of the duration of the impact, it was necessary to consider the contact force between the impact mass and the plate. In figure 7, a plot of the force-time response of the impact event is shown. The force appears to be somewhat erratic as it is computed as the product of the impact mass and the acceleration of the plate node where the mass is lumped. The accelerations

of the node in question reflect considerably higher frequencies than the displacements and, hence, the contact force calculated also contains the high bending mode frequencies.

Evaluations of the minimum value of the forces shown in figure 7 indicate that the impact mass was close to rebounding when the analysis terminated. Additionally, a displacement analysis made with a less refined finite element model indicated that the maximum displacement value for these impact conditions was nearly attained at 0.5 msec. Therefore, for the remainder of the impact analyses, the maximum time allowed for the solution was increased to 8.75×10^{-4} seconds. This corresponds to 350 time steps at the new integration time step of 2.5 μsec.

Stress Solution, Mass Lumped at One Node

Using the new time step described, a full impact analysis with stress solution was performed. This solution progressed until two elemental laminate stiffness matrices became singular due to damage in all plies at the end of thirty time steps.

The displacement time response through the center of the plate along the shorter dimension of the plate is shown in figure 8. Comparing these displacements with those shown in figure 5 demonstrates little, if any, difference between the two solutions. Since in figure 8 considerable damage is present, especially at 7.5×10^{-5} seconds, one would expect significant differences to be present. The reason that these differences are not present is simply that the response shown in both figures 5 and 8 is primarily inertial. Not enough time has passed for the effects of the induced damage to significantly affect the solution. Had the stress solutions continued for a longer time, the differences would have become significant.

In setting up this solution, sufficient displacement printing was specified such that the response of the plate along the longer axis could be observed. The displacement time response through the center of the plate along the longer dimension of the plate is shown

in figure 9. The displacement fields along the long axis of the plate show considerable similarity to those along the shorter axis. The primary difference is that the changes in slope of the curves are slightly more gradual along the longer axis. This was expected since the plate is longer and, hence, more flexible in this direction.

In both figures 8 and 9, the most striking result is the limited area of the plate with significant displacement response during the early moments of the impact event. As time progresses, the displacement "waves" move outward until the entire plate is affected and one would expect high moments and shears corresponding to the compressed displacement fields.

The moment resultants through the plate center along the shorter and longer plate axes are shown in figures 10 and 11 respectively. The moment resultants correspond to $T = 5.0 \times 10^{-5}$ seconds and, hence, the middle displacement fields in figures 8 and 9. The moment resultants depicted in figures 10 and 11 represent averages of the elements on either side of the plate centerlines. The specific values vary slightly on either side of the centerlines due to the bending/twisting coupling described previously. This coupling also produces twisting moment resultants. The twisting moments are not shown, however, since they are of such small magnitude. The maximum twisting moment predicted was less than 8% of the peak M_x value.

The moment resultants shown in figures 10 and 11 demonstrate that the major effect of the impact is highly localized at 5.0×10^{-5} seconds. This is in agreement with the displacement fields depicted in figures 8 and 9.

The transverse shear resultants corresponding to the moment resultants are shown in figures 12 and 13. Once again, the major loading occurs in a local region surrounding the impact site. This is due, of course, to the large moment resultant gradients at the plate center (figs. 10 and 11).

The transverse shear resultants are plotted in the same fashion as the moment resultants. The figures represent averages of the two elements on either side of the plate centerlines. The shear

resultants in individual elements also contain the effects of the bending-twisting coupling and, therefore, are slightly different on either side of the plate centerlines.

The moment and transverse shear resultants depicted in figures 10-13 are sufficiently large to produce significant damage at the center of the plate. At the end of five integration steps, a stress analysis was performed. The elements which suffered in-plane and interlaminar damage at this time are shown in figures 14 and 15 respectively. The grid on which the damage is shown encompasses all elements which were selected for stress analysis.

The ply damage shown in figure 14 consists primarily of transverse (matrix) cracking in the bottom 45° ply. Six of the elements also experience matrix cracking within the next interior ply (0°). Thus, the region shown in figure 14 has sustained considerable damage in terms of surface area but little through the thickness.

The interlaminar damage shown in figure 15 is more interesting. Each of the four elements depicted has experienced delamination at the five innermost interfaces. This damage is quite extensive and indicates that the transverse shear resultants are extremely high in this region and at this time. In practical terms, the material in this region must be considered fully degraded.

The most interesting feature of the interlaminar damage is its presence. Had one simply applied a static point load at the center of the plate, no delamination would have occurred. However, at the very early time at which the stresses were computed, extremely sharp bending gradients are present. This is due to the highly localized displacement response at this early time, as was shown at later times in figures 8 and 9.

In figure 16, the elements with accumulated damage after 2.5×10^{-5} seconds are depicted. Comparing figures 14 and 16, the region of damaged elements can be seen to be growing. The majority of the damaged elements in figure 16 have one or two back face plies damaged. Two of the elements shown have suffered top face damage.

These elements are shown in figure 17. Obviously at 2.5×10^{-5} seconds, the ply damage has become extensive, with elements failing at both outer surfaces.

It is interesting that at 2.5×10^{-5} seconds no additional interlaminar damage is present. The reason for this stems from the method used for computing interlaminar shear stresses. These stresses are computed at ply interfaces only. Since the remaining interface was between 0° and 45° plies, the neutral surface will not be at the ply interface; the maximum shear stress will also not be at the ply interface. Thus, the analysis does not predict the maximum shear stress in this case and the lower stress at the interface may not cause damage.

At 3.75×10^{-5} seconds, the transverse shear resultants are sufficient to produce large interface stresses and additional interlaminar damage is predicted. The new delamination is within the elements which had sustained interlaminar failures at 1.25×10^{-5} seconds. Thus, two of the elements shown in figure 15 have only one remaining intact ply interface. The remaining interface in these elements is between the bottom 0° and 45° plies.

In figures 18, 19 and 20, the accumulation of ply damage during the remainder of the analysis is shown. No additional interlaminar damage occurred.

These figures show a steady increase in the region of impact induced ply damage. The extent of the damage through the thickness at the end of the analysis is depicted in figures 20, 21 and 22. Figure 20 indicates the total planar area of the plate damage. Figure 21 shows which elements in this region have more than one damaged ply and figure 22 shows elements which have sustained fiber damage.

The fiber breakage shown in figure 22 is probably the most critical. In each of the elements, the first occurrence of fiber damage was at 5×10^{-5} seconds. Both elements sustained failures in the bottom -45° ply at this time. At 6.25×10^{-5} seconds, additional damage in the bottom 90° and 0° plies occurred. At 7.5

x 10^{-5} seconds, each ply in these elements had sustained damage and, hence, the solution terminated. There was no material left to carry any additional loading.

The damage accumulated during this solution was very large in its extent, both in the planar dimensions of the plate and through the thickness. The problem with these results was that the experiments carried out at NASA Langley did not indicate damage as extensive as the computer analysis did. The experimental work generated interlaminar separation and transverse ply failure as the two primary damage modes, but apparently did not produce the extensive fiber damage. One reason for this could have been related to the placement of the impacting mass. Since the entire mass was lumped at one node in the analysis, the response of the plate may have been overestimated. It was determined, therefore, that an additional analysis would be made with the impact mass distributed over five nodes rather than lumped at one node.

Stress Solution, Mass Distributed at Five Nodes

The impact mass distribution used in this third analysis was previously depicted in figure 4. This distribution was chosen in an effort to more closely simulate the impact of a sphere on a plate. The diameter encompassed in the distributed mass arrangement corresponds to 20% of the diameter of the sphere used in the experiments at NASA Langley.

The displacement response predicted in this analysis was very similar to the previous analysis. The shapes of the curves were nearly identical to those in figures 8 and 9. One surprising difference was present, however. The solution with the distributed load produced larger peak displacement values. At 2.5 x 10^{-5} seconds, the difference amounted to 3%. When the time increased to 5 x 10^{-5} seconds, the difference decreased to 1%.

This result was surprising since it was anticipated that the spreading of the impact mass would reduce the displacements. The reason for the increased displacements is the initial velocity solution procedure used in the analysis. Since all nodes where the impact mass is applied are given an initial velocity, more of the plate begins the analysis with non-zero velocities. When only one node is impacted, the surrounding nodes lag behind in terms of velocity. When the distributed impact mass is used, these surrounding nodes are excited at the same velocity. Thus, in the solution where the mass is lumped at one node, the velocity lag of the surrounding nodes restrains the displacements. This effect is apparently temporary in the solution procedure as the difference decreases rapidly with time.

The distributions of damage in this solution were somewhat different from those in the previous solution. The extent of the damage was nearly the same, however, and this solution terminated in a fashion similar to the previous case. The increased displacements caused this solution to terminate earlier than the lumped mass solution. The procedures operated for 20 time steps before the damage was too extensive, while the previous solution proceeded for 30 steps.

At the first stress calculation, the predicted ply and interlaminar damage is depicted in figures 23 and 24 respectively. Comparing figures 23 and 14, it can be seen that the extent of the damage is very similar for the distributed mass solution and the lumped mass solution. The type of damage is also similar in that the majority of damaged elements have suffered back ply matrix tensile failures.

Comparing the interlaminar damage predicted in the two solutions (figures 15 and 24) demonstrates that the distributed mass solution produces considerably more delamination, although the extent of this damage through the thickness of the plate was comparable for the two solutions. Each of the damaged elements in figure 24 has suffered delaminations between all plies except the outer 45°/0° interfaces. As in the previous solution, this extensive delamination must be considered as total failure in these elements. The solution procedure continued, however, since most of the individual plies remained intact.

The damage growth during the remainder of the analysis is depicted in figures 25 through 27. With each stress calculation, the number of damaged elements grows, as does the extent of the damage within the elements. Comparing figures 27 and 19 indicates that the number of damaged elements at 5×10^{-5} seconds is identical for the two solutions. The types of damage within the elements are very different, however. The damage in the central four elements (fig. 28) includes considerable fiber breakage. The solution terminated because two of these central elements had sustained fiber damage in all plies except the upper 0° ply. This ply had suffered matrix damage, however. Thus, no material remained for carrying the load.

The delamination predicted in the distributed mass solution never progressed beyond the twelve elements shown in figure 24. The amount of delamination within these elements did increase, however. At 2.5×10^{-5} seconds, the four central elements (fig. 29) had no remaining ply interfaces. During the subsequent stress calculation at 3.75×10^{-5} seconds, four additional elements experienced increased interlaminar damage. These elements are shown in figure 30. The last remaining interface in the elements was the bottom 0°/45° ply junction. At the end of the analysis, no additional delamination had occurred.

After reviewing the results of the second stress analysis, it was decided that a third should be performed. The decision was made in an effort to determine the damage subsequent to the point at which the two stress solutions had terminated.

Stress Solution with Modified Finite Element Model

In order to continue the solution process beyond the point at which an element has no remaining plies, two approaches were considered. The first approach involved modifying the computer code to simply ignore the element after the damage occurred. The time involved in adopting this method was not available, however, and

a simple approach was needed. The approach taken involved simply removing the four central elements from the finite element model before beginning the analysis. It was felt that this approach would eliminate the most critical elements and allow the solution to proceed to conclusion. Since these four elements had already been shown to sustain damage throughout the laminate, removing them would simulate the response after they had failed.

The finite element model used for this analysis was previously shown in figure 3 and the impact mass distribution demonstrated in figure 4.

The solution with this modified finite element model progressed through 30 time steps, as had the original stress solution. After 30 steps, the solution again terminated due to the lack of material left in an element. The progression of damage growth for this solution is shown in figures 31 through 37. The only major difference between this solution and the previous ones relates to the location of the element which caused the solution to terminate.

In the previous analyses, the element which failed totally had always been one of the four central elements. In the modified model solution, these elements were removed. The element which caused the execution to terminate in the modified model solution was simply an adjacent element. Hence, the effort to continue the analysis beyond 7.5×10^{-5} seconds was in vain.

IV. DISCUSSION AND RECOMMENDATIONS

The computerized analysis methodology has been utilized to predict the response, including damage initiation and propagation, for a specific low velocity, low mass impact event. The analysis has been shown to be an effective tool in predicting the response of the plate structure. The damaged nodes and locations predicted were consistent and correspond reasonably well with experimental work as described to MSC by NASA Langley. Several significant features of the analysis predictions and methodology warrant further discussions.

In each of the stress solutions performed, significant interlaminar separations occurred at the first stress computation. The time at which the calculations were made was 1.25×10^{-5} seconds. The elements which suffered interlaminar separation at this time were the only elements affected by delamination. These two features identify two significant elements of the stress and damage predictions.

The fact that the delamination occurred at the first stress solution demonstrates that interlaminar failures initiate very early in the impact event. The delamination is a function of the transverse shear forces, which are highest very early in the impact event because of the localized nature of the displacement response at that time. Since the significantly non-zero displacements are restricted to a small region at the center of the plate, severe moment gradients also exist at the plate center. The high moment gradients produce the large transverse shear forces. As the impact event progresses, the displacement fields spread, and the moment gradients decrease and the propensity for interlaminar damage initiation decreases.

As delamination occurs, shear deformations increase due to singular shear stresses at the crack tip. The singular shear stresses tend to promote propagation of the crack. These effects cannot be modeled, however, since shear deformation is not included in the current analysis.

This is an area where further work could significantly improve the usefulness of the CLIP code. The propagation of interlaminar damage might be handled in one of two ways.

One approach would involve the inclusion of shear deformation in the displacement solution. With the inclusion of shear deformation, damaged elements could be given a reduced stiffness to promote increased shear stresses in adjacent elements equal to the average increase produced by the shear stress singularity. This would then promote delamination propagation.

The other approach would involve the use of an analysis to be used subsequent to the impact analysis. This method would use the delamination predicted during the impact analysis. The material surrounding the delamination would then be subjected to the shear and moment distributions predicted in the impact analysis after the instant at which the damage occurred. The areas where the delamination connected with intact material could then be analyzed utilizing fracture mechanics to predict the delamination growth. Noting that the effects of shear deformation are small in undamaged materials, this damage growth need not be included in the impact analysis if the affected area is small.

Another area which warrants discussion involves the extent of the ply damage predicted in the impact analyses made. In all of the stress solutions made, the damage eventually propagated completely through the thickness of the central finite elements. This led to an immediate problem in that the solution terminated at this point. Modifications to the CLIP code to allow the solution to proceed beyond this point would be most helpful. The solution could be modified to continue until the damaged region reached an area equivalent to the impacting mass. At this point one would assume that the mass had penetrated the plate.

Because the solutions terminated, the full extent of the damage which would have been induced in the plate was never determined. It was apparent, however, that the predictions of damage exceeded the damage measured in the experimental work performed at NASA Langley. This was primarily related to the damage through the thickness

predicted at the plate center and this would tend to indicate that the energy impacted to the system in the analysis was too great. The excess energy in the analysis is probably a function of two effects not modeled. The first of these, and probably the most important, is related to energy which should be lost due to local surface crushing at the point of impact. It is known from Hertzian contact analyses that the local contact stresses can be quite large and could cause significant permanent local deformations. These deformations would absorb a significant portion of the impact energy. Modifications to account for this effect would improve the analytical predictions. These modifications could be effected utilizing the contact forces prediction already in the CLIP code coupled with a Hertzian contact analysis and a local, non-linear material model.

The other contributor to the energy loss is material damping. The effects of damping very early in the impact event are probably small but at later times they must surely become significant. The CLIP code has provisions for damping but this feature was not used due to a lack of data.

Another area of discussion relates to the effects of utilizing a distributed impact mass in the analysis. As was demonstrated, distributing the impact mass produced a slightly increased displacement field when the opposite should have been true. The effect was seen to be short-lived and may be insignificant. It is disconcerting, however, and modifications could be made to correct the situation. These modifications would involve applying the mass and velocity initially at one node and spreading the mass as a function of the contact force as the solution progressed. This would more closely simulate the actual impact event.

A final area of consideration relates to the effects of a static prestress on the impact analysis. The procedure utilized in the current analysis is simply a superposition of the static and dynamic displacement fields. This is applicable if in-plane static loads are tensile or if shear or compressive loadings are small enough that buckling is not a consideration. If buckling is a real possibility then the inclusion of a stability analysis would be

required.

A stability analysis in the finite element procedure would require considerable modifications to the code and substantially decrease the efficiency of the analysis. A stability analysis requires the formulation of a modified stiffness matrix and an eigenvalue extraction. The modified stiffness matrix is based on the strain field present when the buckling analysis is performed. The eigenvalue problem is not compatible with the direct integration of the equations of motion as currently used for the impact displacement response. Thus, a new analysis procedure would be needed. Additionally, the eigenvalue problem would have to be solved at each time step since the buckling loads are a function of the strain field present. This would effectively double the solution time. Thus, while the inclusion of a stability analysis would be possible, it would not be practical.

In summation, while the analysis is functioning well and provides significant insight into the phenomenon of low velocity impact, further work would be most helpful.

The areas of these future efforts should include:

1) Inclusion of a disbond growth model either through shear deformation or fracture mechanics;
2) Modification to allow continued program execution after local complete element failure;
3) Inclusion of energy loss mechanisms due to non-linear contact effects; and
4) More realistic modeling of the impact mass distribution.

The addition of these capabilities to the analysis procedure would provide better modeling of the impact event. This would allow for increased confidence in the analysis and facilitate its use in evaluating the relative merits of various laminates when subjected to low velocity impact.

As optimum laminates are determined from impact related criteria, further evaluations could then be performed with regard to residual static strength, subsequent impact events, and fatigue life. The static and fatigue evaluations could be made using a modification of a code developed for fatigue of notched composite laminates (reference 18) while subsequent impact events might be evaluated using a modification of the code developed here.

REFERENCES

1. Willis, J. R., "Hertzian Contact of Anisotropic Bodies," Journal of Mechanics of Physical Solids, Vol. 14, 1966, pp. 163-176.
2. Timoshenko, S. P., "Zur Frage nach der Wirkung eines Stosses auf einer Balken," Z. Math. Phys., Vol. 62, 1913, No. 2, p. 198.
3. Goldsmith, W., Impact. E. Arnold Ltd. (Publishers) 1960, Chapter IV.
4. Karas, K., "Platten Unter Seitlichem Stoss," Ingenieur-Archiv, Vol. 10, 1939, p. 237.
5. Sun, C. T., and Chattopadhyay, S., "Dynamic Response of Anisotropic Plates Under Initial Stress due to Impact of a Mass," Trans. A.S.M.E., J. Appl. Mech., Vol. 42, 1975, p. 693.
6. Moon, F. C. "Wave Surfaces Due to Impact on Anisotropic Plates," Journal of Composite Materials, Vol. 6, 1972, p. 62.
7. Moon, F. C. "Theoretical Analysis of Impact in Composite Plates," NASA CR-12110, Princeton University, 1973.
8. Mindlin, R. D., "High Frequency Vibrations of Crystal Plates," Quarterly of Applied Mathematics, Vol. 19, 1961, p. 51.
9. Chou, P. C. Flis, W. J. and Miller, H. "Low Speed Impact of Plates of Composite Materials," NADC 78259-60, 1978.
10. Clebsch, A., Theorie de l'elasticite des corp solides, trans. B. de St.-Venant and M. Flamant, Dunod, Paris, 1883.
11. McQuillen, E. J., Llorens, R. E., and Gause, L. W., "Low Velocity Transverse Normal Impact of Graphite-Epoxy Composite Laminates," Report No. NADC-75119-30, Naval Air Development Center, Warminster, PA, June 1975.
12. Chou, P. C., Flis, W. J., Miller, H., "Certification of Composite Aircraft Structures under Impact Fatigue, and Environmental Conditions. Part I. Low Speed Impact of Plates of Composite Materials," NADC-78259-60, January 1978.
13. Llorens, R. E., McQuillen, E. J., "Off Center, Low Velocity, Transverse Normal Impact of a Viscoelastic Beam," NADC-78237-60, September 1978.

14. Bathe, K. J., Wilson, E. L., Peterson, F. E., "SAP IV, A Structural Analysis Program for Static and Dynamic Response of Linear Systems" EERC 73-11, June 1973.
15. Bathe, K. J. and Wilson, E. L., Numerical Methods in Finite Element Analyses, Prentice-Hall Inc., 1976.
16. Advanced Composites Design Guide, prepared by Rockwell International Corp., Contract #F33615-71-C-1362 for AFML, 1973.
17. Ashton, J. E. and Whitney, J. M., Theory of Laminated Plates, Technomic, Inc., 1970.
18. Humphreys, E. A. and Rosen, B. Walter, "Development of a Realistic Stress Analysis for Fatigue of Notched Composite Laminates" NASA-CR-159119, May 1979.

Table 1. Failure Criteria

Tensile Fiber Mode

$$\frac{\sigma_{11}}{\sigma_A^+} = 1$$

Compressive Fiber Mode

$$\frac{\sigma_{11}}{\sigma_A^-} = 1$$

Tensile In-Plane Matrix Mode $(\sigma_{22} > 0.0)$

$$\frac{\sigma_{22}^2}{(\sigma_T^+)^2} + \frac{\sigma_{12}^2}{(\tau_A)^2} = 1$$

Compressive In-Plane Matrix Mode $(\sigma_{22} < 0.0)$

$$\frac{\sigma_{22}}{\sigma_T^-}\left[\left(\frac{\sigma_T^-}{2\tau_T}\right)^2 - 1\right] + \frac{\sigma_{22}^2}{(2\tau_T)^2} + \frac{\sigma_{12}^2}{(\tau_A)^2} = 1$$

Table 1 (cont'd.). Failure Criteria

Tensile Interlaminar Mode $(\sigma_{33} > 0.0)$

$$\frac{\sigma_{33}^2}{(\sigma_T^+)^2} + \frac{\sigma_{23}^2}{(\tau_T)^2} + \frac{\sigma_{13}^2}{(\tau_T)^2} = 1$$

Compressive Interlaminar Mode $(\sigma_{33} < 0.0)$

$$\frac{\sigma_{33}}{\sigma_T^-}\left[\left(\frac{\sigma_T^-}{2\tau_T}\right)^2 - 1\right] + \frac{\sigma_{33}^2}{(2\tau_T)^2} + \frac{1}{(\tau_T)^2}\left[\sigma_{23}^2+\sigma_{13}^2\right] = 1$$

where:

σ_A^+ = axial tensile strength

σ_A^- = axial compressive strength

σ_T^+ = transverse tensile strength

σ_T^- = transverse compressive strength

τ_A = axial shear strength

τ_T = transverse shear strength

Table 2. T300/5208 Properties

E_A	=	153 GPa
E_T	=	10.9 GPa
G_A	=	5.6 GPa
ν_{AT}	=	0.30
ρ	=	1.55 g/cc
V_F	=	0.70
σ_A^+	=	689.5 MPa
σ_A^-	=	758.5 MPa
σ_T^+	=	27.6 MPa
σ_T^-	=	96.5 MPa
τ_A	=	62.1 MPa
τ_T	=	62.1 MPa

Table 3. Impact Parameters

IMPACT MASS	= 16.45 g
IMPACT VELOCITY	= 9.4 m/s

Table 4. Comparison Groupings of Predicted Damage

Figures 14 - 22	Predicted damage in solution with mass lumped at one node
Figures 23 - 30	Predicted damage in solution with mass distributed over five nodes
Figures 31 - 37	Predicted damage in solution with modified finite element model (four central elements removed)

ONE NODE IMPACT

Figures	Comparison
14, 16 - 20	Figures show the extent of elements with predicted ply damage as a function of time
14, 15	A comparison of the prediction of elements with ply damage vs. elements with interlaminar damage at $T = 1.25 \times 10^{-5}$ sec
16, 17	A comparison of the number of elements with predicted top ply damage vs. the number of elements with ply damage anywhere through the laminate thickness at $T = 2.5 \times 10^{-5}$ sec
20 - 22	A description of the extent of ply damage through the thickness of the laminate

FIVE NODE IMPACT

Figures	Comparison
23, 25 - 27	Figures show the extent of elements with predicted ply damage as a function of time
23, 24	A comparison of the prediction of elements with ply damage vs. elements with interlaminar damage at $T = 1.25 \times 10^{-5}$ sec
27 - 30	Figures depict the extent of damage in the laminate including ply damage, fiber damage and interlaminar damage

Table 4 (continued). Comparison Groupings of Predicted Damage

MODIFIED FINITE ELEMENT MODEL

Figures	Comparison
31, 33, 34 - 37	Figures show the extent of elements with predicted ply damage as a function of time
36, 37	A comparison of elements with predicted ply damage vs. elements with interlaminar damage at $T = 1.25 \times 10^{-5}$ sec

COMPARISONS BETWEEN ANALYSES

Figures	Comparison
15, 24, 32	A comparison of the number of elements which have sustained interlaminar damage in each of the three solutions
19, 27, 35	A comparison of the number of elements which have sustained ply damage at $T = 5.0 \times 10^{-5}$ sec in each of the three solutions
20, 27, 37	A comparison of the number of elements with predicted ply damage at the end of each solution
20, 28	A comparison of the number of elements which have sustained fiber damage in the solution with one impacted node vs. the solution with five impacted nodes

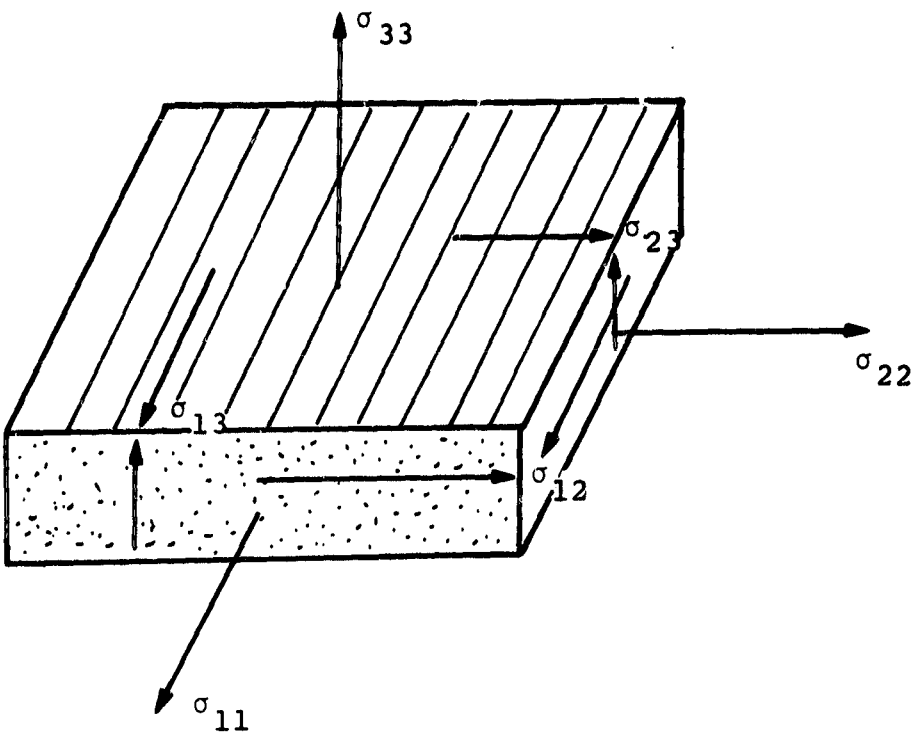

Figure 1. Unidirectional Ply Stress Components

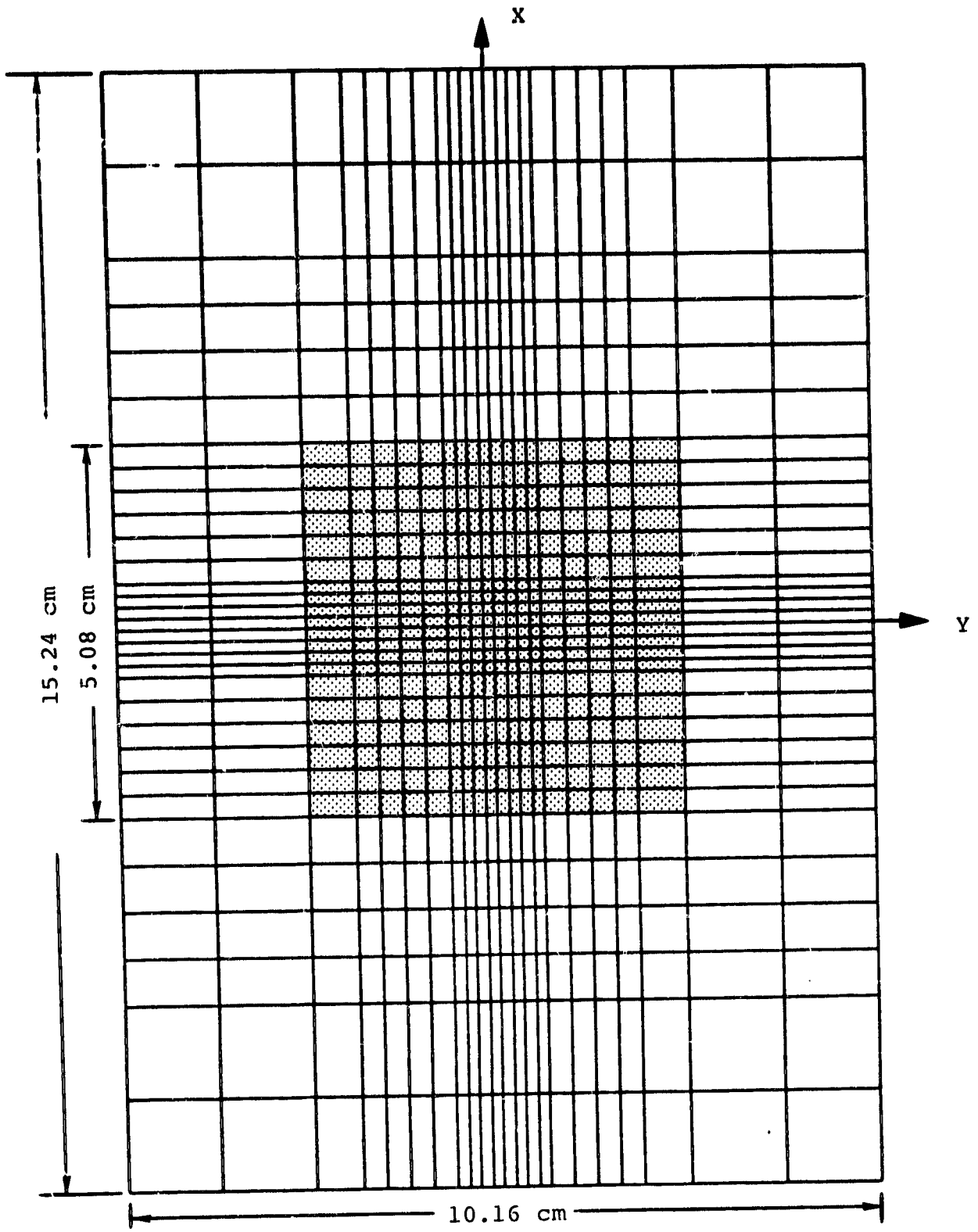

Figure 2. Finite Element Model

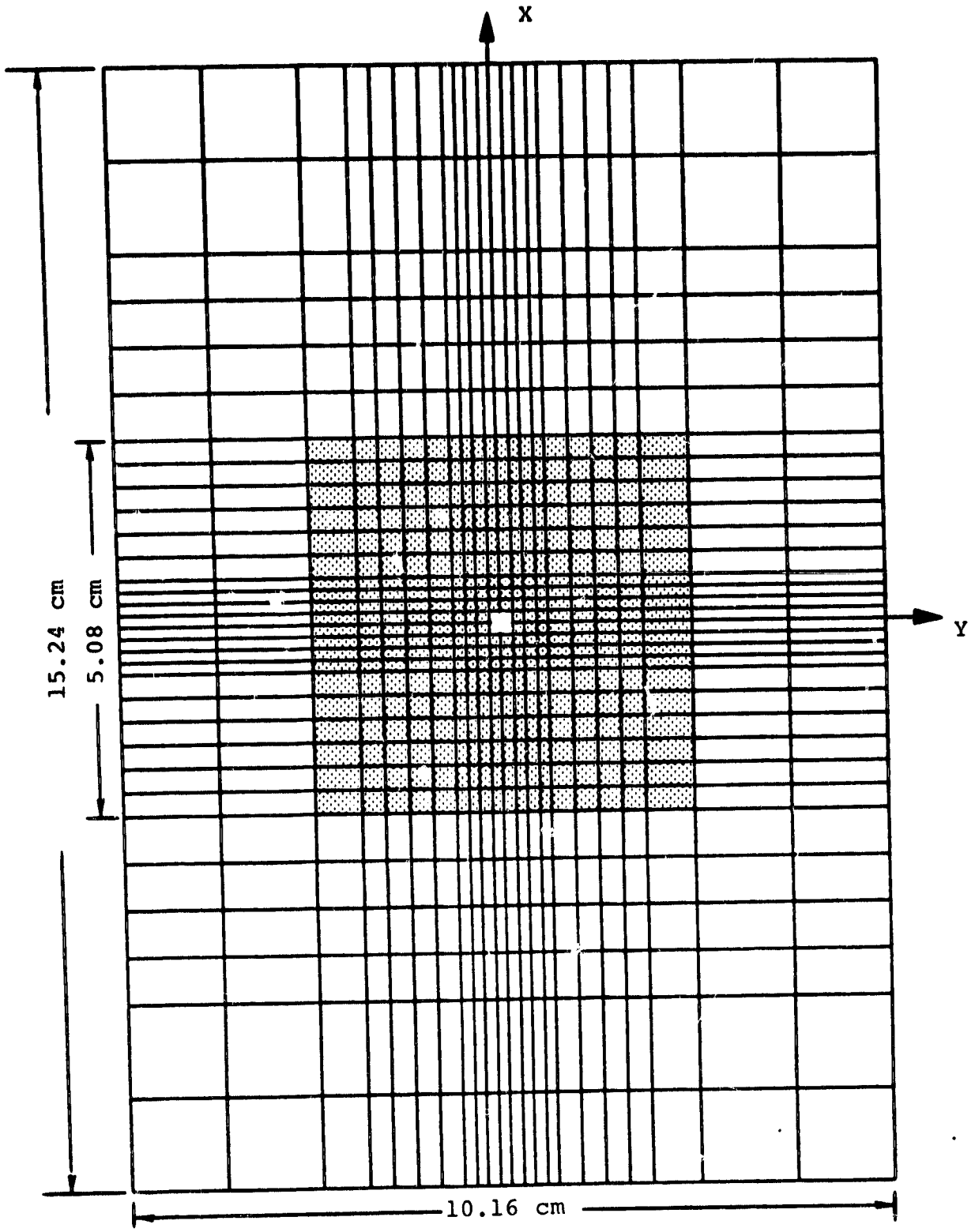

Figure 3. Modified Finite Element Model

a) 1 Node

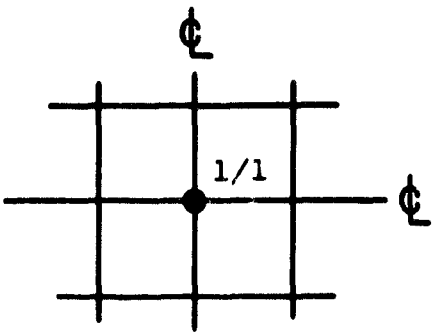

b) 5 Nodes

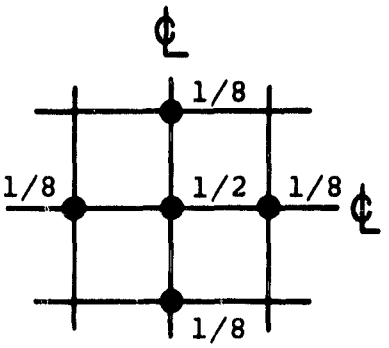

c) Modified

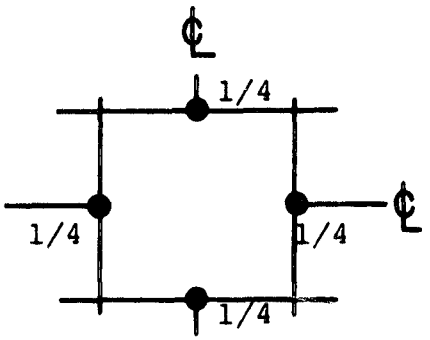

Figure 4. Impactor Mass Distributions

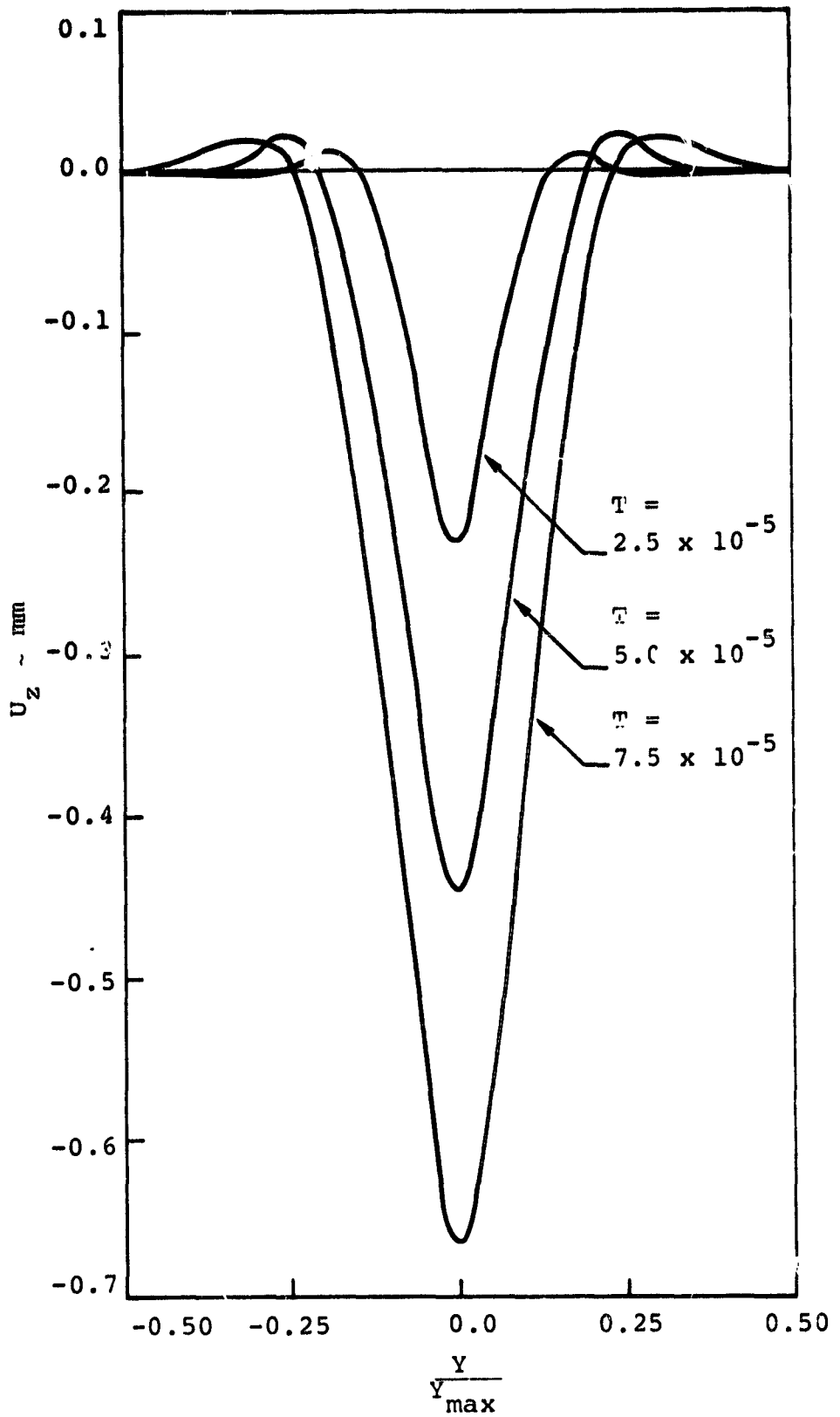

Figure 5. Displacement Response Through the Plate Center Along the Shorter Axis, Displacement Solution.

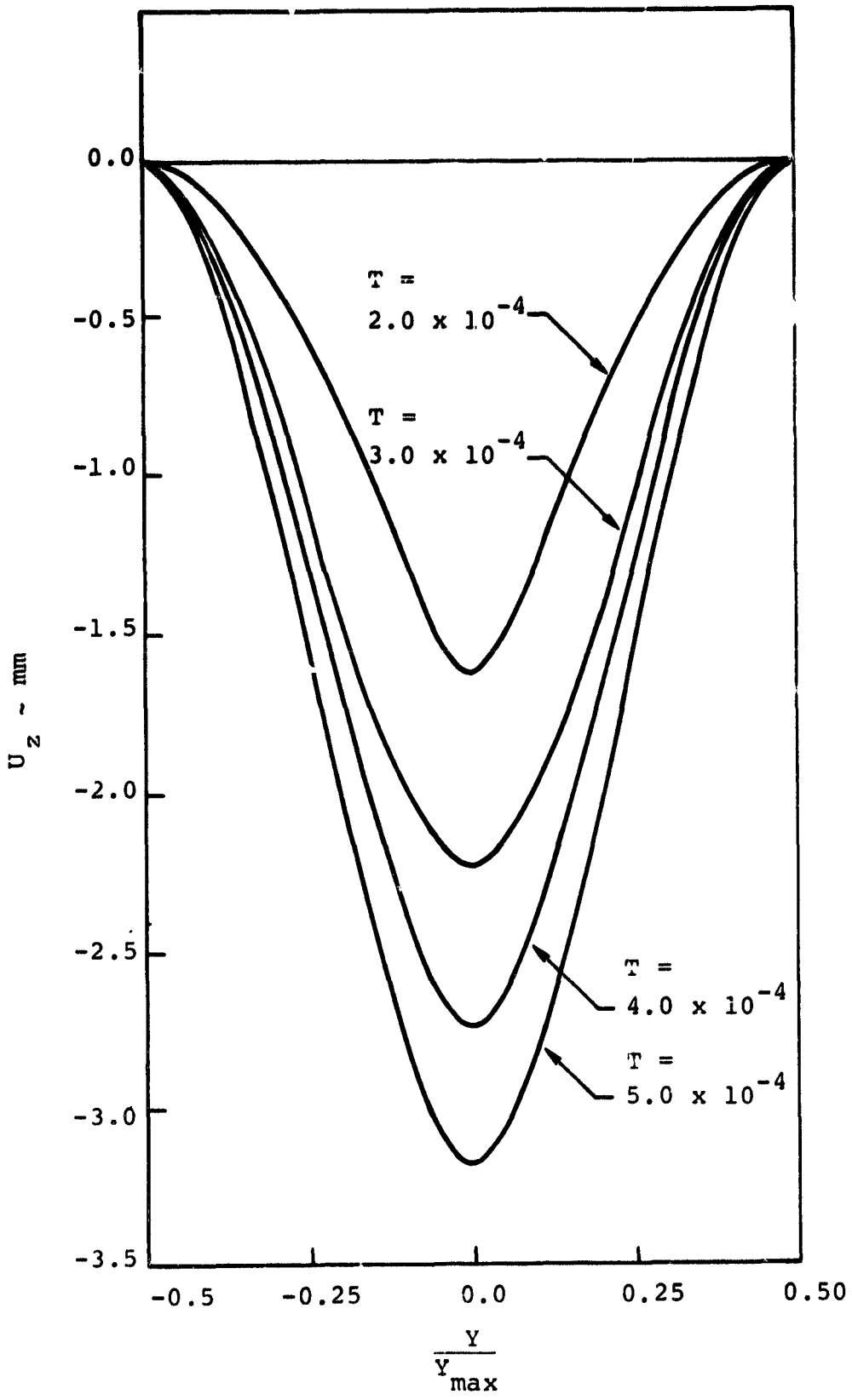

Figure 6. Displacement Response Through the Plate Center Along the Shorter Axis, Displacement Solution.

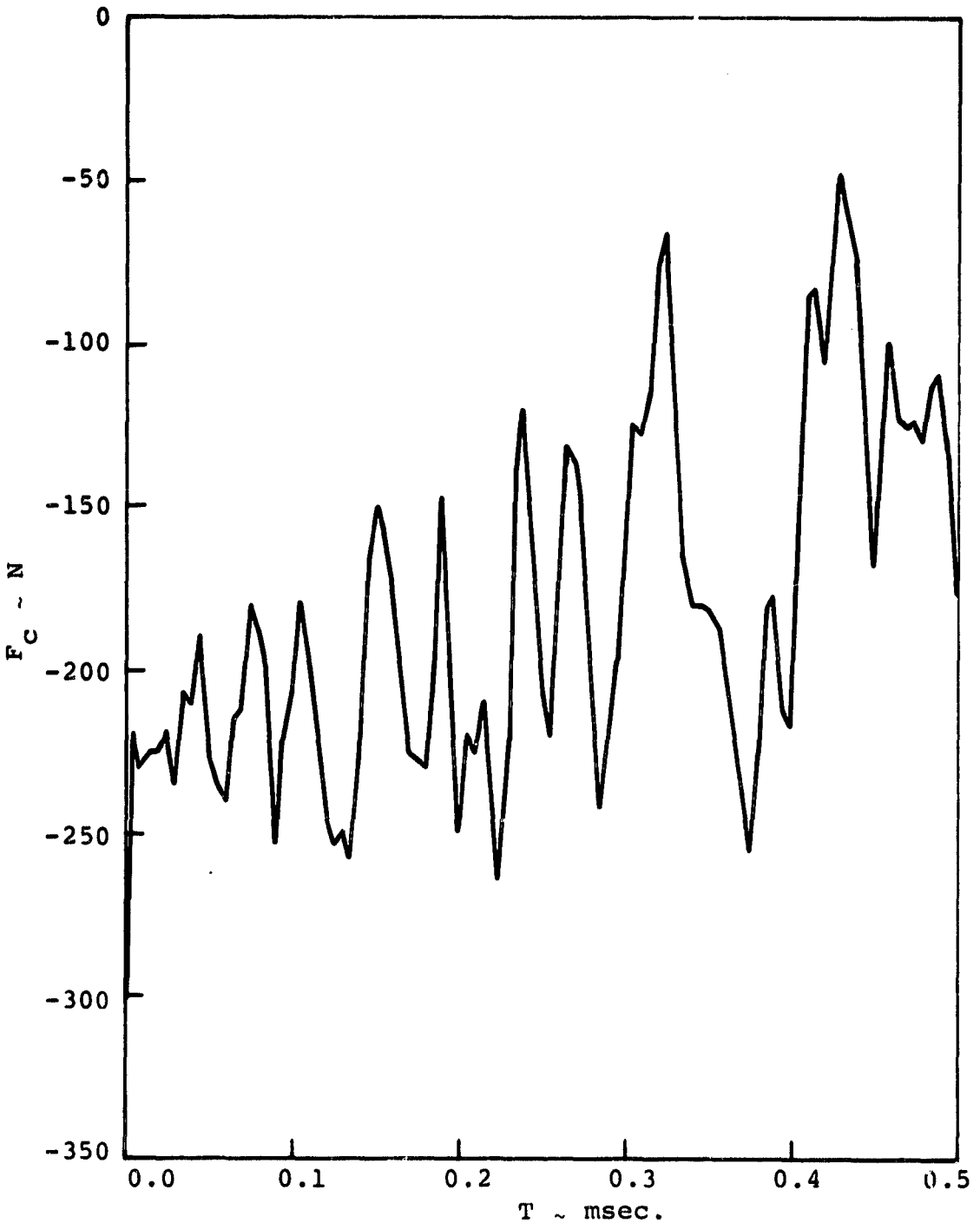

Figure 7. Contact Force, Displacement Solution

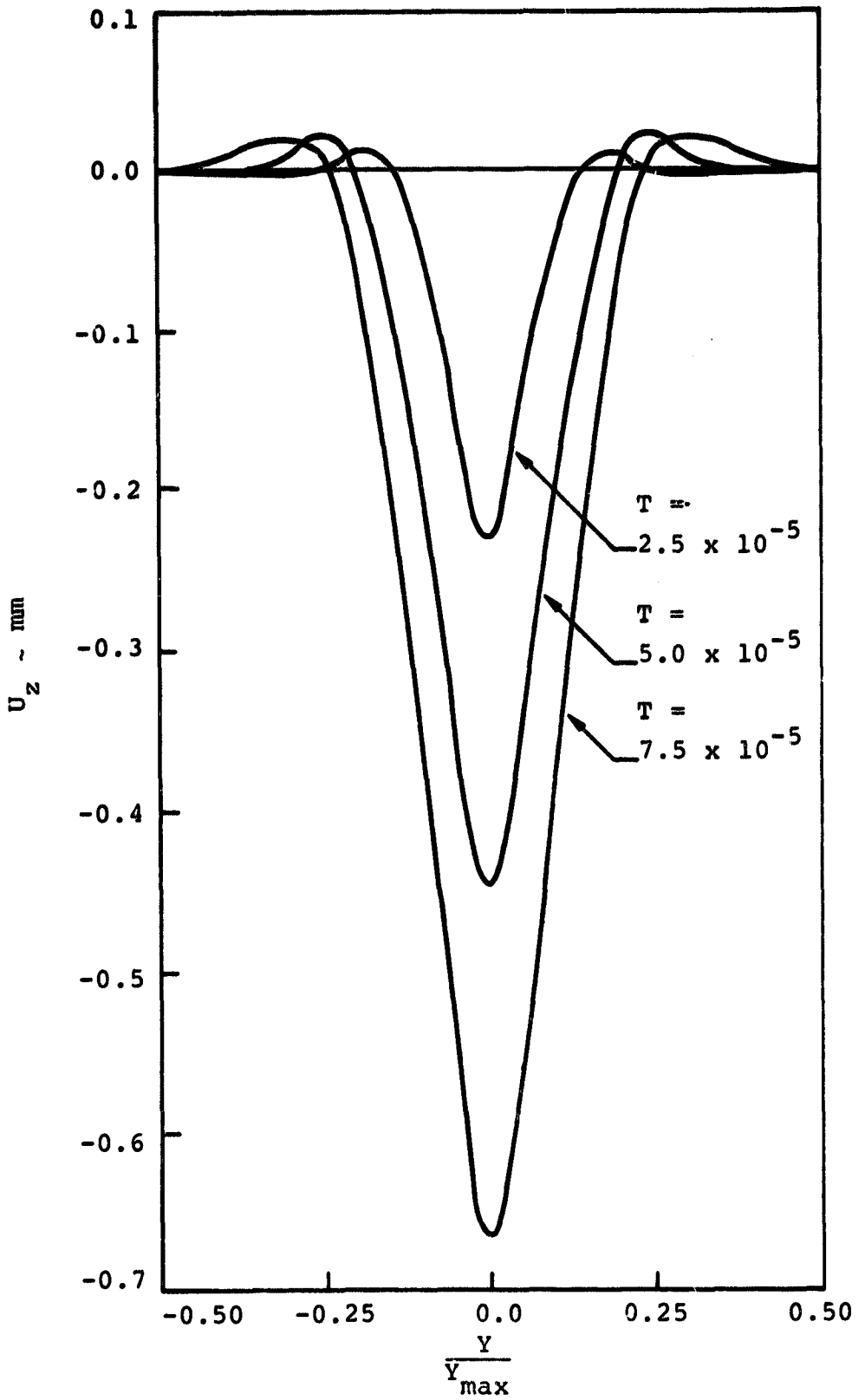

Figure 8. Displacement Response Through the Plate Center Along the Shorter Axis, Stress Solution, Mass Lumped at One Node.

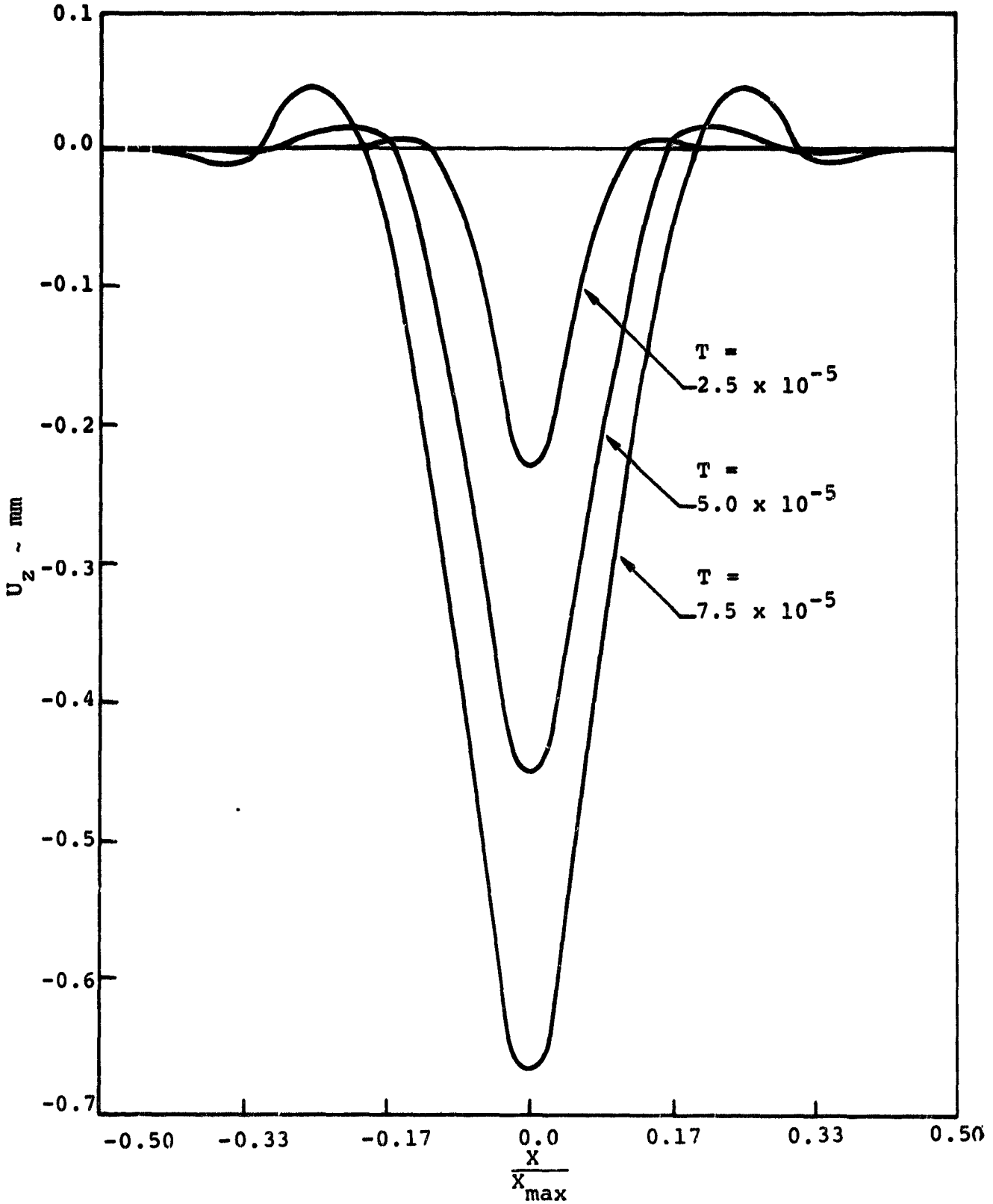

Figure 9. Displacement Response Through the Plate Center Along the Longer Axis, Stress Solution, Mass Lumped at One Node.

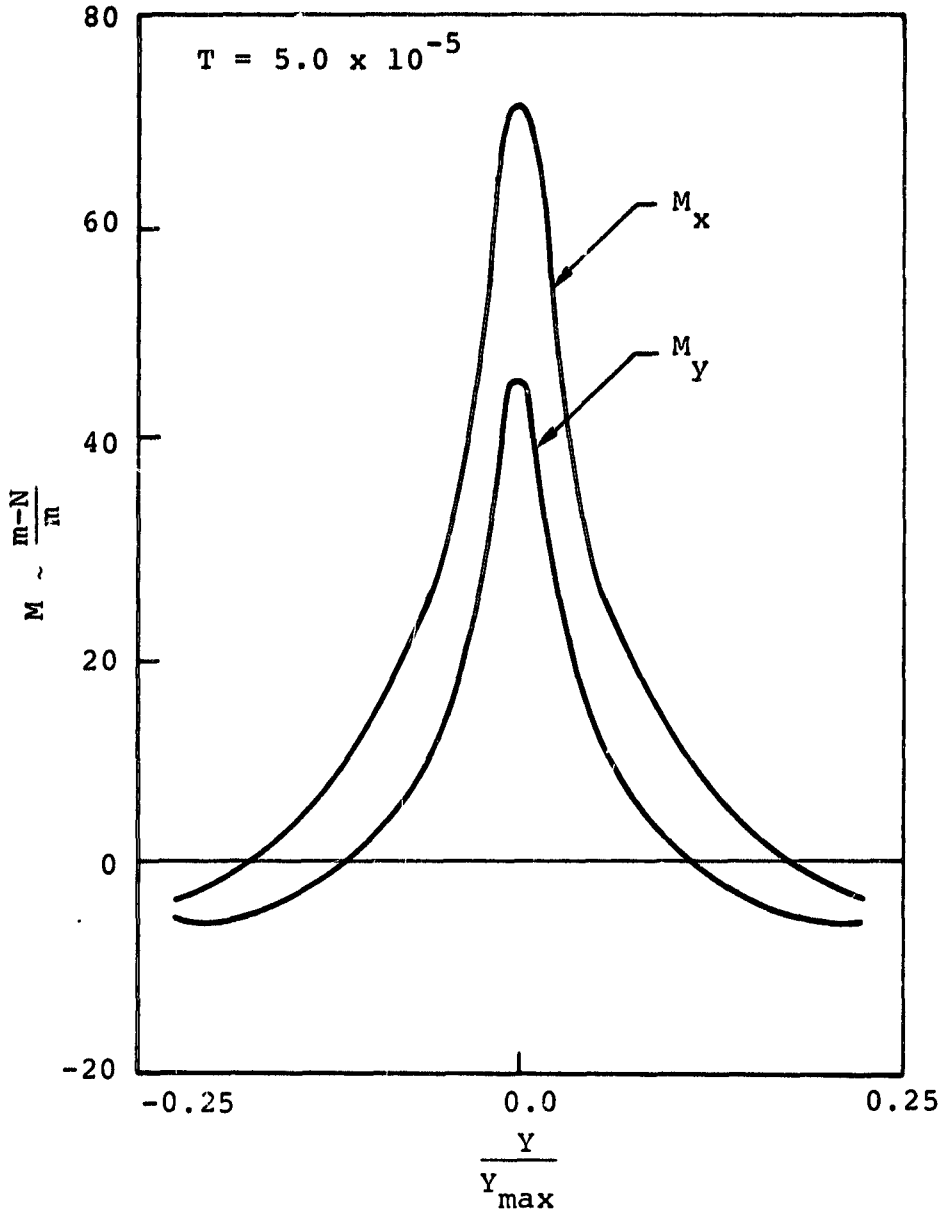

Figure 10. Moment Resultants Through the Plate Center Along the Shorter Axis, Stress Solution, Mass Lumped at One Node.

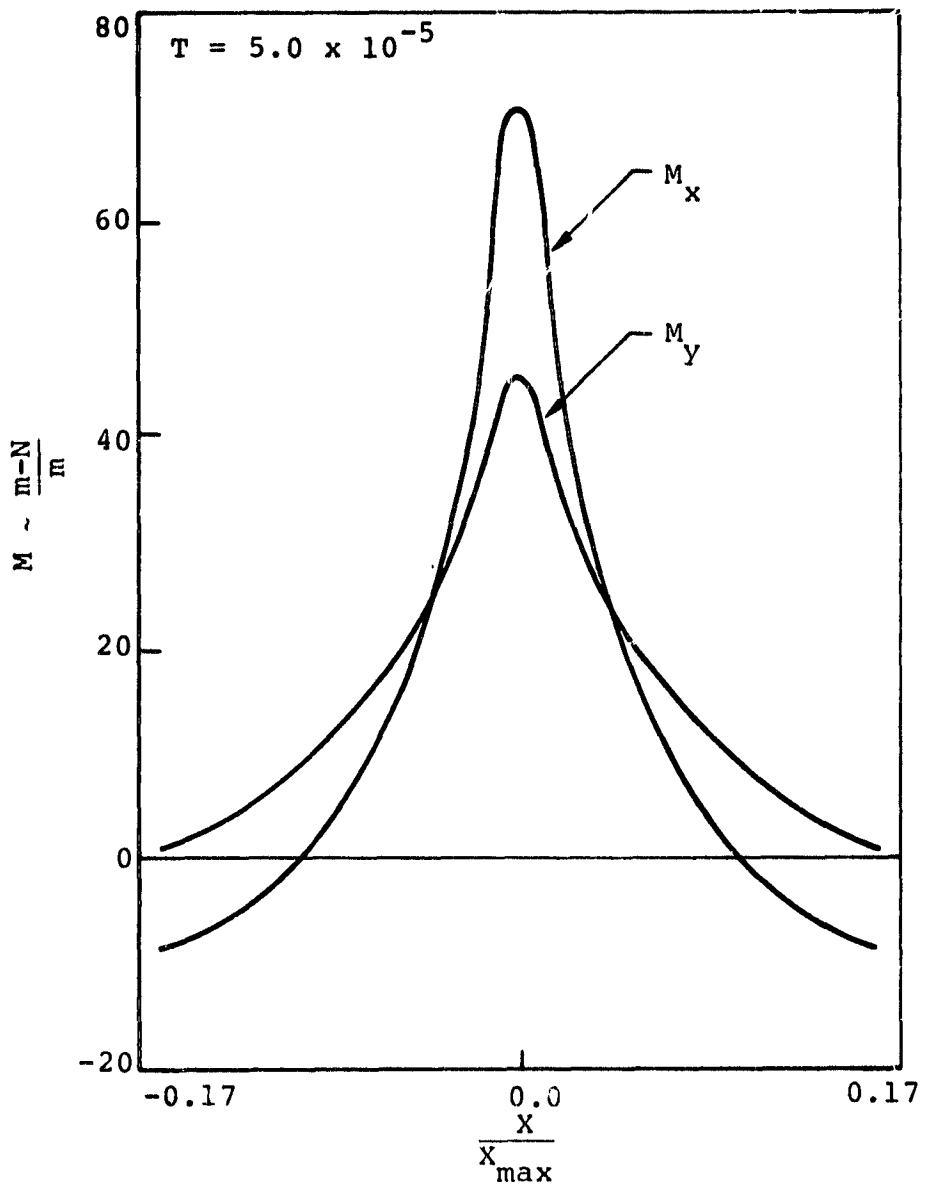

Figure 11. Moment Resultants Through the Plate Center Along the Longer Axis, Stress Solution, Mass Lumped at One Node.

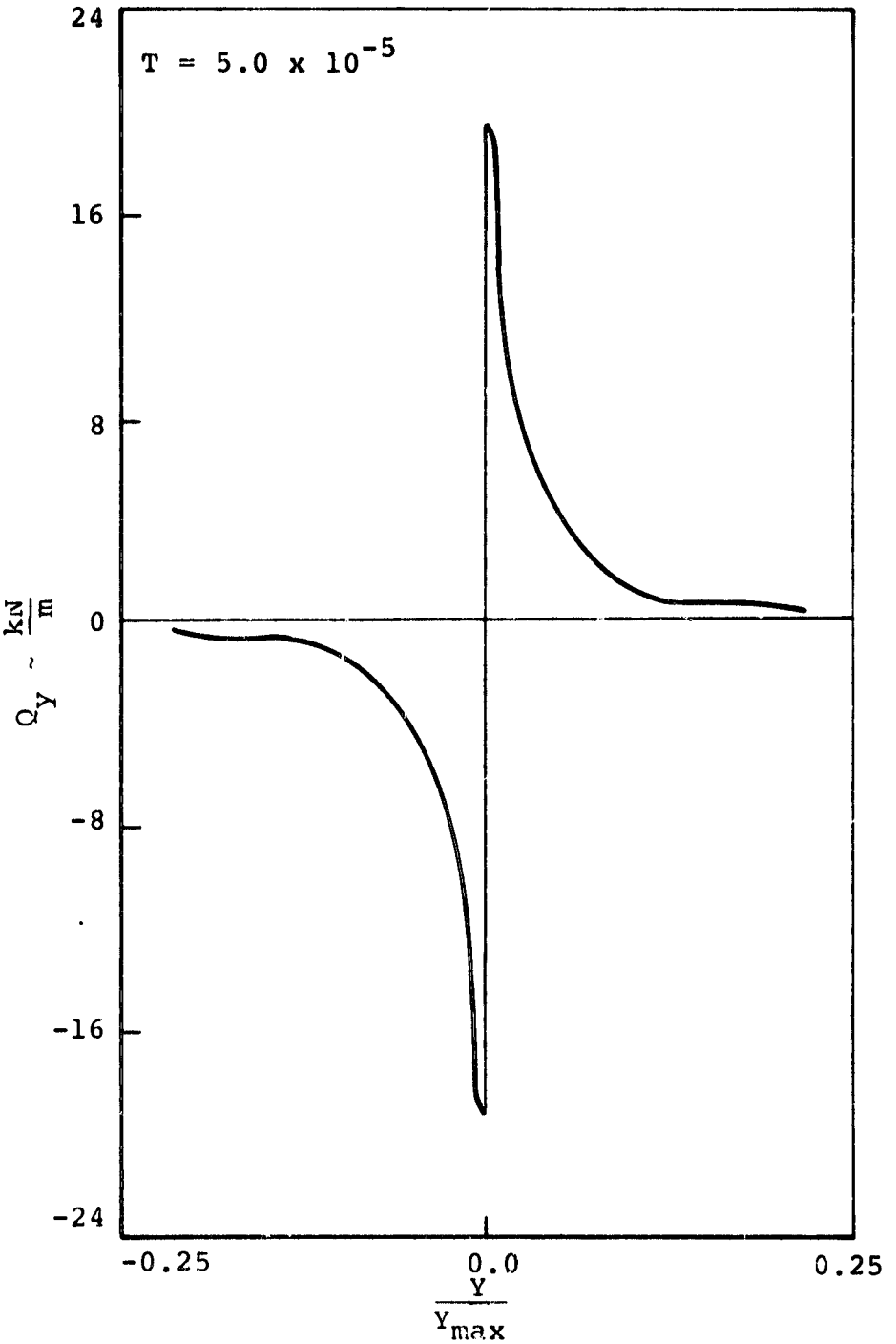

Figure 12. Transverse Shear Resultant, Q_y, Through the Plate Center Along the Shorter Axis, Stress Solution, Mass Lumped at One Node.

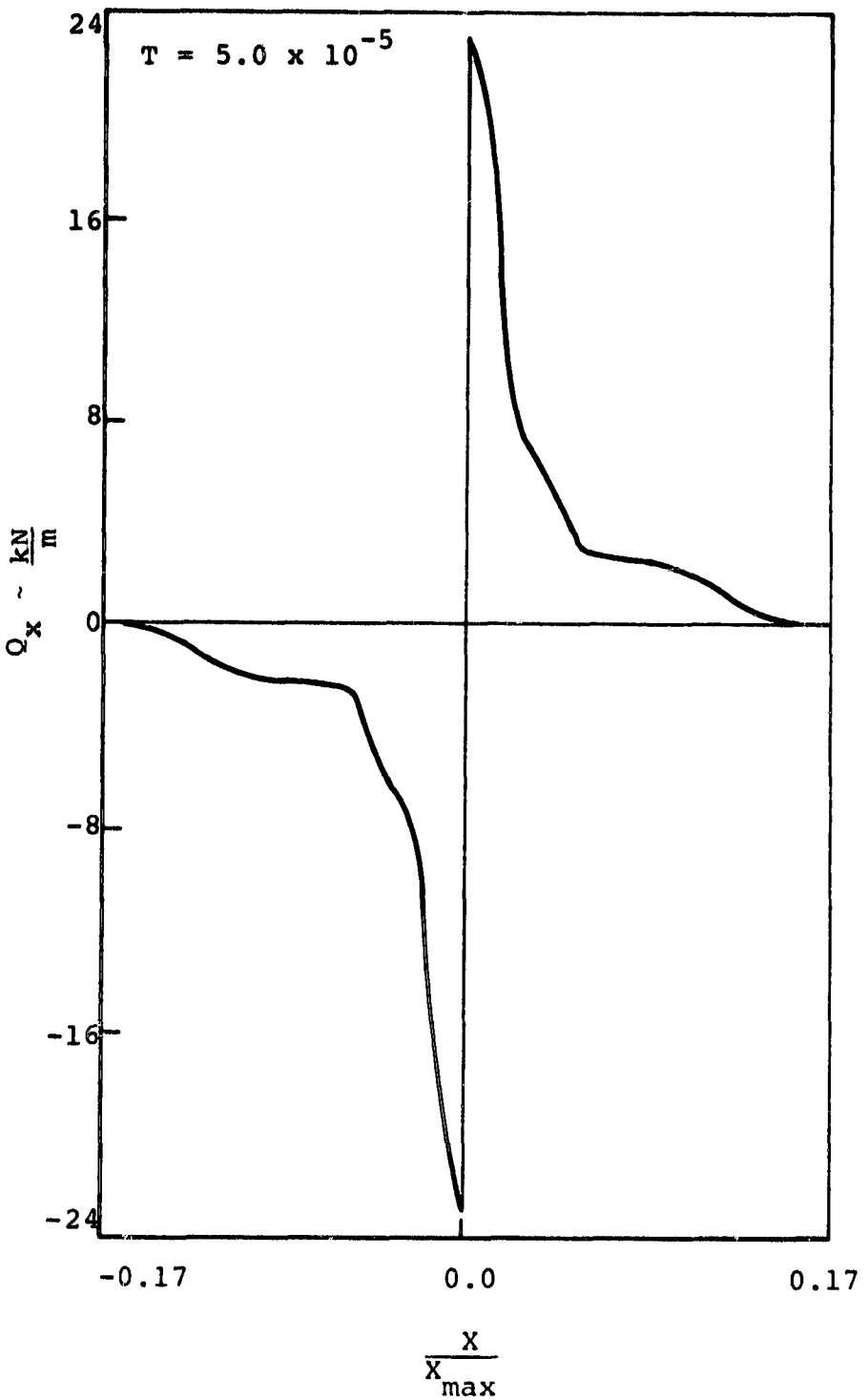

Figure 13. Transverse Shear Resultant, Q_x, Through the Plate Center Along the Longer Axis, Stress Solution, Mass Lumped at One Node

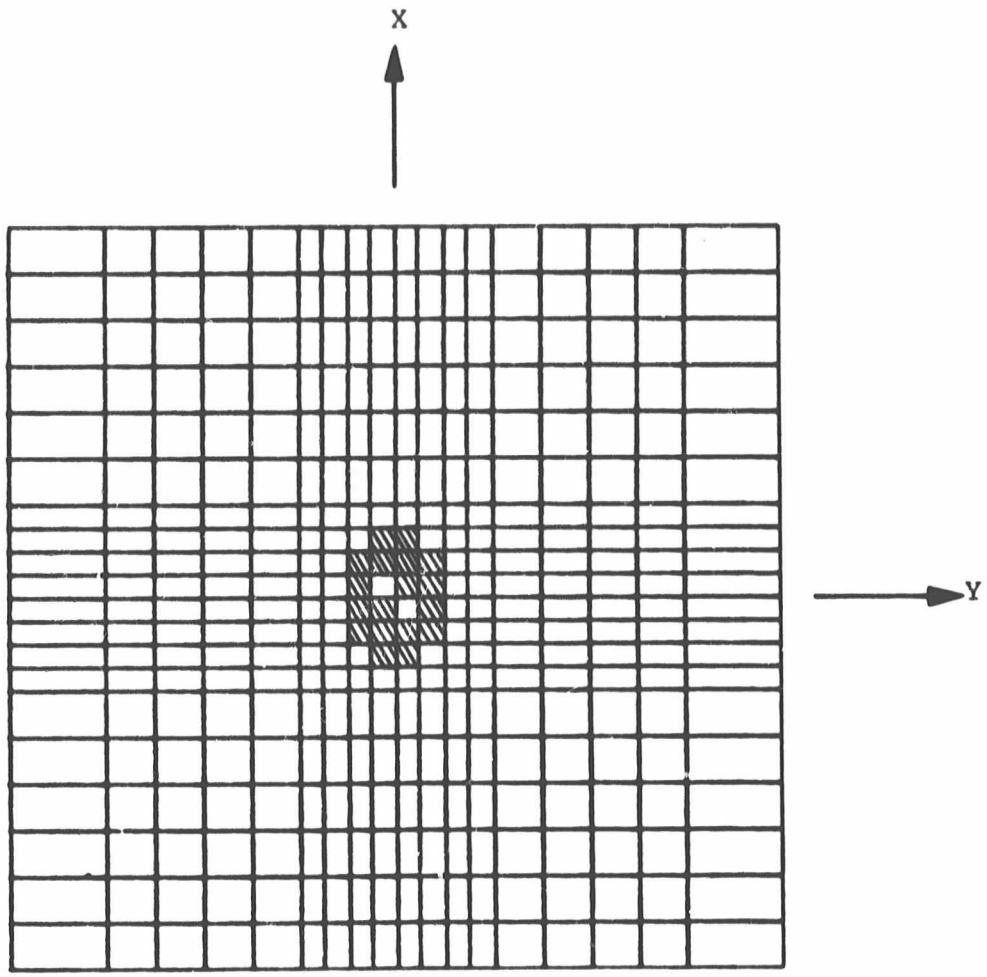

Figure 14. Elements With Ply Damage, T = 1.25×10^{-5} sec., Stress Solution, Mass Lumped at One Node

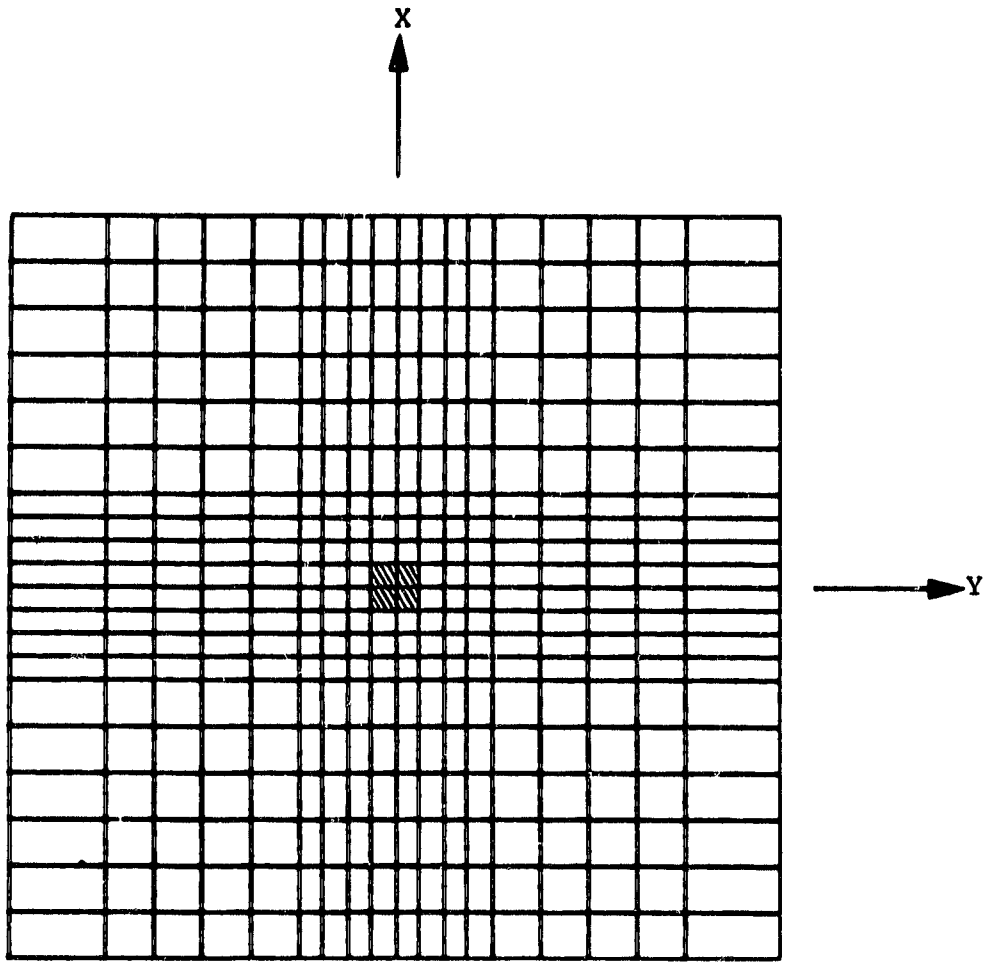

Figure 15. Elements with Interlaminar Damage, T = 1.25×10^{-5} sec., Stress Solution, Mass Lumped at One Node

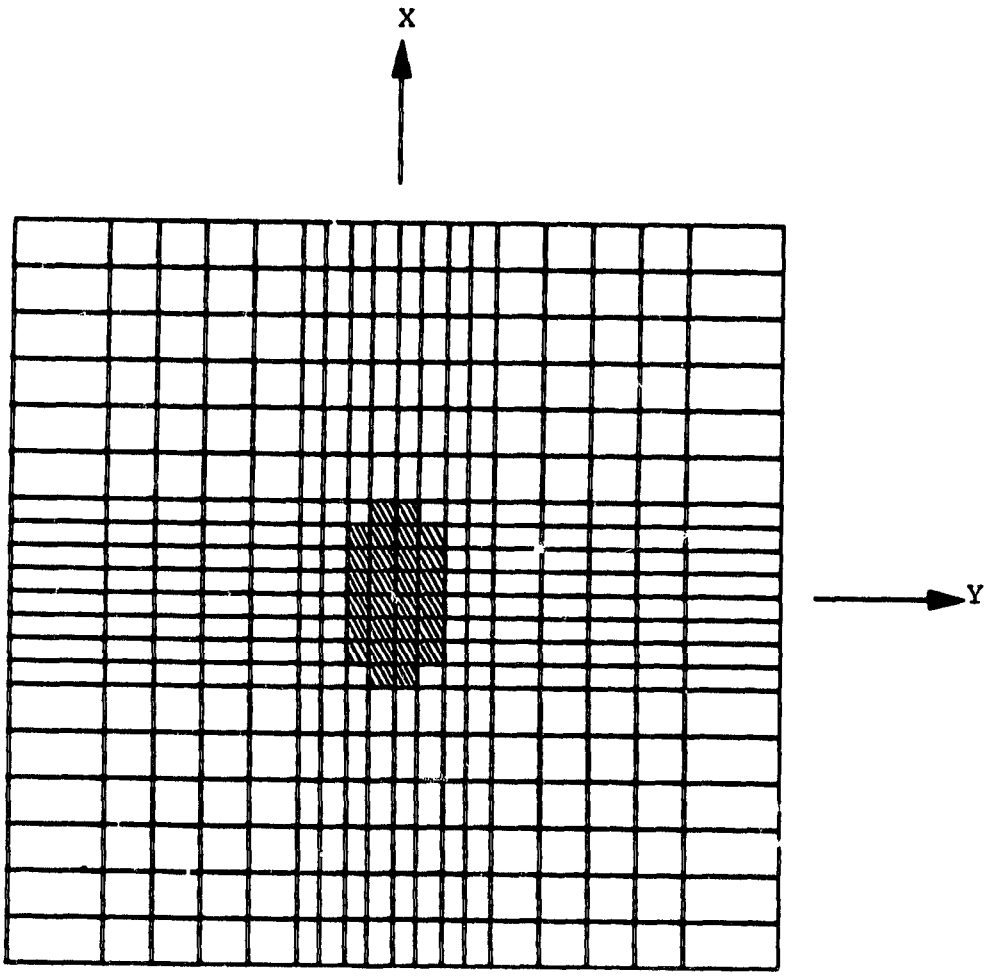

Figure 16. Elements with Ply Damage, T = 2.5×10^{-5} sec., Stress Solution, Mass Lumped at One Node

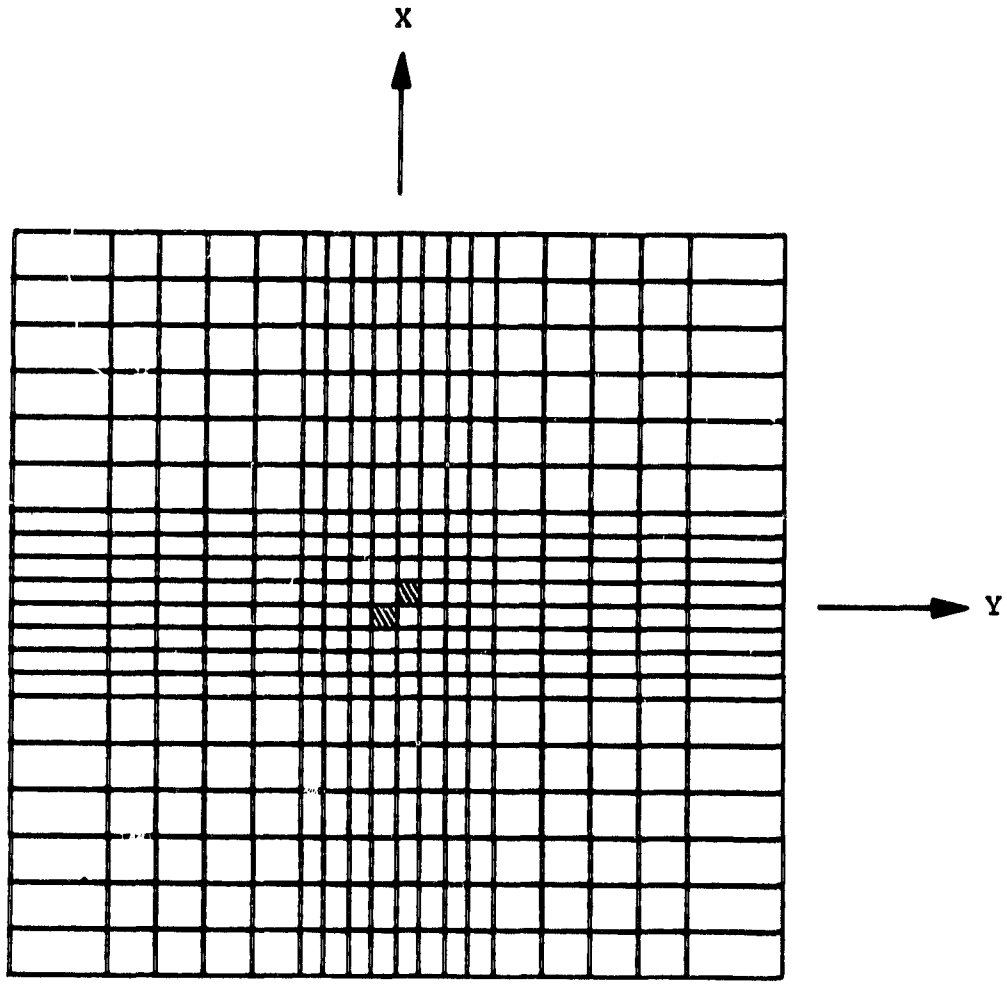

Figure 17. Elements with Top Ply Damage, T = 2.5 x 10^{-5} sec., Stress Solution, Mass Lumped at One Node

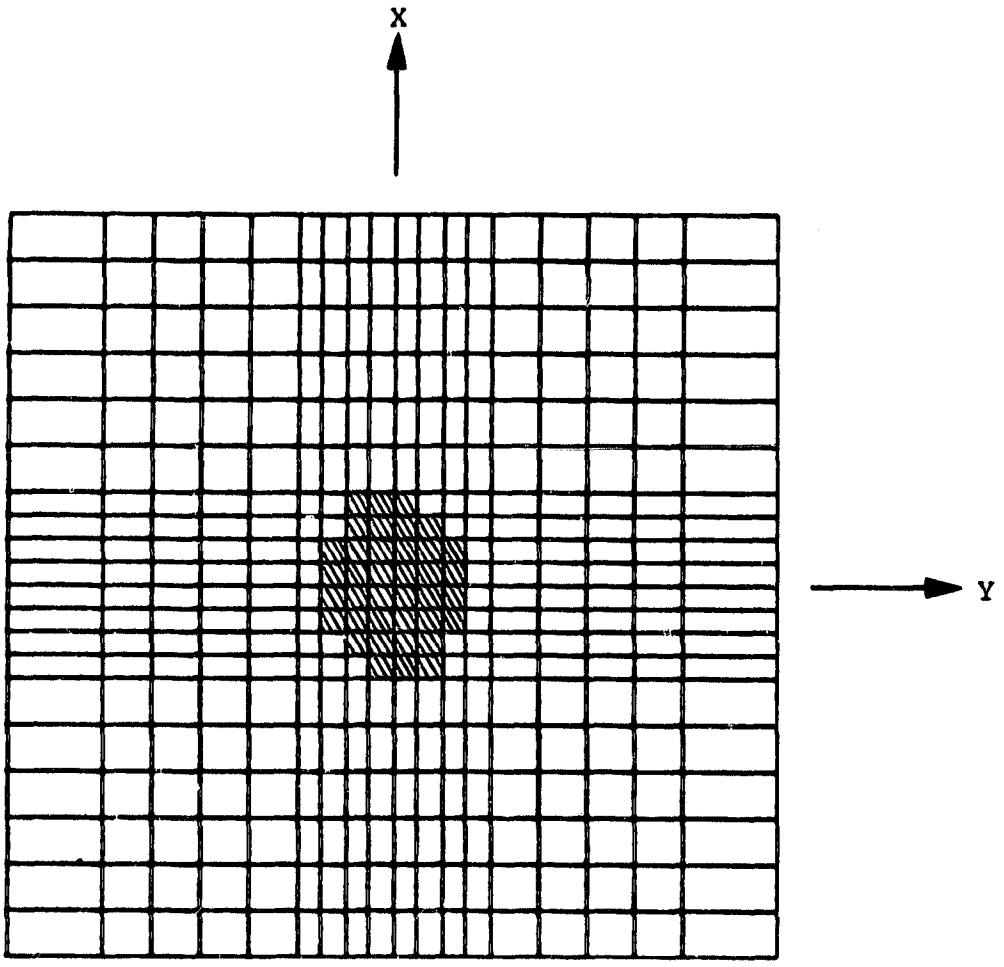

Figure 18. Elements with Ply Damage, T = 3.75×10^{-5} sec., Stress Solution, Mass Lumped at One Node

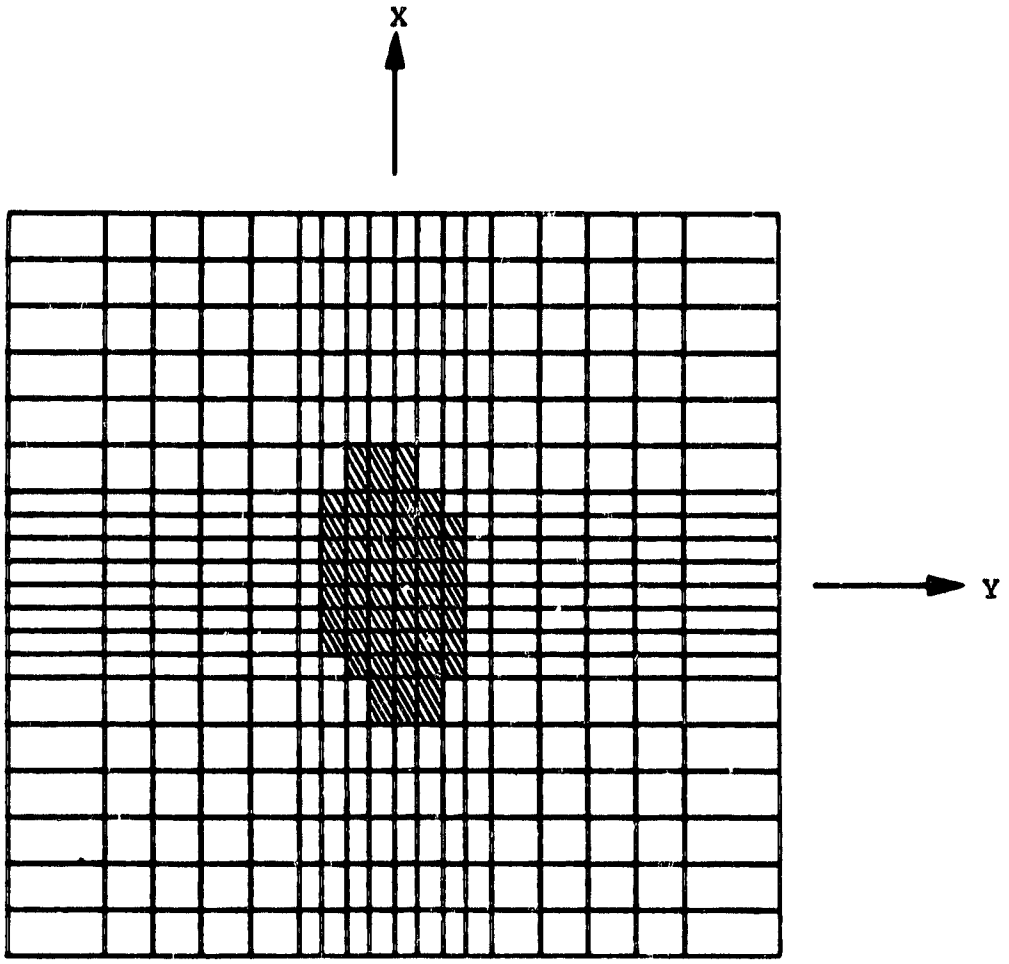

Figure 19. Elements with Ply Damage, T = 5.0 x 10^{-5} sec., Stress Solution, Mass Lumped at One Node

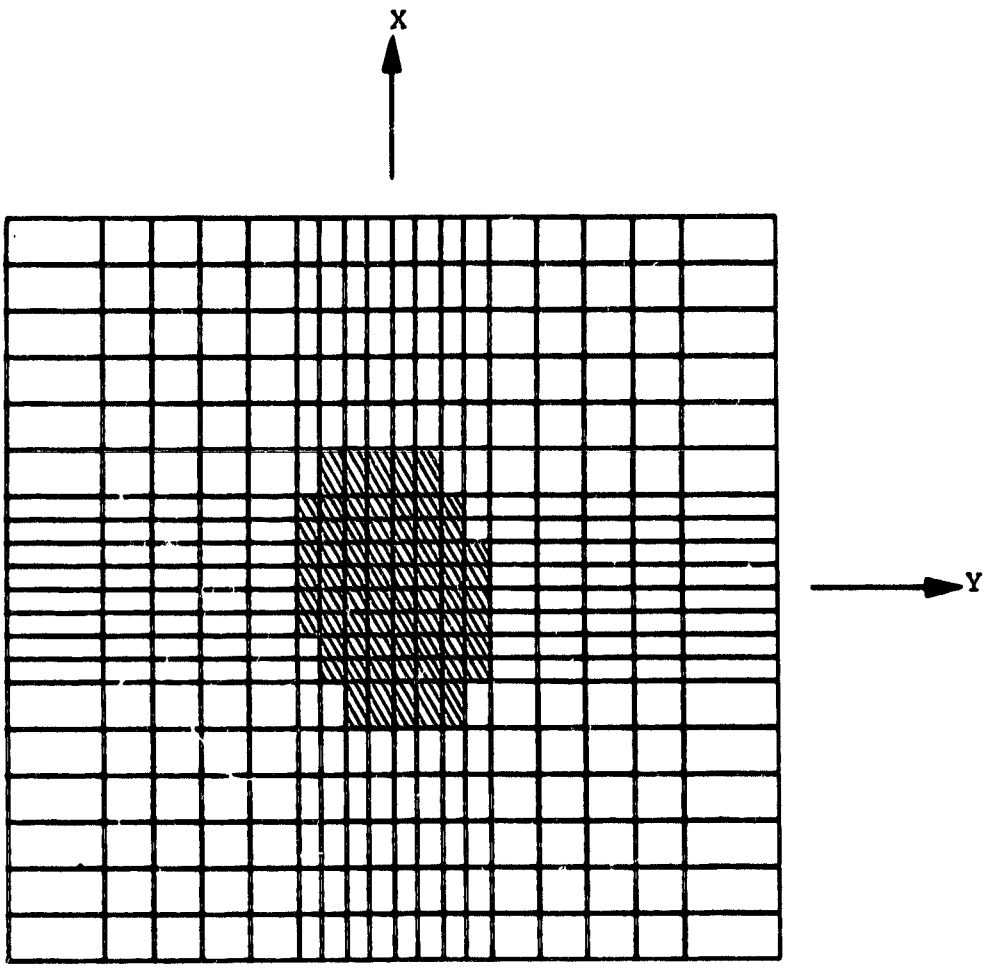

Figure 20. Elements with Ply Damage, T = 7.5 x 10^{-5} sec., Stress Solution, Mass Lumped at One Node

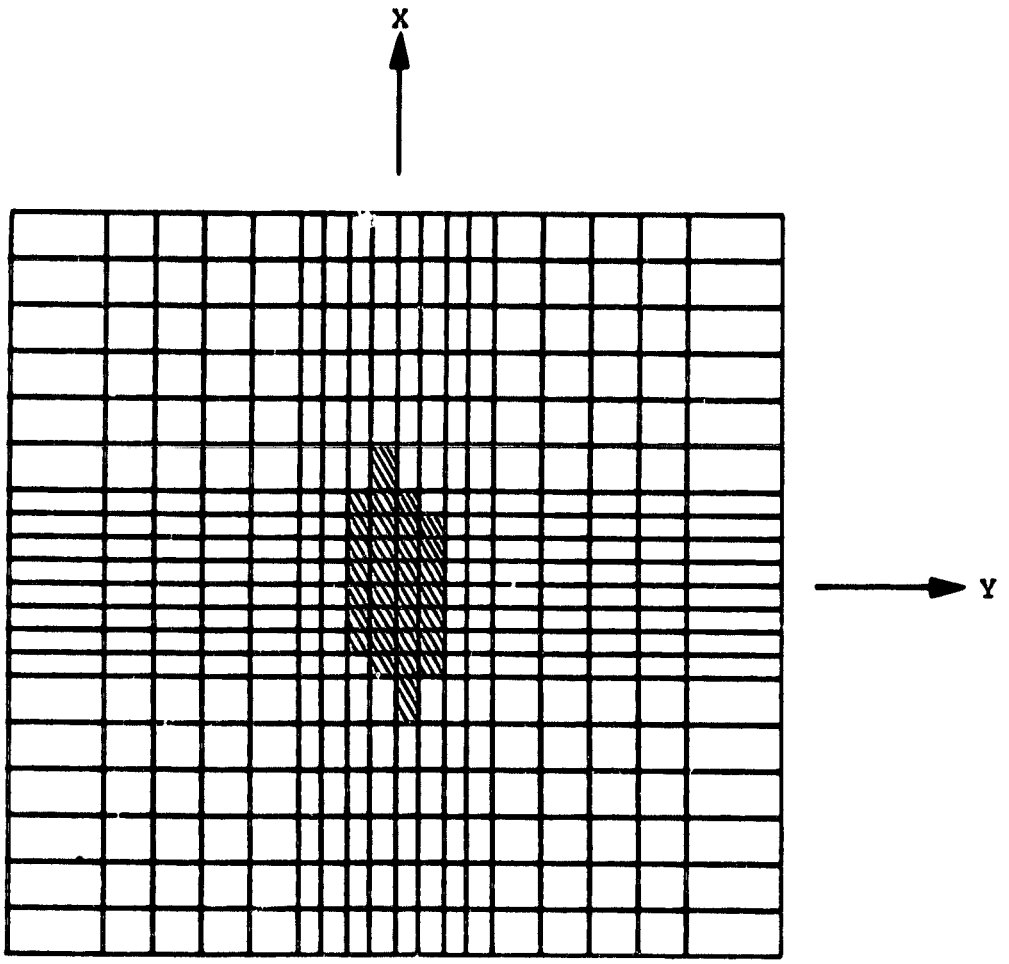

Figure 21. Elements with More Than One Failed Ply, $T = 7.5 \times 10^{-5}$ sec., Stress Solution, Mass Lumped at One Node

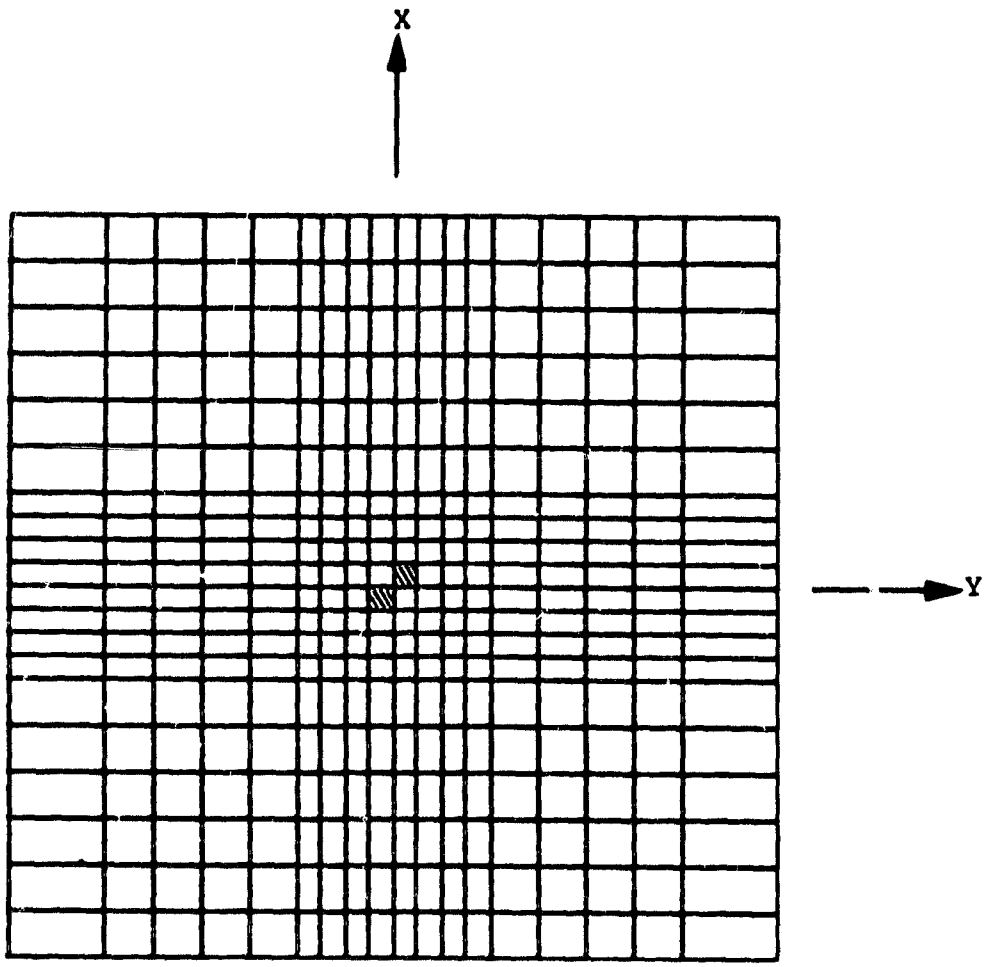

Figure 22. Elements with Fiber Failure, T = 7.5 x 10^{-5} sec., Stress Solution, Mass Lumped at One Node

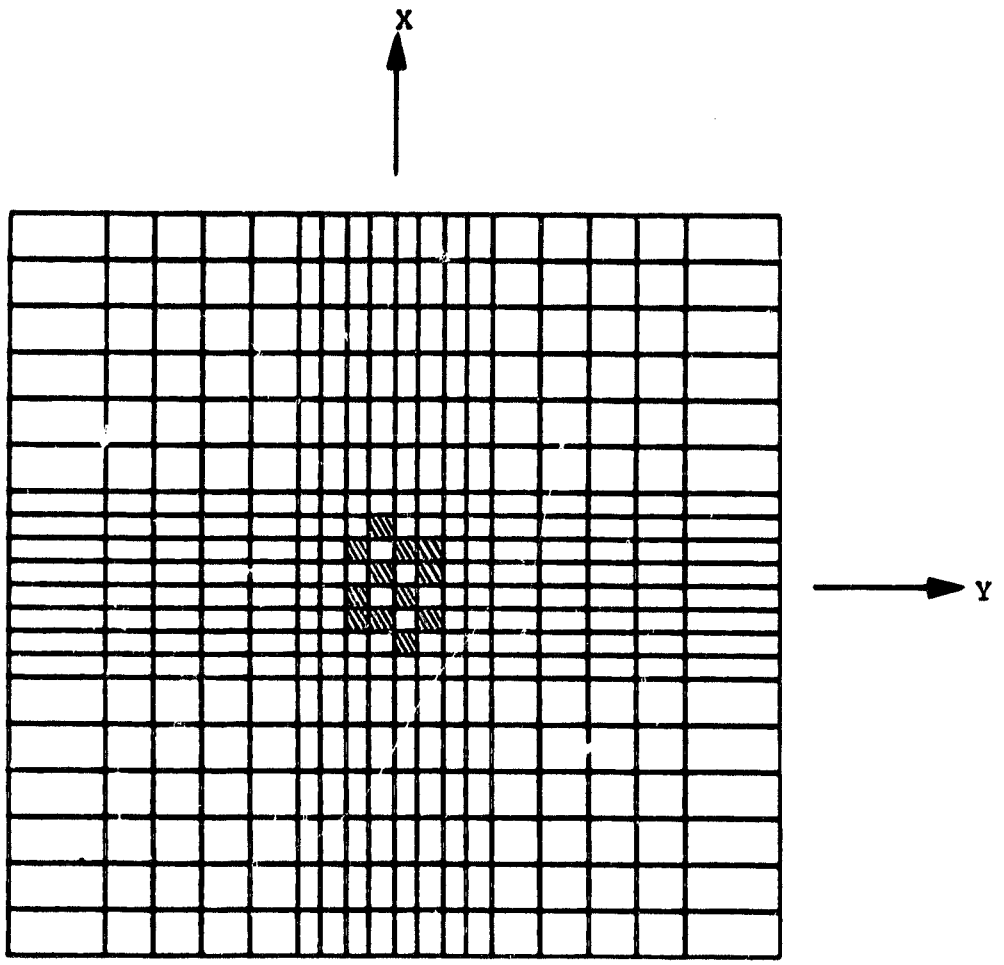

Figure 23. Elements with Ply Damage, T = 1.25×10^{-5} sec., Stress Solution, Mass Distributed at 5 Nodes

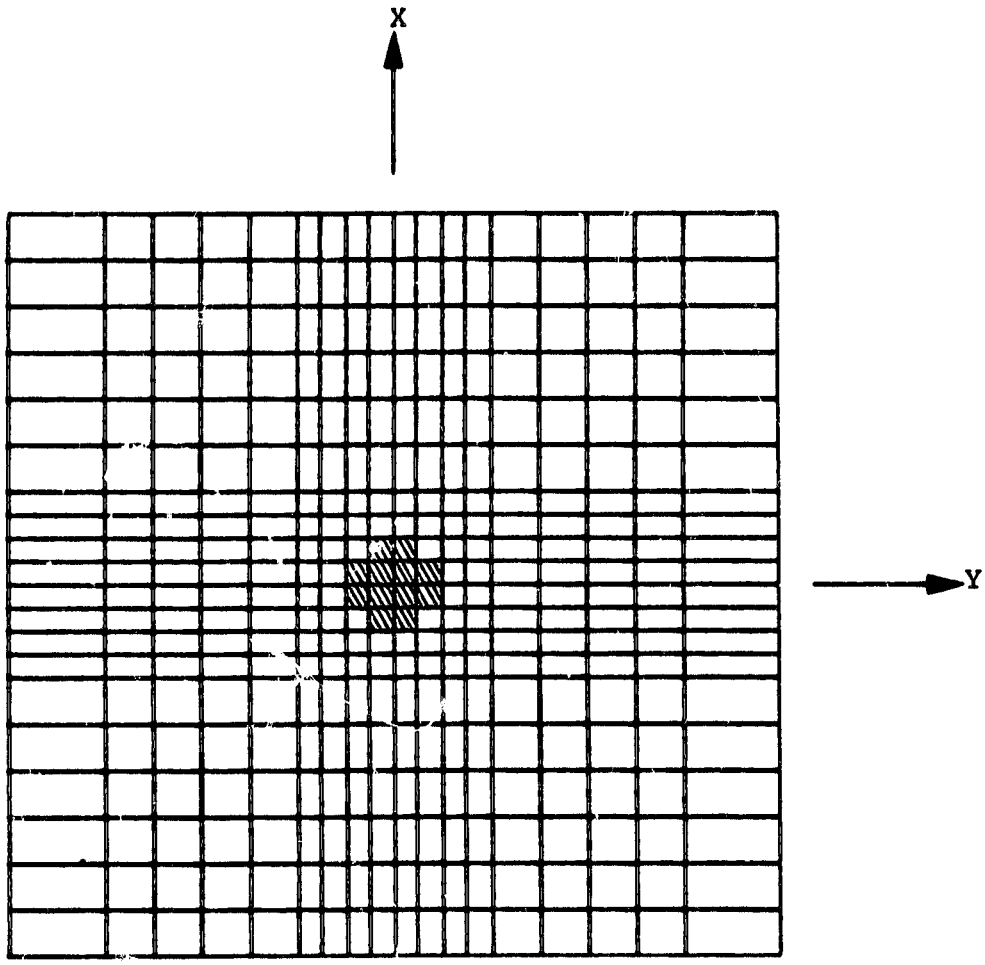

Figure 24. Elements with Interlaminar Damage, T = 1.25×10^{-5} sec., Stress Solution, Mass Distributed at 5 Nodes

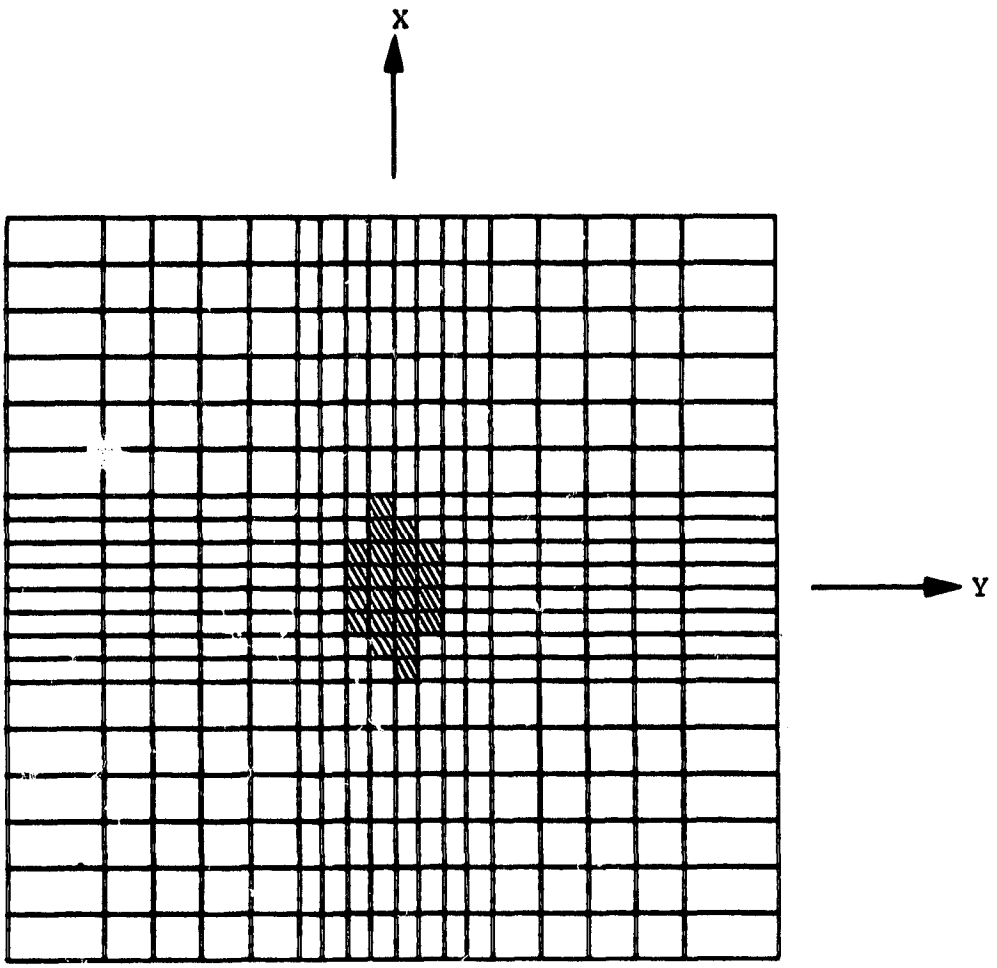

Figure 25. Elements with Ply Damage, T = 2.5 x 10^{-5} sec., Stress Solution, Mass Distributed at 5 Nodes

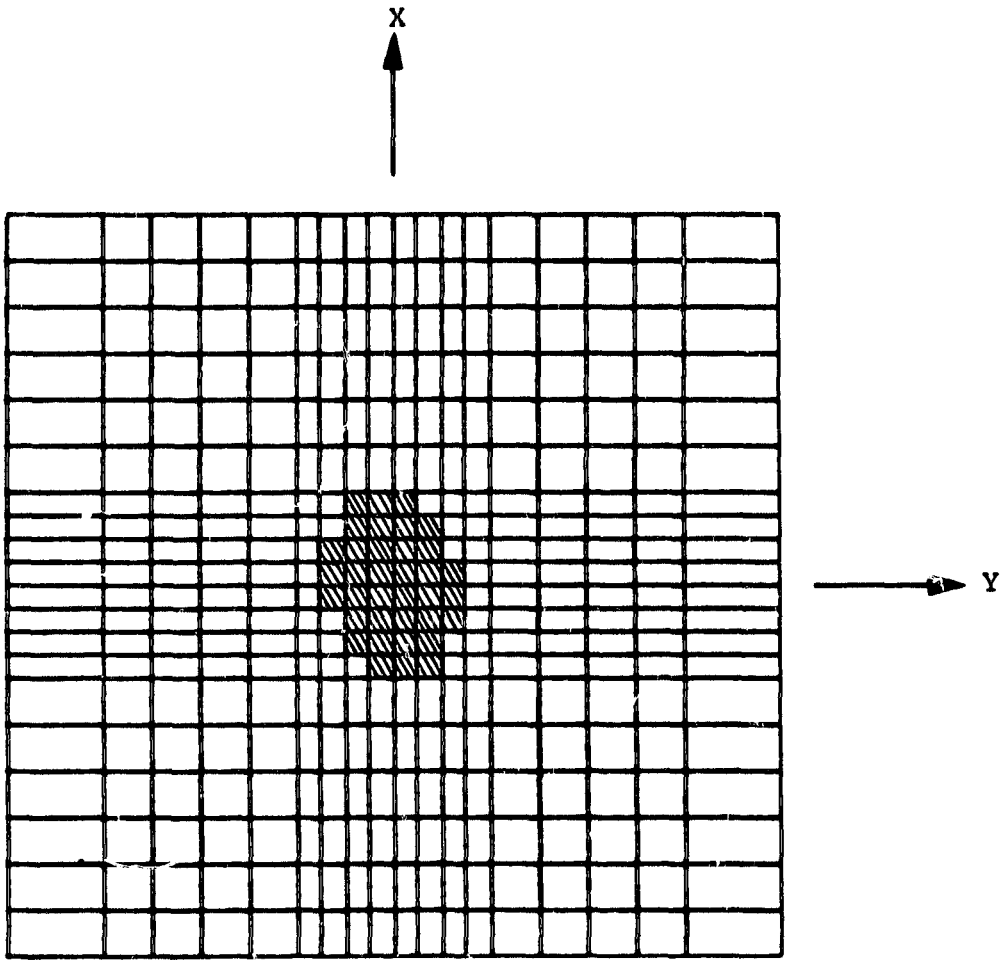

Figure 26. Elements with Ply Damage, T = 3.75 x 10^{-5} sec., Stress Solution, Mass Distributed at 5 Nodes

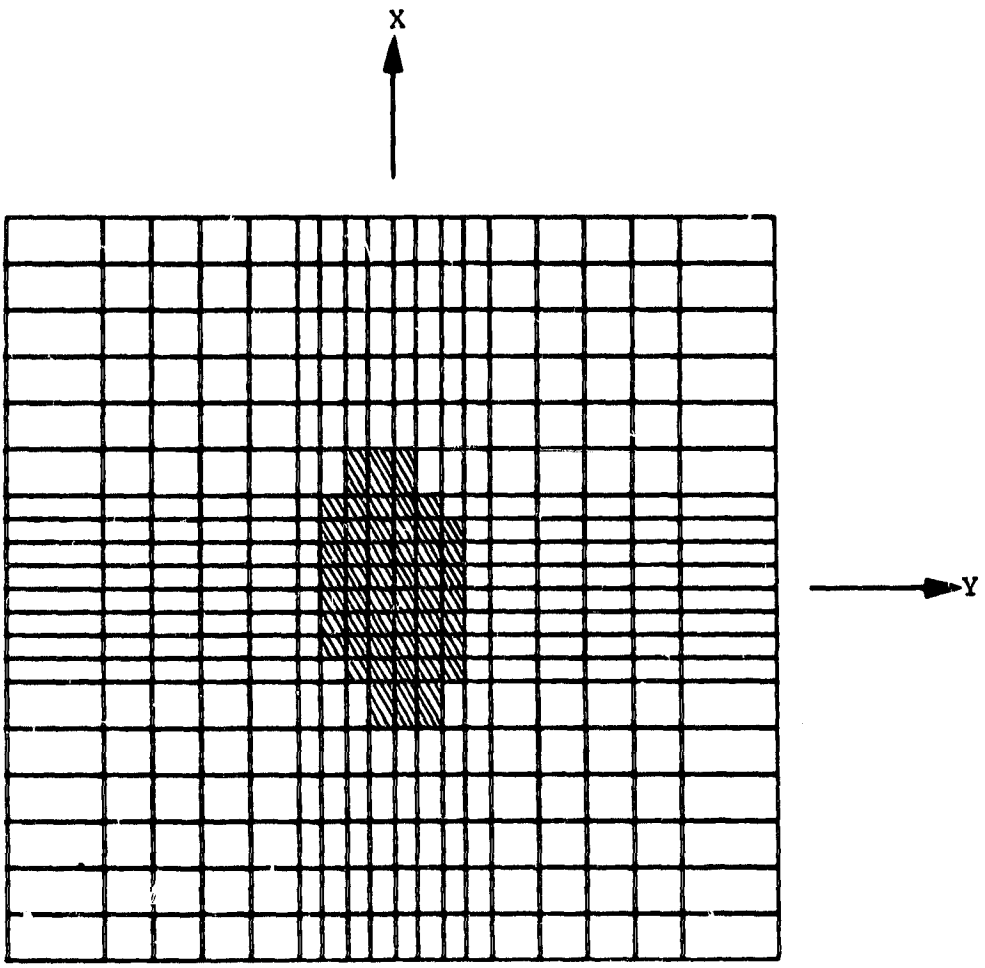

Figure 27. Elements with Ply Damage, T = 5.0 x 10^{-5} sec., Stress Solution, Mass Distributed at 5 Nodes

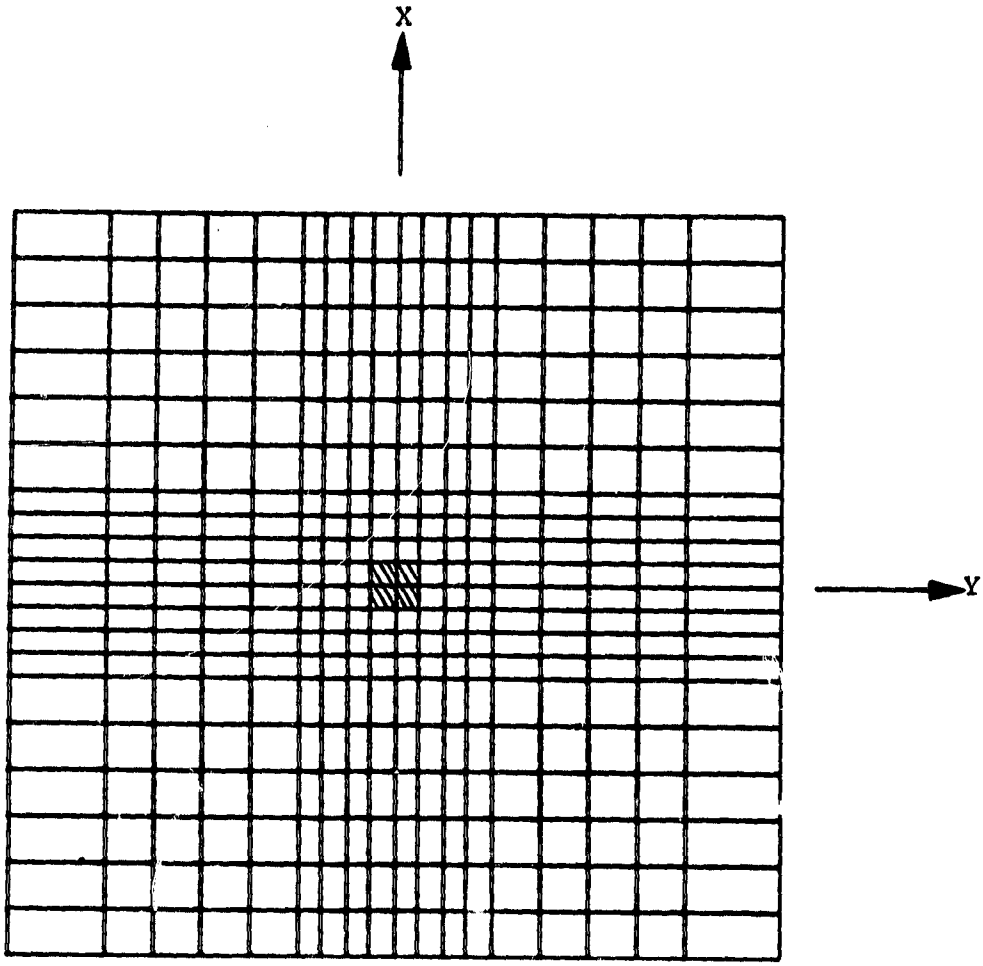

Figure 28. Elements with Fiber Damage, T = 5.0×10^{-5} sec., Stress Solution, Mass Distributed at 5 Nodes

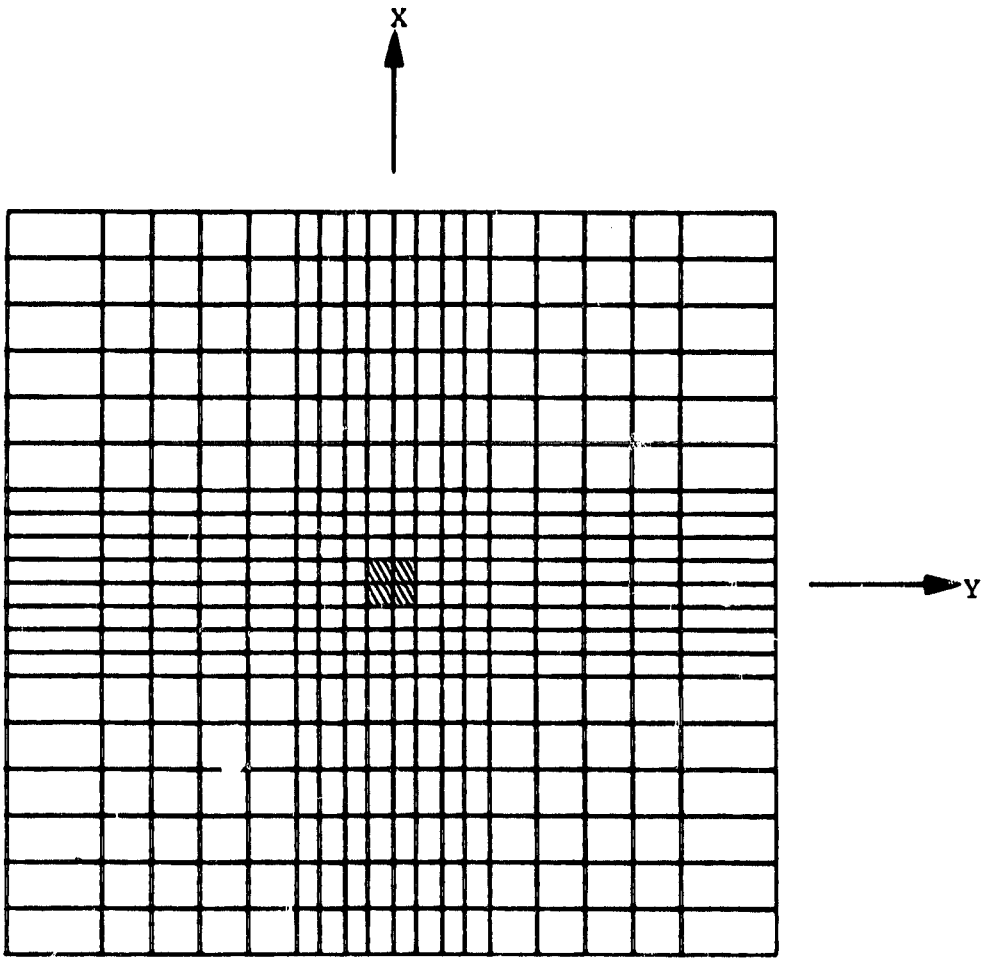

Figure 29. Elements with No Remaining Intact Ply Interfaces, $T = 2.5 \times 10^{-5}$ sec., Stress Solution, Mass Distributed at 5 Nodes

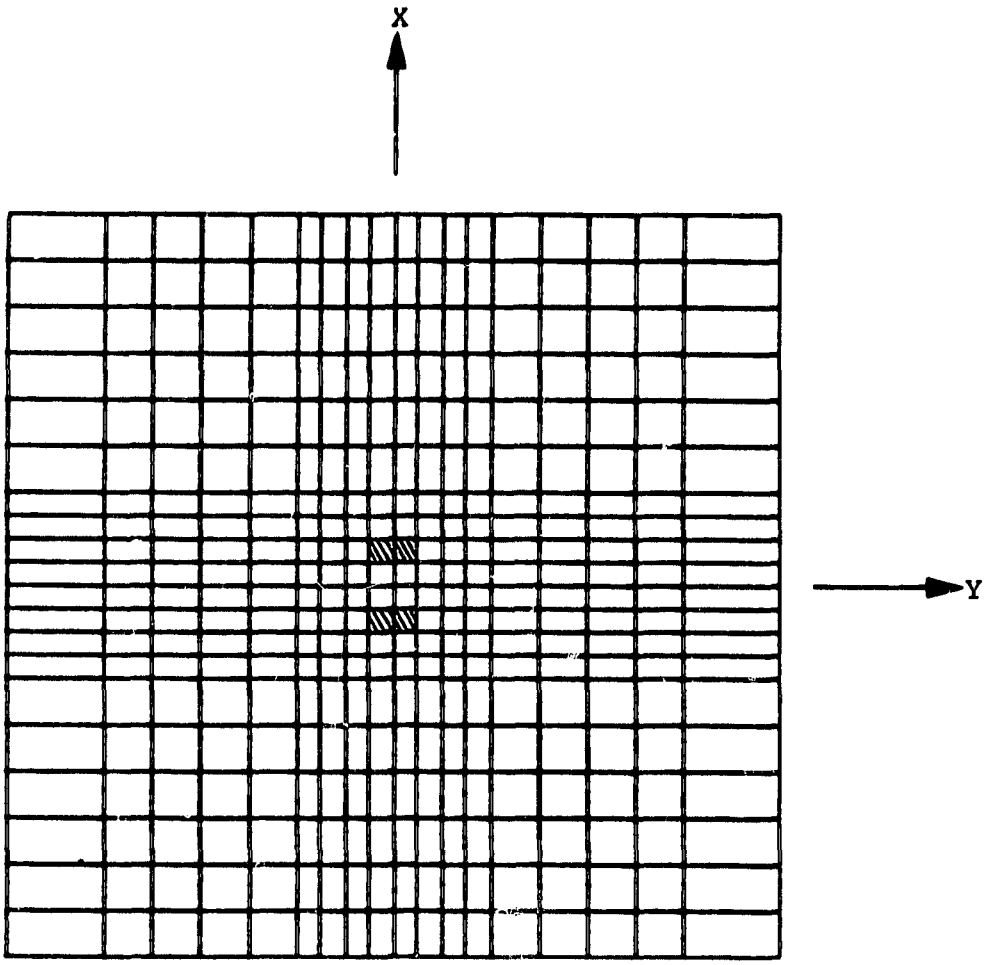

Figure 30. Elements with One Remaining Intact Ply Interface, $T = 3.75 \times 10^{-5}$ sec., Stress Solution, Mass Distributed at 5 Nodes

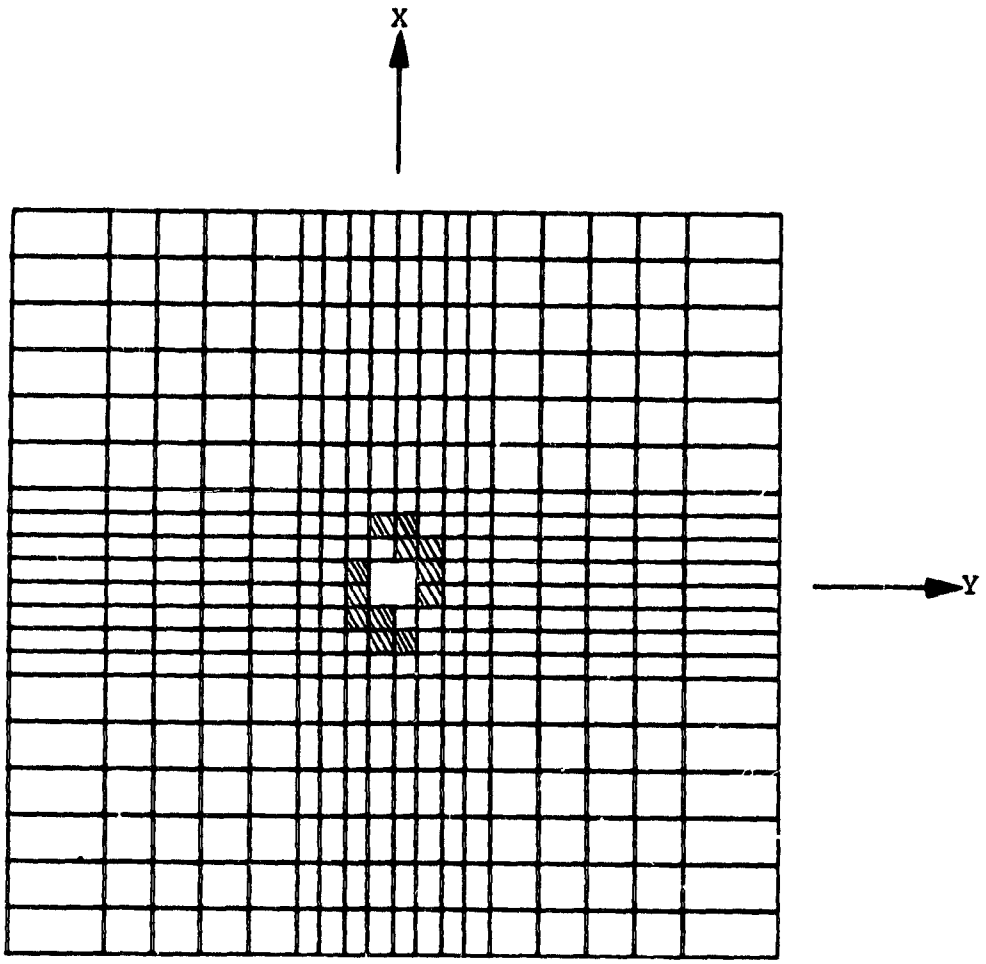

Figure 31. Elements with Ply Damage, T = 1.25×10^{-5} sec., Stress Solution, Modified Model

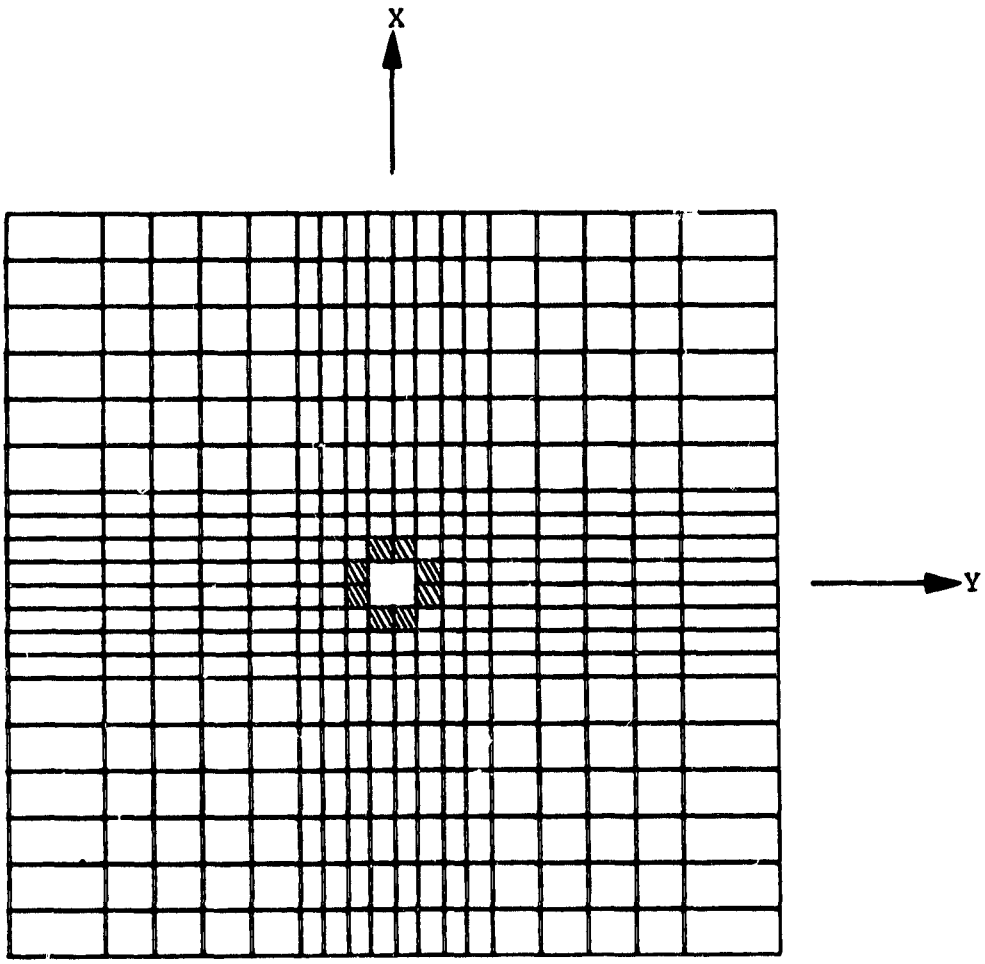

Figure 32. Elements with Interlaminar Damage, T = 1.25 x 10^{-5} sec., Stress Solution, Modified Model

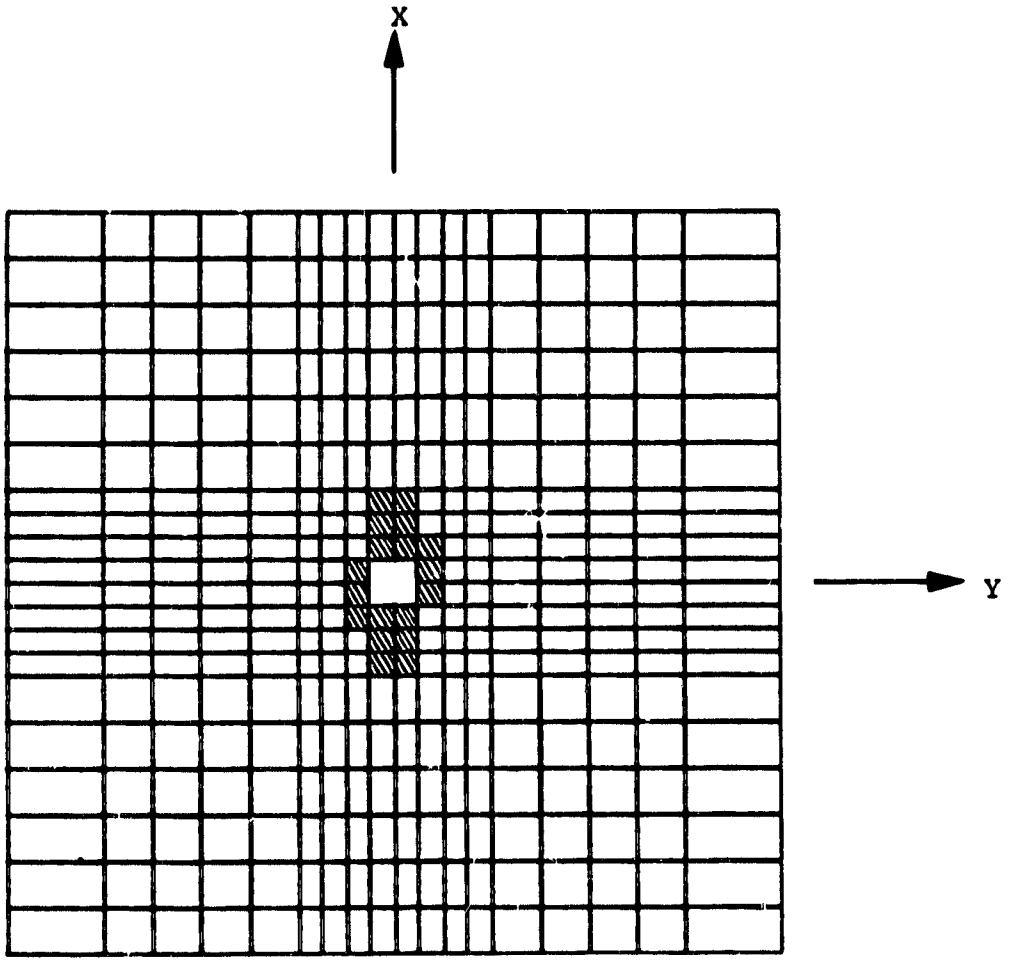

Figure 33. Elements with Ply Damage, T = 2.5 x 10^{-5} sec., Stress Solution, Modified Model

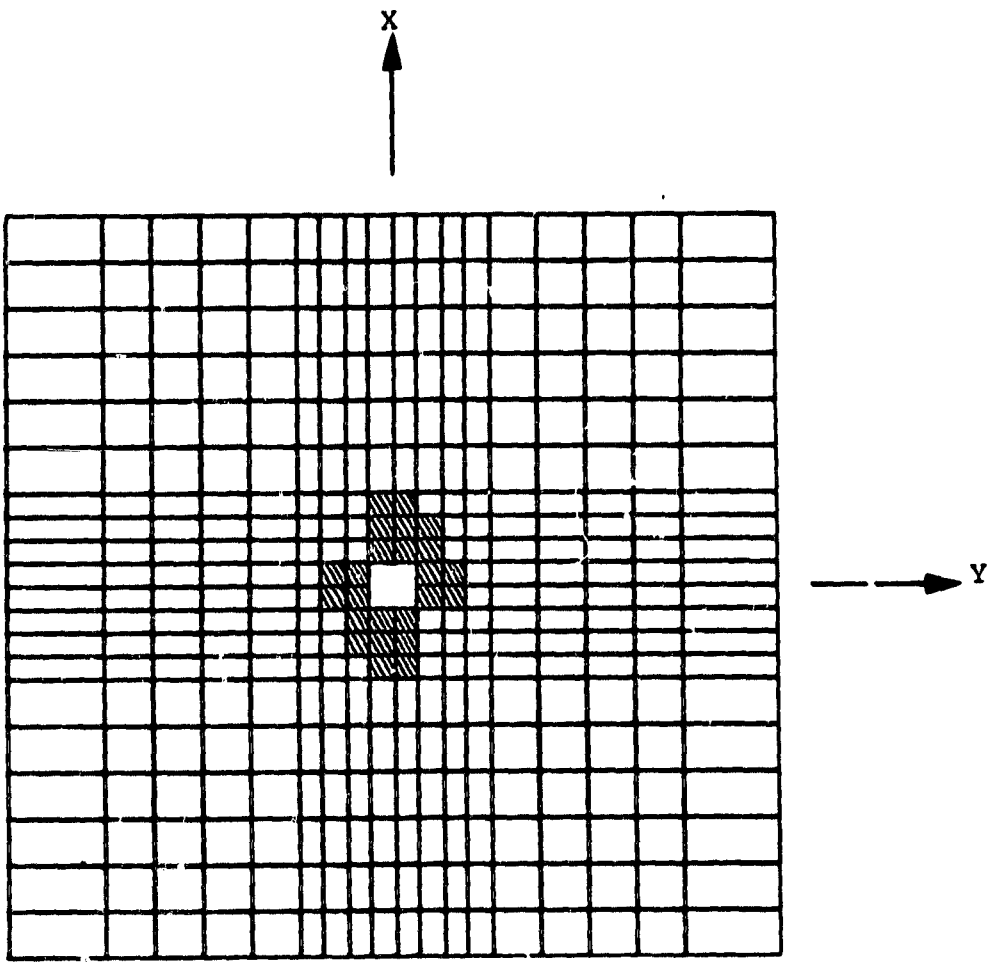

Figure ... Elements with Ply Damage, T = 3.75×10^{-5} sec., Stress Solution, Modified Model

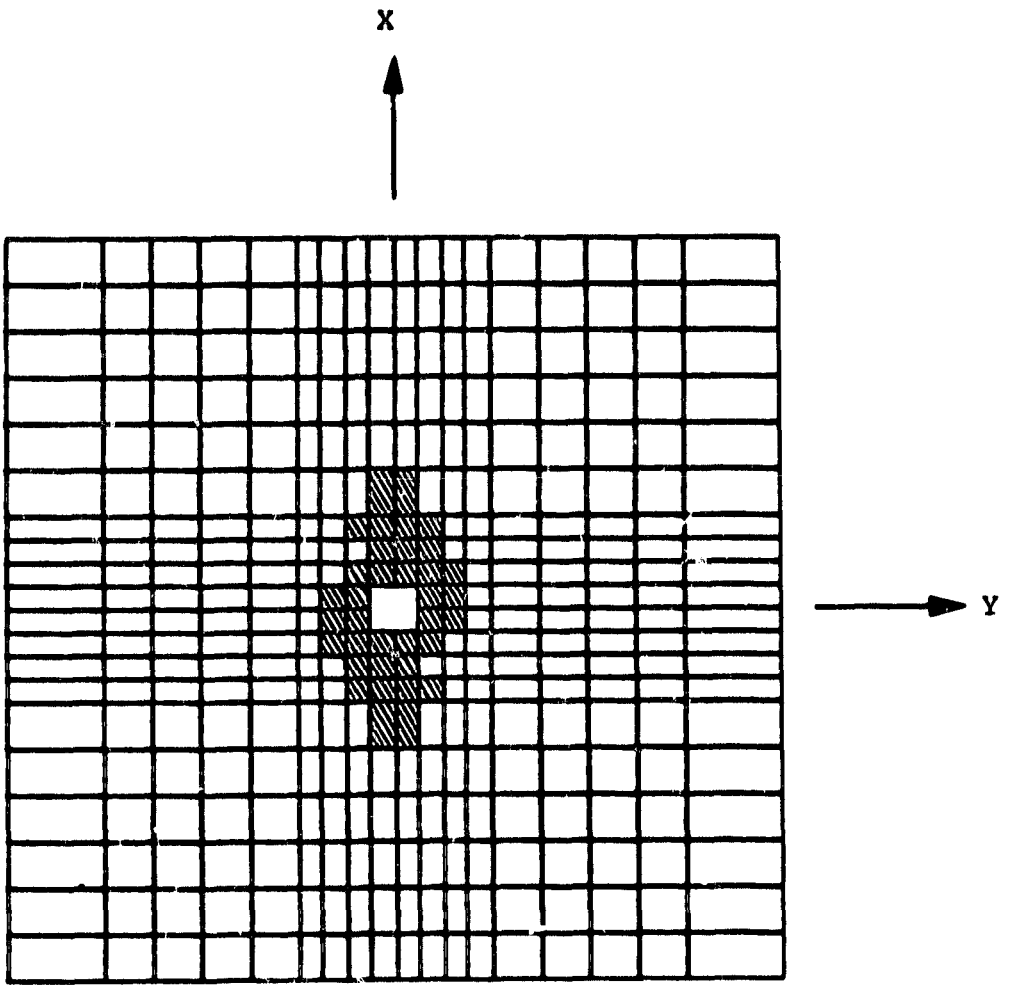

Figure 35. Elements with Ply Damage, T = 5.0 x 10^{-5} sec., Stress Solution, Modified Model

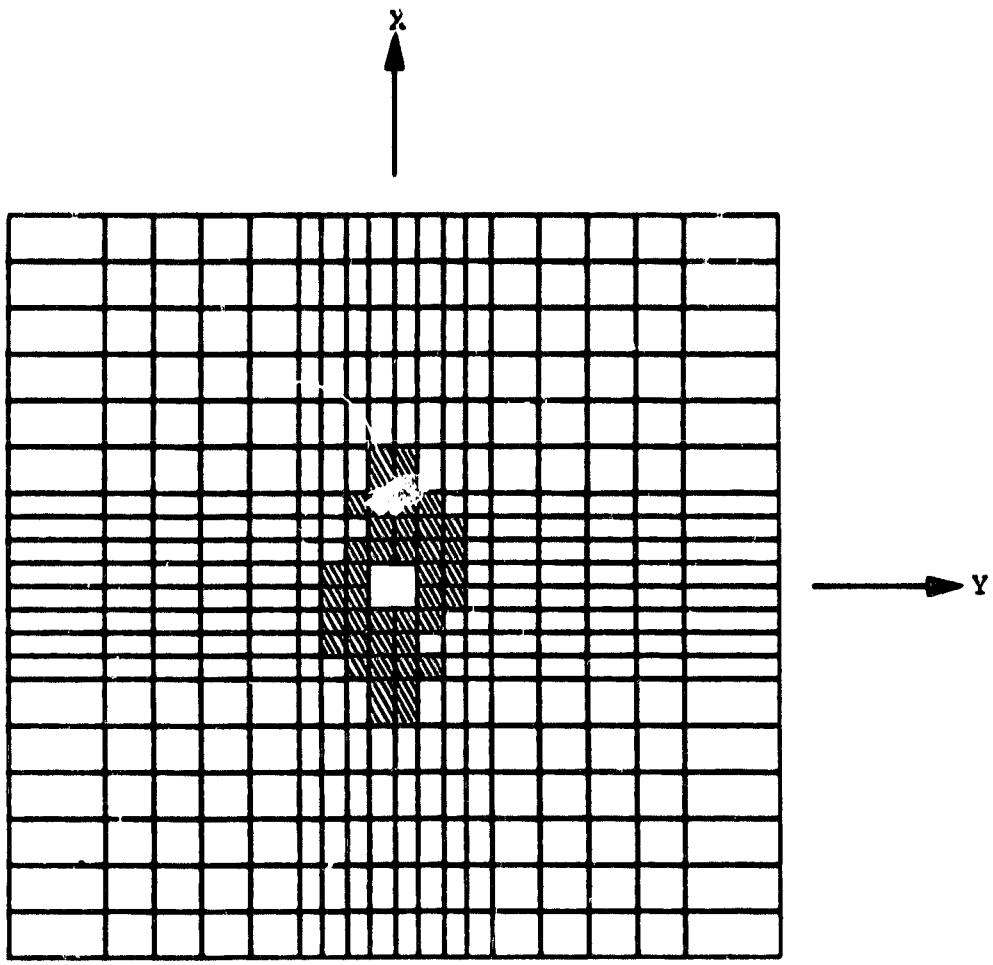

Figure 36. Elements with Ply Damage, T = 6.25×10^{-5} sec., Stress Solution, Modified Model

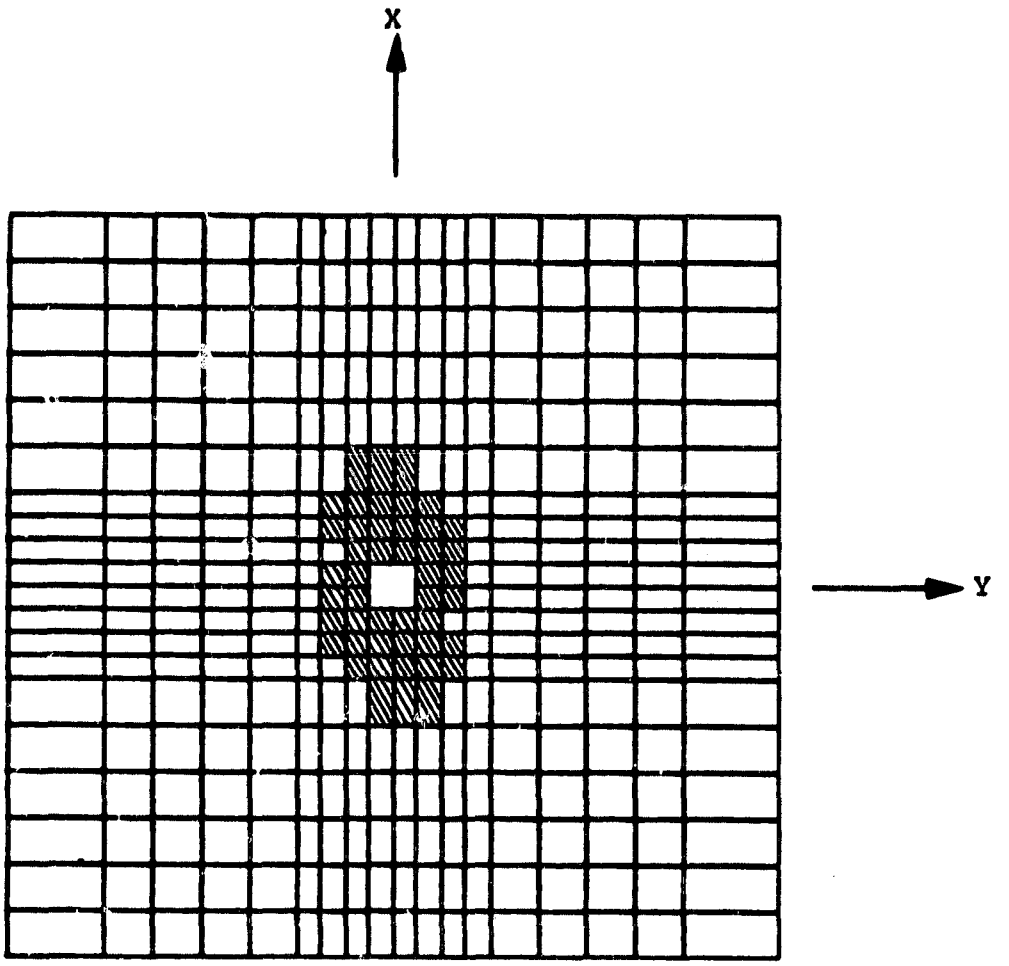

Figure 37. Elements with Ply Damage, T = 7.5 x 10^{-5} sec., Stress Solution, Modified Model

APPENDIX A
STRESS, MOMENT, AND TRANSVERSE SHEAR RESULTANTS

In order to perform the composite stress analysis required for failure prediction, it is necessary to determine stress, moment, and transverse shear resultants. The thin shell finite element taken from SAP IV has the capability for stress and moment resultants but lacks the ability to compute transverse shear resultants. It was necessary, therefore, to add the capability for this transverse shear prediction.

Since the primary focus of the current contract involved material response and not the development of general purpose finite element routines, the simplest approach available for computing transverse shear resultants was adopted. In the course of this effort, it was determined that since the restrictions inherent in the simple transverse shear computations effectively remove the necessity for the complex stress and moment resultant computation, the SAP IV routines which perform these analyses were not required. Therefore, the entire stress recovery procedure is based on the simplifying element orientations required for transverse shear as described below.

The primary restriction invoked by the simple transverse shear resultant computation involves the elemental geometry. No attempt was made to determine transformations of forces from the global coordinate system to an arbitrary elemental coordinate system. Therefore, it is required that the local elemental coordinates coincide with the global coordinates. Additionally, no provisions were made for elemental geometric irregularities. This requires that all elements be rectangular. The second restriction applies only to the stress recovery procedures. The displacement response is computed correctly for elements which are not rectangular if the element coordinate system is defined coincident with the global coordinate system. This restriction is required so that the laminate properties are utilized correctly.

In figures A-1 and A-2, the elemental nodal forces and moments are depicted. The forces and moments are shown in a global positive

scene. The element is required to be rectangular and oriented with the global coordinate system as mentioned previously and, thus, the relations for stress and moment resultants can be written directly as given in tables A-1 and A-2. It can easily be seen that the relations in tables A-1 and A-2 are invalid if either of the two restrictions mentioned are violated.

The computation of transverse shear stress resultants is slightly more complicated. In figure A-3 the moments and shear resultants required for equilibrium are depicted. In the analysis used, the transverse shear forces are computed from moment equilibrium since shear deformation is not included in the displacement solution.

The transverse shear resultants can be determined quite easily from equilibrium considerations as:

$$Q_x = \frac{\partial M_x}{\partial x} + \frac{\partial M_{xy}}{\partial y}$$

$$Q_y = -\frac{\partial M_{xy}}{\partial x} - \frac{\partial M_y}{\partial y} \; . \qquad \text{(A.1)}$$

If it is assumed that all quantities vary linearly within the finite element, equations [A.1] can be rewritten as:

$$Q_x = \frac{\Delta M_x}{\Delta x} + \frac{\Delta M_{xy}}{\Delta y}$$

$$Q_y = -\frac{\Delta M_{xy}}{\Delta x} - \frac{\Delta M_y}{\Delta y} \; . \qquad \text{(A.2)}$$

Each of the quotients in equations [A.2] can then be written in terms of the nodal moments of figure A-2. When this is done, a difficulty is immediately encountered.

The various terms of equation [A.2] are found to be:

$$\frac{\Delta M_x}{\Delta x} = - [M_y^i + M_y^j + M_y^k + M_y^\ell] \frac{1}{\Delta x \Delta y}$$

$$\frac{\Delta M_y}{\Delta y} = [M_x^i + M_x^j + M_x^k + M_x^\ell] \frac{1}{\Delta x \Delta y}$$

$$\frac{\Delta M_{xy}}{\Delta x} = [M_x^i + M_x^j + M_x^k + M_x^\ell] \frac{1}{\Delta x \Delta y} \qquad \text{(A.3)}$$

$$\frac{\Delta M_{xy}}{\Delta y} = - [M_y^i + M_y^j + M_y^k + M_y^\ell] \frac{1}{\Delta x \Delta y}$$

It is immediately apparent that in terms of the nodal moments, the two terms required for Q_x are identical, as are the two terms in the Q_y expression. This result is demonstrating that, in terms of the nodal moments, it is not possible to separate the contributions of the bending and twisting moments. This is easily confirmed by considering a one-dimensional case. The shear force computed is twice the proper value if the full expressions of equations [A.2] are utilized.

The resolution of this problem involves simply dropping the twisting components from equation [A.2] and using the expressions:

$$Q_x = \frac{\Delta M_x}{\Delta x}$$

$$Q_y = - \frac{\Delta M_y}{\Delta y} \, . \qquad \text{(A.4)}$$

It must be remembered that the contributions of the twisting moments have not been neglected in equations [A.4]. These contributions are included implicitly in equations [A.4] through the computations of the two quotients involved.

Table A-1. Stress Resultants

$$N_x = [(F_x^j + F_x^k) - (F_x^i + F_x^\ell)] \frac{1}{2} \frac{1}{\Delta y}$$

$$N_y = [(F_y^\ell + F_y^k) - (F_y^i + F_y^j)] \frac{1}{2} \frac{1}{\Delta x}$$

$$N_{xy} = [(F_x^\ell + F_x^k) - (F_x^i + F_x^j)] \frac{1}{2} \frac{1}{\Delta x}$$

$$= [(F_y^j + F_y^k) - (F_y^i + F_y^\ell)] \frac{1}{2} \frac{1}{\Delta y}$$

Table A-2. Moment Resultants

$$M_x = [(M_y^i + M_y^\ell) - (M_y^j + M_y^k)] \frac{1}{2} \frac{1}{\Delta y}$$

$$M_y = [(M_x^\ell + M_x^k) - (M_x^i + M_x^j)] \frac{1}{2} \frac{1}{\Delta x}$$

$$M_{xy} = [(M_x^k + M_x^j) - (M_x^i + M_x^\ell)] \frac{1}{2} \frac{1}{\Delta y}$$

$$= [(M_y^\ell + M_y^k) - (M_y^i + M_y^j)] \frac{1}{2} \frac{1}{\Delta x}$$

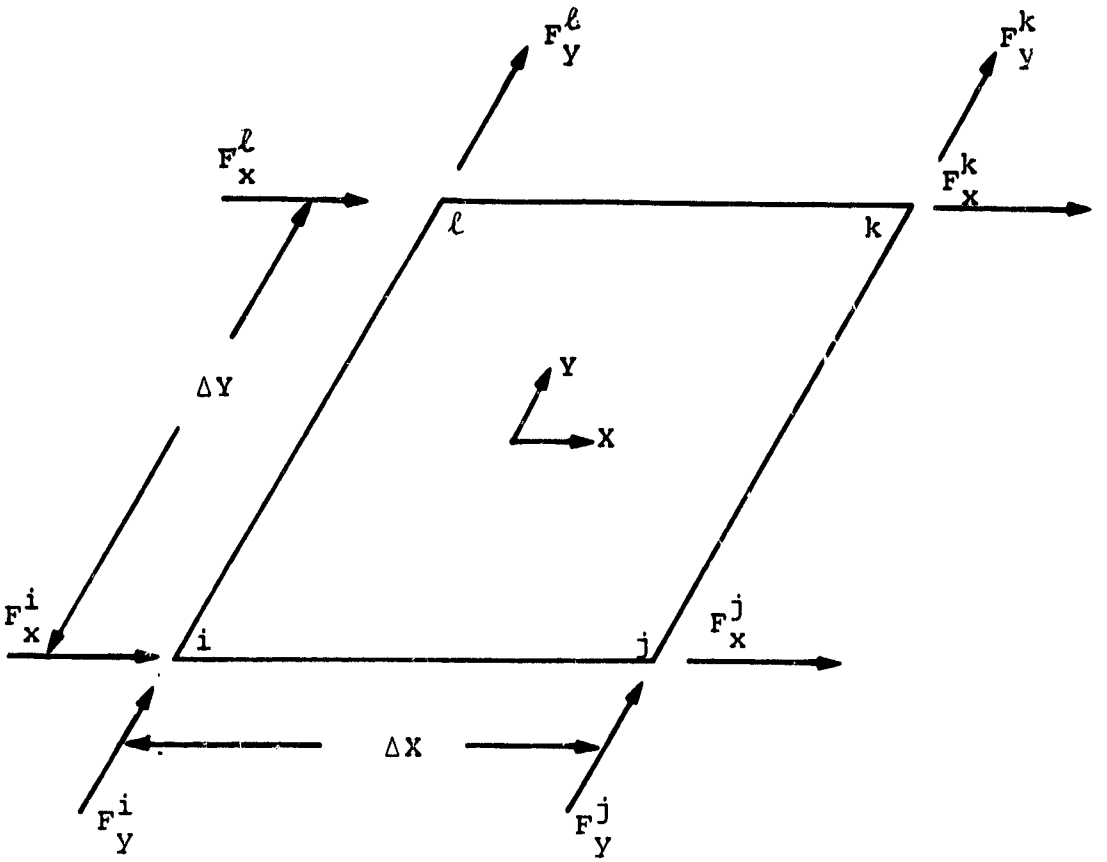

Figure A-1. In-Plane Elemental Nodal Forces

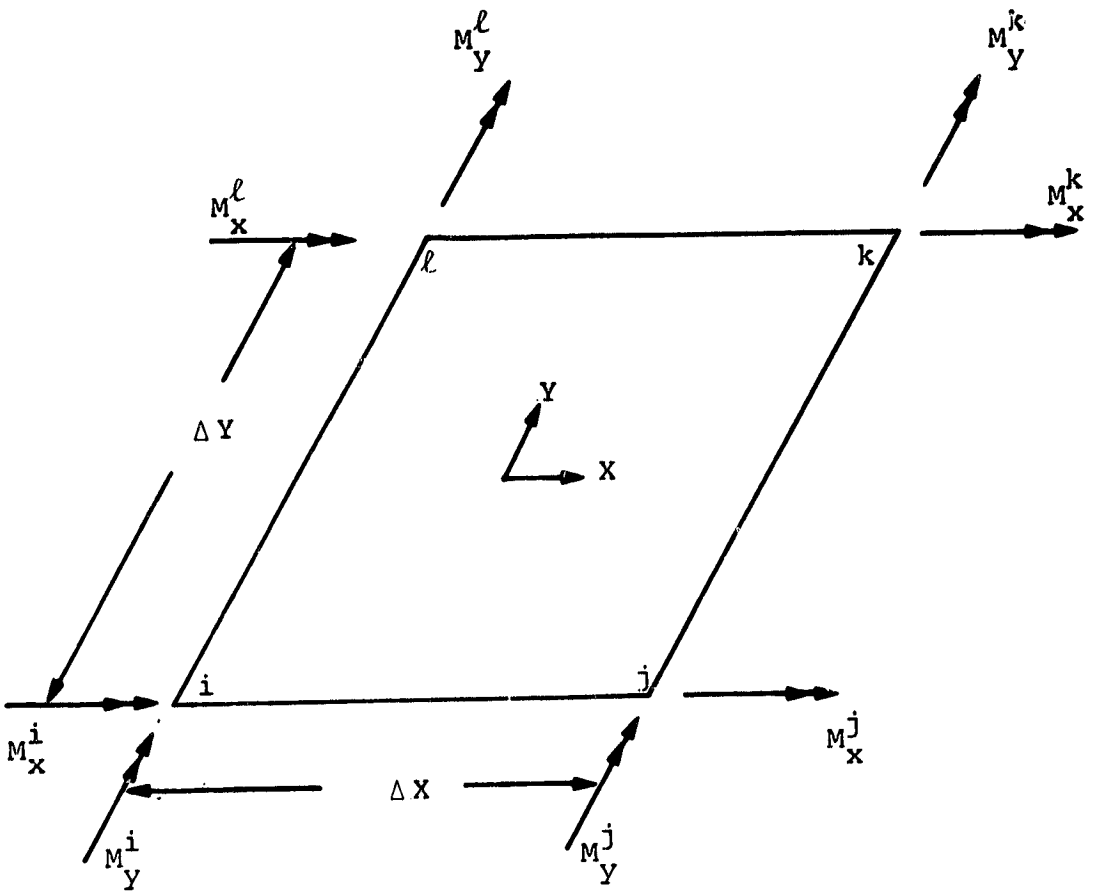

Figure A-2. Elemental Nodal Moments

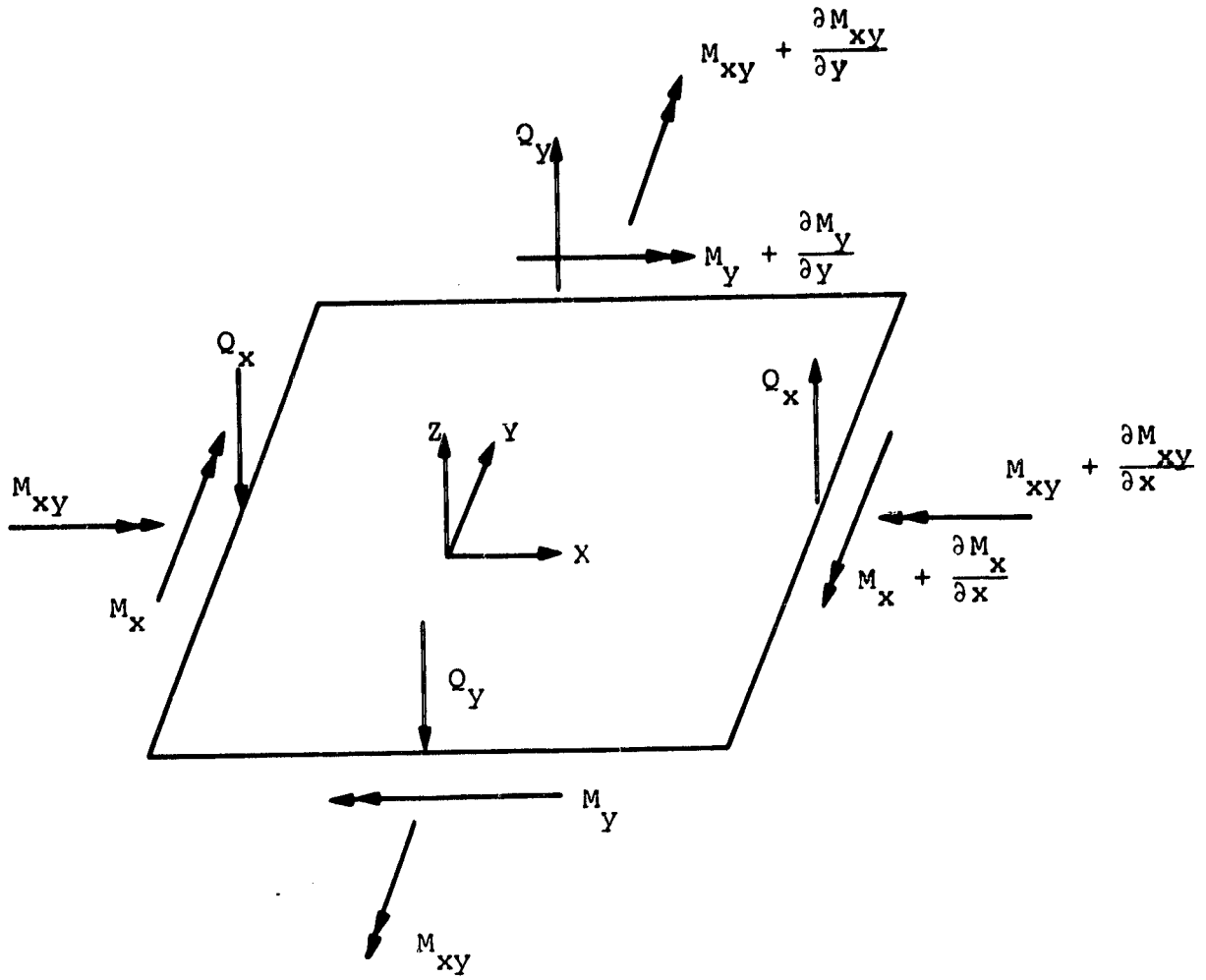

Figure A-3. Moment Equilibrium and Transverse Shear Forces

APPENDIX B
INTERLAMINAR SHEAR STRESSES

The analysis used in the CLIP code for computing interlaminar shear stresses is based upon bending equilibrium. In Appendix A, the derivation of the transverse shear stress resultants is given. These resultants are then used to compute transverse shear stresses at the ply interfaces within the laminate. The method used for computing the interlaminar shear stresses is based on an extension of classical methods used for bending shear stresses in homogeneous beams.

In the analysis, it is necessary to compute interlaminar shear for two different cases. Interlaminar stresses must be computed in elements which have sustained damage as well as those which have not. The methods used in both cases are described here.

INTERLAMINAR SHEAR IN INTACT ELEMENTS

In order to compute interlaminar shear stresses in undamaged elements, the transverse shear stress resultants are converted to moments by multiplying by the appropriate shell element dimensions (see eqn. A.4). These two moments then represent the change in moment across the element in both the X and Y coordinates. This is demonstrated for a one-dimensional case in figure B-1. It is readily apparent in figure B-1 that the shear stresses represent the balancing force required for moment equilibrium.

The moment differentials derived from the transverse shear resultants are then applied to the laminate model. This produces three in-plane stresses within each ply. These ply stresses are then converted to forces and summed through the thickness in both the X and Y coordinate directions. In figure B-2, the three in-plane stresses and resulting interlaminar shear stresses are shown for an outer ply of the laminate and an applied moment differential. Equilibrium in the X-direction yields forces

$$\sigma_x \Delta y \Delta z + \sigma_{xy} \Delta x \Delta z + \sigma_{xz} \Delta x \Delta y = 0 \qquad \text{(B.1)}$$

and in the Y-direction

$$\sigma_y \Delta x \Delta z + \sigma_{xy} \Delta y \Delta z + \sigma_{yz} \Delta x \Delta y = 0. \qquad \text{(B.2)}$$

Thus, the interlaminar shear stresses are simply

$$\sigma_{xz} = \frac{-(\sigma_x \Delta y \Delta z + \sigma_{xy} \Delta x \Delta z)}{\Delta x \Delta y}$$

$$\sigma_{yz} = \frac{-(\sigma_y \Delta x \Delta z + \sigma_{xy} \Delta y \Delta z)}{\Delta x \Delta y} \qquad \text{(B.3)}$$

To compute interlaminar shear stresses on interior ply interfaces, it is only required that the X and Y forces represented by the σ_{xy} and σ_{yz} terms respectively in equation B.1 be summed through the laminate to the interface in question.

INTERLAMINAR SHEAR IN DAMAGED ELEMENTS

In order to compute interlaminar shear stresses in an element which has sustained damage prior to the stress calculation, it is first necessary to determine how the laminate responds to loading when damage is present. In figure B-3 the bending stresses through a localized delamination are shown. Since the delamination is small, the material away from the delamination effectively forces the curvature and strain field to remain unchanged. The material above and below the delamination bend as two independent laminates while the constraint of the adjacent, undamaged material adds opposing membrane forces. Thus, the net effect produces no change in the bending stress field. This is the basis for not reformulating the elemental stiffness for interlaminar delaminations.

This model cannot account for a moment gradient, however. In order to evaluate the effects of a moment gradient, it is required that the two sublaminates behave entirely independently. The opposing membrane forces must not be present in the shear analysis. If a moment gradient is applied to this type of model, then the membrane forces must also exhibit a gradient. This is not possible since it would require a shear force transfer across the delamination. This is a drawback related to the lack of shear deformation in the analysis.

To model the moment gradient, it is necessary to compute the bending stiffnesses of the sublaminates independently. The bending stiffnesses are then added to give the stiffnesses of the assemblage of partial laminates. This, however, leads to bending/extensional coupling at both the laminate and sublaminate levels. It is required, therefore, that the [B] matrices be accounted for. This can easily be accomplished by noting that the membrane forces must be zero for the applied transverse shear forces (moment gradients).

The force/moment - strain/curvature relations for a general laminate are

$$\{N\} = [A]\{\varepsilon^{o}\} + [B]\{\kappa\}$$
$$\{M\} = [B]\{\varepsilon^{o}\} + [D]\{\kappa\} \qquad (B.4)$$

where the matrices have the usual connotations. Remembering that

$$\{N\} = 0 \qquad (B.5)$$

the mid-plane strains due to a bending load are

$$\{\varepsilon^{o}\} = -[A]^{-1}[B]\{\kappa\}. \qquad (B.6)$$

These strains actually represent a neutral axis shift from the mid-surface of the unsymmetric laminate to the proper neutral surface.

Using the strains of equation (B.6), an effective bending stiffness matrix can be determined.

$$\{M\} = [B]\{\varepsilon^{o}\} + [D]\{\kappa\} \tag{B.7}$$

$$= -[B][A]^{-1}[B]\{\kappa\} + [D]\{\kappa\} \tag{B.8}$$

$$= ([D] - [B][A]^{-1}[B])\{\kappa\} \tag{B.9}$$

$$= [D^*]\{\kappa\} \tag{B.10}$$

The bending stiffness matrix in (B.10) relates moments and curvatures about the neutral surfaces rather than the mid-surface.

The bending stiffness matrix for the total laminate is then given as

$$[D^*] = \sum_{I=1}^{N} [D^*]^{I}, \quad N \text{ - number of sublaminates.} \tag{B.11}$$

With the bending stiffness of the assemblage of sublaminates given in eqn. (B.11), a curvature vector can easily be found for the applied moment differentials. Using the curvature for the whole laminate and eqn. (B.6), the ply stresses for each sublaminate can be determined and summation of forces depicted in figure B-2 and equations B.1 through B.3 carried out. Thus, the interlaminar stresses in damaged elements are predicted.

When an element contains both ply damage and interlaminar damage, the same method is used. In figure B-4 the sublaminates for a laminate which has sustained general damage are shown. For ply damage, the entire ply is removed from interlaminar shear calculations.

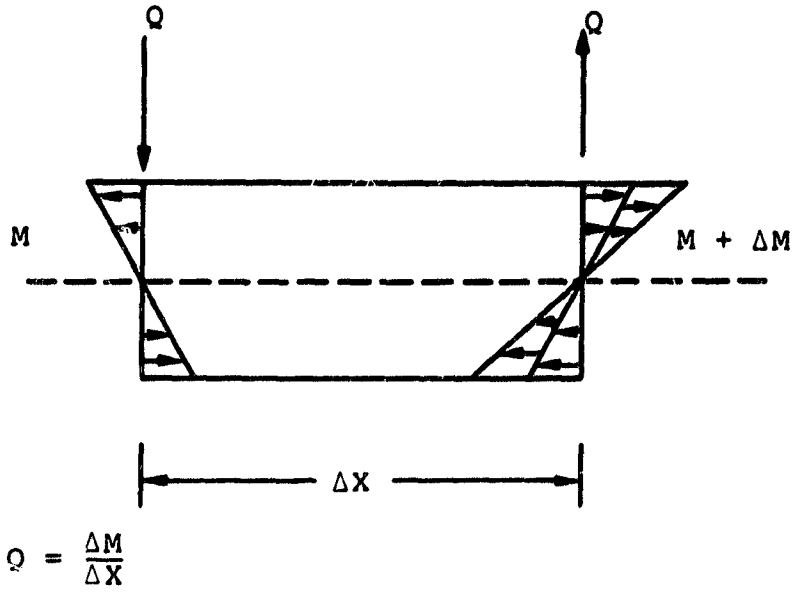

Figure B-1. One-Dimensional Shear/Moment Relationship

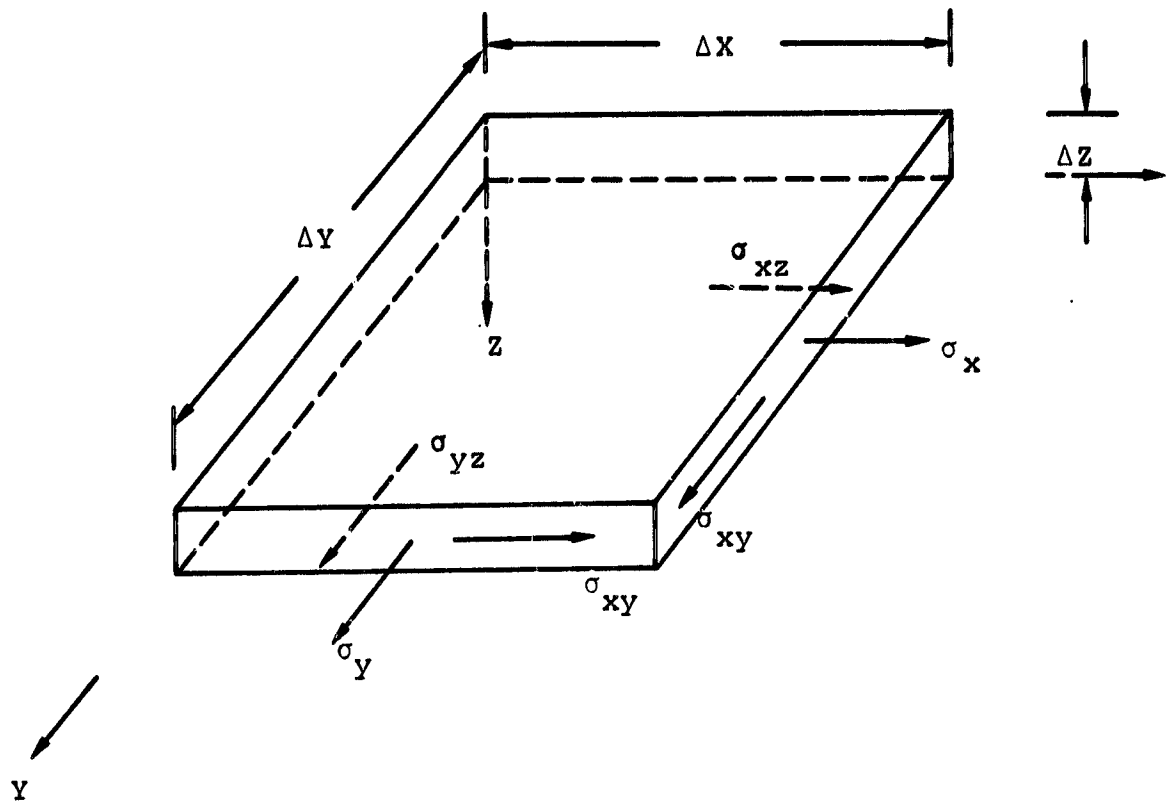

Figure B-2. Interlaminar Shear Stresses

C-2

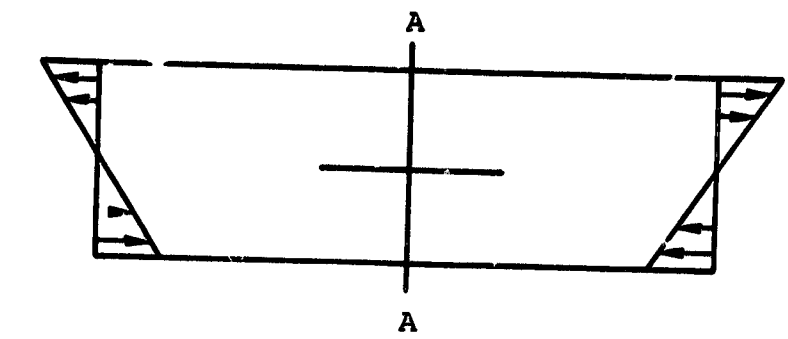

A-A

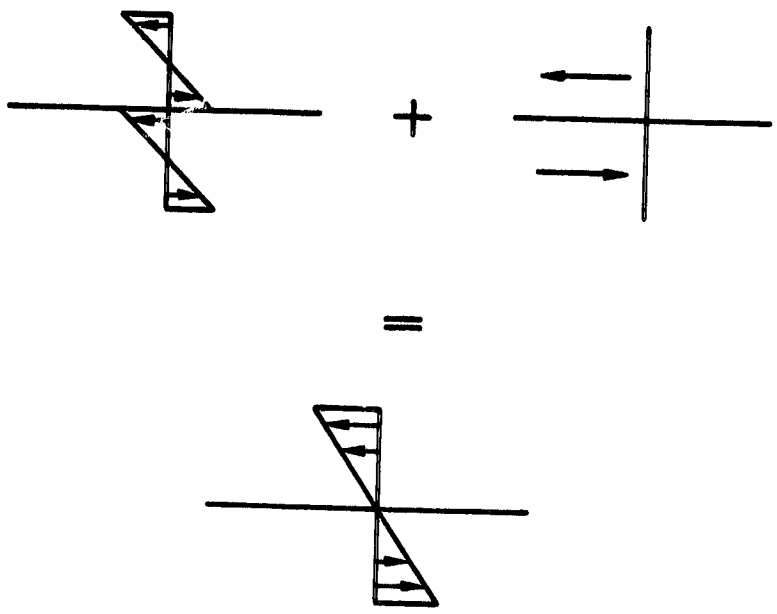

Figure B-3. Bending Stresses with an Interlaminar Delamination

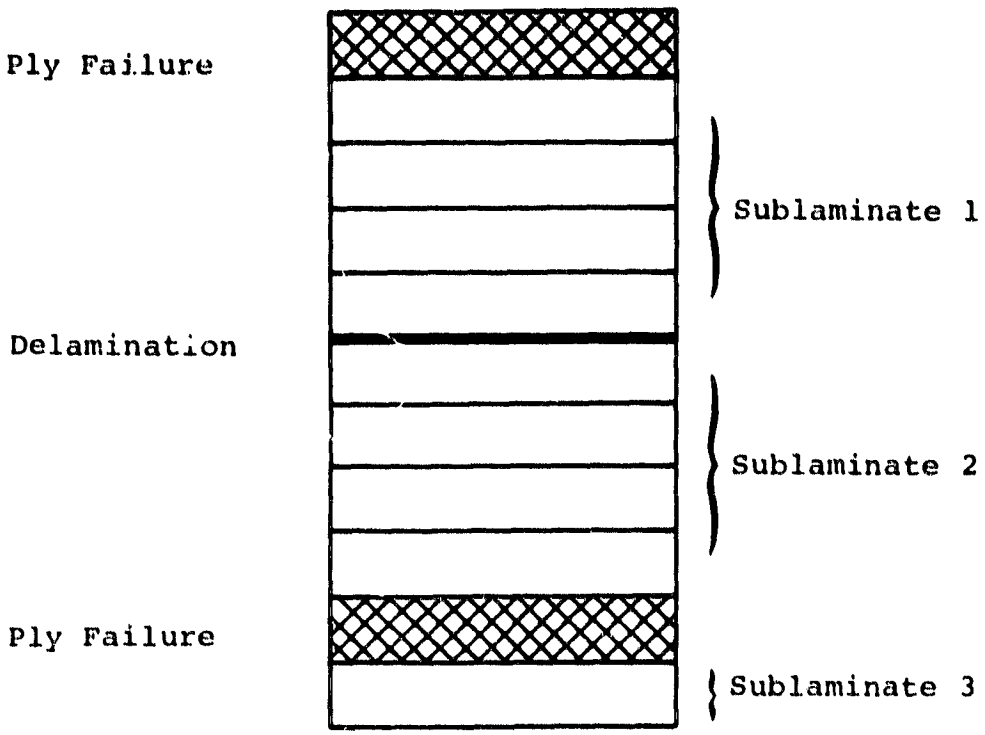

Figure B-4. Typical Failed Laminate

APPENDIX C
COMPOSITE LAMINATE IMPACT PROGRAM (CLIP)

The computer program developed for predicting damage initiation and growth during low velocity impact consists of a transient dynamics finite element code coupled with composite stress and failure analysis procedures. In conjunction with the failure analysis routines is the capability to incorporate predicted damage into the transient analysis. Thus, the damage predicted during any time step is incorporated into the dynamic solution at future time steps. This coupling of damage and dynamic response is the heart of the computerized procedure.

The transient dynamic finite element procedures used were taken from the SAP IV code (ref. 14). The portions of the SAP IV code used include the thin shell element routines and the time integration routines. The composite stress and failure analysis routines were developed specifically for use in the CLIP code.

In figure C-1, a simplified flow chart of the analysis performed by the CLIP code is shown. The branches and loops shown represent the procedures required for incorporating the effects of predicted damage into the analysis and removing the impact mass after the contact force becomes tensile. The various computer program segments which perform the analysis are listed in table C-1 along with a brief description of their functions.

PROGRAM OPERATION

The CLIP code has been written with several different solution options. The different options offer the user considerable flexibility in using the code. The options available include data check mode, static analysis alone, static analysis to generate a prestress condition for a dynamic analysis, dynamic analysis without stress calculation and dynamic analysis with stress calculation.

The data check mode of operation is useful in insuring that all input data parameters are correct. This option is essential in any large program.

The static solution mode has, basically, two uses. First, a static test case is an easy method to prove the validity of a finite element model. It is extremely difficult to verify the results of a dynamic analysis directly. The second use of the static analysis is to generate a pre-stress condition at the beginning of the dynamic analysis. This allows the static stresses to be included directly with the dynamically induced stresses.

The inclusion of the static solution is performed by direct superposition. The static displacement vector is saved at the end of each time step. In this way the static displacements do not act as an initial condition in the dynamic response. It must be remembered that this is a direct superposition of results. There is no coupling of the static and dynamic responses.

The dynamic solution can be performed with or without stress calculations. The dynamic analysis made without stress calculations is considerably less costly and time consuming than a similar analysis with a complete stress analysis. The solution cost reductions are a result of two factors. First, the stress analysis procedures are by-passed in the analysis and secondly, there are no damage calculations which would require reformulation of elemental and global stiffness matrices and subsequent decomposition. Because of this, the dynamic solution without stress analysis can be used to determine the length of time required to characterize the impact event at a moderate cost. This mode of analysis can also be used to verify the integration time step selected.

When using the dynamic solution without stress analysis, it should be remembered that the response of the plate will be different when stress calculations are included. The amount of this difference will be a function of the amount of damage sustained in the plate when stress calculations are included.

When damage predicted in an element is ply damage (either matrix or fiber), the elemental stiffness matrix is modified. These modifications are then included in the global stiffness matrix for incorporation in subsequent time steps. Thus, the plate stiffness is changed forcing a plate response change.

The dynamic solution mode which includes stress analysis is the primary mode of operation of the CLIP code. This mode is used for simulating the actual response of a composite plate subjected to low velocity impact.

The use of the analysis in this mode requires some thought on the part of the user. The code is written such that the user selects how often the stress calculations are performed. If the stress calculations are not performed often enough, it is possible to miss considerable damage. This is especially true at the beginning of the analysis when very localized deformations are the predominant response of the plate.

In an effort to achieve computational economy, the CLIP code performs stress analysis only for elements which the user selects. This option saves considerable computer time since many of the finite elements in the model will typically never sustain damage. If, however, an element, which should fail under the dynamic loading, is not selected for stress analysis, this damage is lost. It is never computed and, hence, is not included in the dynamic response. Thus, it is important to select the proper group of elements for stress calculations. Insight into the elements which should be included can be obtained by examining the plate response without stress calculations.

PROGRAM OUTPUT

The output of the CLIP code can be divided into two distinct entities. First, the program echos the input data such that a record of this data is generated, and secondly, the results of the analysis are printed. In each of these two areas, the user has considerable flexibility in determining the extent of the output generated.

In terms of the input data echo, the user can suppress printing of the nodal points or the elemental data or both. Other input data including the impact parameters, lamina materials and laminate con-

figuration as well as data generated by the analysis code with respect to problem size and laminate elastic constants are always printed.

In terms of the solution output, the user selects the frequency of output for the various data generated as well as the nodal points (displacements, velocities, accelerations) and elements (element forces, laminate coordinate stresses, layer coordinate stresses, failure calculations, failure locations) where data are to be printed.

For the nodal output data, the user can select different printout frequencies for the displacements, velocities and accelerations as long as the velocity and acceleration print frequencies are even multiples of the displacement frequency. Thus, the displacements may be printed every five time steps while the velocities print every fifty steps and the accelerations every 20 steps. The print frequencies are left to the discretion of the user.

The elemental data are printed in a similar fashion where each printout frequency must be an even multiple of the stress calculation frequency. As an example, the user must not select a stress calculation frequency of every ten steps while requesting a layer coordinate stress printing every three time steps. The result of this particular arrangement would produce layer stress printing only every thirty time steps. There is no requirement that the individual data print frequencies be multiples of each other, however.

The elemental data which can be printed consist of elemental forces, ply stresses in two coordinate systems, calculations of the failure analyses, and locations of damage. The elemental forces consist of stress, moment and transverse shear resultants and top surface stress corresponding to the impactor/plate contact force distributed over all elements adjoining the impacted nodes.

Layer stress can be printed in the laminate coordinate system (global X-Y) or the local ply coordinate systems, or both. Stresses are printed for each ply in the laminate under study as well as each

ply interface including the top and bottom free surfaces. Thus, there is always one more interface than there are plies.

The calculations of the failure criteria, if selected for printing, produce data for each ply and interface. The data printed are simply the sum of the terms in the various failure criteria modes (see table 1). These data can be used to identify locations and modes of damage within the elemental laminate models.

If the details of these calculations are not required, the user can select that failure location printing be activated. This output details the ply or interface which has failed within a damaged element. For the case of ply damage, information is also printed indicating whether matrix or fiber failure has occurred. It is possible to specify both failure calculation printing and failure location printing. To do so, however, is somewhat redundant.

Composite Laminate Impact Program

I. PROGRAM CONTROL DATA

Card 1 — **Title Card** — **20A4**

Columns		Contents
1-80	HED(20)	Program Title Card

Card 2 — **Control Data** — **4I5**

Columns		Contents
1-5	NUMNP	Number of nodes
6-10	MODEX	Execution code, =0 execute
11-15	NSTR	Stress calculation code =0, no stress calculation =N, stress calculation every N time steps
16-20	ISTAT	Static analysis code =0, no static pre-stress

Card 3 — **Dynamic Analysis Control Data** — **I5,3F10.0**

Columns		Contents
1-5	NT	Maximum number of time steps
6-15	DT	Time step
16-25	ALFA	Mass proportional damping coefficient
26-35	BETA	Stiffness proportional damping coefficient

Card 4		Print Control Data	10I5
Columns			Contents
1-5	KEY(1)		Node print code, ≠0 print node data
6-10	KEY(2)		Element print code, ≠0 print element data
11-15	KEY(3)		Displacement print code
16-20	KEY(4)		Velocity print code
21-25	KEY(5)		Acceleration print code
26-30	KEY(6)		Element force print code
30-35	KEY(7)		Laminate coordinate stress print code
36-40	KEY(8)		Lamina coordinate stress print code
41-45	KEY(9)		Failure calculation print code
46-50	KEY(10)		Failure location print code

NOTES: Card 4

KEY(3)-KEY(10)	=0, suppress printing =N, print every N time steps
KEY(6)-KEY(10)	Codes not used if NSTR, Card 2, =0

Card 5		Print Control Data	20I5
Column			Contents
1-5	NDISP		Number of nodal print groups ≤ 100
6-10	NSTRP		Number of element stress calculation groups ≤ 100

NOTES: Card 5

If NDISP =0, print data for all nodes,
do not include Card 6
If NSTRP =0, compute stresses for all elements,
do not include card 7

Card 6	Print Control Data	2015

Column		Contents
1-5	KEYS (I,1)	First node, print group I
6-10	KEYS (I,2)	Last node, print group I
11-15	KEYS (J,1)	First node, print group J
16-20	KEYS (J,2)	Last node, print group J

Continue through NDISP groups, more than 1 card
if necessary

Card 7	Print Control Data	2015

Column		Contents
1-5	KEYS (I,1)	First element stress calculation, Group I
6-10	KEYS (I,2)	Last element stress calculation, Group I
11-15	KEYS (J,1)	First element stress calculation, Group J
16-20	KEYS (J,2)	Last element, print group J

Continue through NSTRP groups, more than 1 card
if necessary

NOTES: Cards 5,7

Stress calculations are performed only for element identified in these groups.

II. IMPACT CONTROL DATA

Card 1	Node Data	I5

Columns		Contents
1-5	NUMIMP	Number of impacted nodes $0 \leq$ NUMIMP ≤ 20

Card 2	Node Data	20I5

Columns		Contents
1-5	IMN(I)	Impacted node
6-10	IMN(I+1)	Impacted node

Continue through NUMIMP nodes.

Card 3	Impact Conditions	2F10.0

Columns		Contents
1-10	TOTMAS	Total impactor mass
11-20	TERMV	Impact velocity

Card 4	Impact Mass Distribution	8F10.0

Columns		Contents
1-10	XMFRAC(I)	Impact mass fraction, node I
11-20	XMFRAC(J)	Impact mass fraction, node J

Continue through NUMIMP nodes.

III. LAMINATE DATA

Card 1 — **Laminate Geometry Control Data** — 2I5

Columns		Contents
1-5	NMAT	Number of different materials ≤ 2
6-10	NPLY	Number of plies ≤ 25

Card 2 — **Lamina Elastic Constants** — 5F10.0

Columns		Contents
1-10	E1(I)	Lamina Axial Modulus E_{11}, material I
11-20	E2(I)	Lamina Transverse Modulus, E_{22}, material I
21-30	G(I)	Lamina Axial Shear Modulus, G_{12}, material I
31-40	ANU(I)	Lamina Major Poissons Ratio ν_{12}, material I
41-50	RHO(I)	Lamina Mass Density, material I

Continue through NMAT materials.

Notes : Card 2

Major Poissons Ratio, $\nu_{12} = E_{11}\nu_{21}/E_{22}$

Card 3 — **Lamina Material Strengths** — 6F10.0

Columns		Contents
1-10	STREN(1,I)	Axial tensile strength, material I
11-20	STREN(2,I)	Axial compressive strength, material I

21-30	STREN(3,I)	Transverse tensile strength, material I
31-40	STREN(4,I)	Transverse compressive strength, material I
41-50	STREN(5,I)	Axial shear strength, material I
51-60	STREN(6,I)	Transverse shear strength, material I

Continue through NMAT materials.

Card 4 — Lamina Geometries — 2F10.0,I5

Columns		Contents
1-10	THIK(I)	Ply thickness
11-20	THET(I)	Ply orientation, degrees
21-25	MAT(I)	Ply material number

Continue through NPLY plies.

IV. NODAL DATA

Card 1 — Nodal Input Data — 7I5,3F10.0

Columns		Contents
1-5	N	Nodal point number
6-10	ID(N,1)	Boundary condition code, global X - direction
11-15	ID(N,2)	Boundary condition code, global Y - direction
16-20	ID(N,3)	Boundary condition code, global Z - direction
21-25	ID(N,4)	Boundary condition code, global X - rotation
26-30	ID(N,5)	Boundary condition code global Y - rotation
31-35	ID(N,6)	Boundary condition code global Z- rotation
36-45	X(N)	X - Coordinate
46-55	Y(N)	Y - Coordinate
56-65	Z(N)	Z - Coordinate

Continue through NUMNP nodes

NOTES: Card 1,

ID(I,J)=0, Force boundary condition
=1, Zero displacement boundary condition

V. ELEMENT DATA

Card 1	Element Input Data	I5

Columns		Contents
1-5	NUMEL	Number of elements

Card 2	Element input data	6I5,F10.0

Columns		Contents
1-5	MM	Element number
6-10	IY(1)	Element node I
11-15	IY(2)	Element node J
16-20	IY(3)	Element node K
21-25	IY(4)	Element node L
26-30	IY(5)	Element stiffness re-use code =0, form new stiffness =1, re-use previous stiffness
31-40	PRESSU	Uniform lateral pressure load

Continue through NUMEL cards.

NOTES: Card 2

IY(1) - IY(4),

1. Element must be rectangular
2. Nodes IY(1), IY(2) must lie along global X-Axis
3. IY(1)-IY(2) Define local positive X-Axis
4. Element must be defined counter-clockwise

IY(5), for stiffness matrix re-use.
Element geometry must be identical to previous element

PRESSU, Used in static analysis only
Ignored if ISTAT =0, Section I, Card 2

VI STATIC NODAL LOADS

Card 1 — Nodal Load Input — I5,F10.0

Columns		Contents
1-5	N	Node number
6-15	TR(1)	X-Axis load
16-25	TR(2)	Y-Axis load
26-35	TR(3)	Z-Axis load
36-45	TR(4)	X-Axis moment
46-55	TR(5)	Y-Axis moment

NOTES: Card 2

Used in static analysis only, but at least one blank card must be included.

N - If N=0 or blank, terminate nodal load input

Z- Axis moments are not permitted since only flat models are allowed and thus no Z-rotational stiffness exists

- END OF INPUT DATA -

GENERAL PROGRAM NOTES:

1. Units for the various input parameters need only be consistent, with the exception of ply orientation angles, which must be input as degrees.

2. When inputting nodal boundary condition codes, it is advisable to use zero-displacement wherever possible. These serve to reduce program size and running time. Specifically, Z-axis rotations should be excluded. X and Y axis displacements should be excluded unless membrane forces are included in static prestress conditions.

3. Z - coordinate location must be identical for all nodes. This restriction, along with the restriction that elements be rectangular and aligned with the global X-axis, is required for proper stress calculation.

4. Damping coefficients need not be included if no damping is desired in the dynamic analysis.

5. The laminate input, Section III, should be symmetric as the displacement solution ignores bending/extensional coupling.

TABLE C-1. CLIP ROUTINES

CLIP	Main Program. Supervises the data input. Sets internal storage parameters. Supervises element and global stiffness formulation.
TIMER	Computes and prints elapsed CPU Time.
IMPIN	Reads impact parameters.
LAMIN	Reads laminate materials and orientations. Formulates laminate stiffness matrices. Computes effective plane stress matrices for shell element routines.
INPUTJ	Reads modal data. Determines equation numbers. Sets impacted mode numbers to degree of freedom numbers.
ELT6	Sets storage for shell element routines.
TPLATE	Supervises shell element formulation.
STRETR, QTSHEL, QOCOS, TDCOS, TRFPRD, SLST, SLCCT	Shell element routines.
CALBAN	Finds global stiffness band width and saves elemental matrices for global stiffness formulation.

ERROR	Compares required storage and available storage
INL	Reads and processes static nodal loads.
ADDSTF	Forms global stiffness, mass and force matrices. Computes impact velocity for momentum conservation.
ADSTF2	Modifies existing global stiffness matrix for damage incorporation.
STEP	Supervises time integration analysis. Sets internal storage for integration analysis.
STATIC	Supervises solution for static displacement vector.
ADDMAS	Converts blocked mass and force vectors (from ADDSTF) to single, unblocked vectors.
MASSIN	Reads mass vector into core after damaged element reformulations. Modifies global mass and stiffness for impact mass separation.
SOLSTP	Performs time integration analysis.
TRIFAC	Decomposes stiffness matrix.
REDVK	Solves for displacement vector.
PR	Prints displacements, velocities and accelerations.
STRREC	Supervises stress recovery procedure.
PLYSTR	Performs composite stress analysis.
FAIL	Performs failure analysis.
BSTIF	Computes properties for interlaminar shear calculations in damaged elements.
INVRTS	Matrix inversion routine.
MATPRD	Matrix multiplication routine.
STOPPR	Terminates program execution.

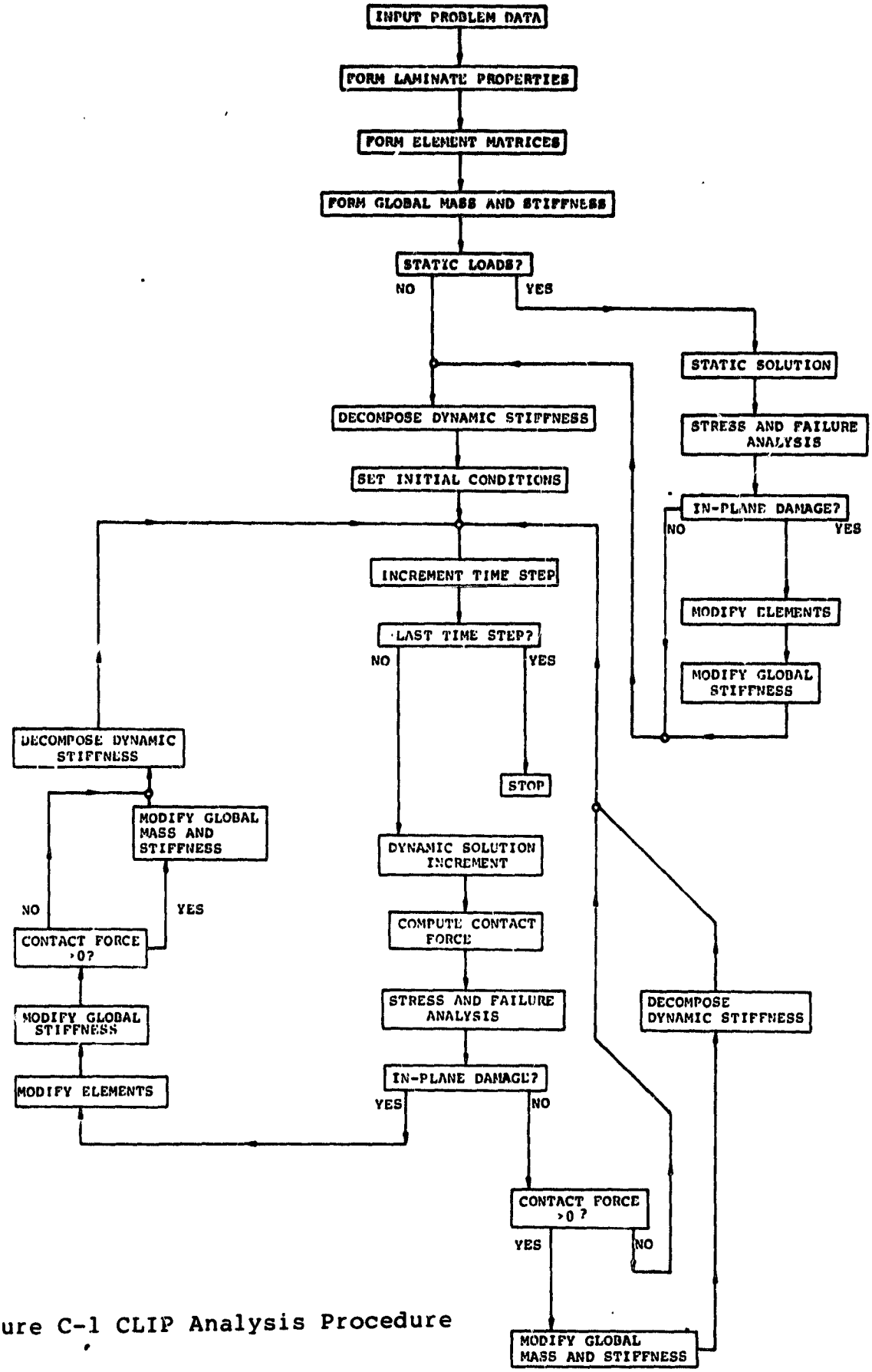

Figure C-1 CLIP Analysis Procedure